

**DEVELOPMENT AND CHARACTERIZATION OF HA BASED
MICROWAVE ASSISTED BIOMEDICAL COATINGS ON
SURGICAL GRADE STAINLESS STEEL**

Thesis Submitted for the Award of the Degree of

DOCTOR OF PHILOSOPHY

in

MECHANICAL ENGINEERING

By

PARDEEP SINGH

Registration Number: 41900777

Supervised By

Dr.Hitesh Vasudev (24804)

School of Mechanical Engineering

(Professor)

Lovely Professional University, Punjab

Co-Supervised by

Dr. Amit Bansal

Mechanical Engineering (Assistant Professor)

IKGPTU, Jalandhar

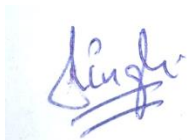


LOVELY PROFESSIONAL UNIVERSITY, PUNJAB

2023

DECLARATION

I, hereby declared that the presented work in the thesis entitled “Development and characterization of HA based microwave assisted biomedical coatings on surgical grade stainless steel” in fulfilment of degree of **Doctor of Philosophy (Ph.D.)** is outcome of research work carried out by me under the supervision Dr. Hitesh Vasudev working as Professor, in the School of Mechanical Engineering at Lovely Professional University, Punjab, India. In keeping with general practice of reporting scientific observations, due acknowledgements have been made whenever work described here has been based on findings of other investigator. This work has not been submitted in part or full to any other University or Institute for the award of any degree.



(Signature of Scholar)

Name of the scholar: Pardeep Singh

Registration No.: 41900777

Department/school: School of Mechanical Engineering

Lovely Professional University, Punjab, India

CERTIFICATE

This is to certify that the work reported in the Ph.D. thesis entitled “Development and characterization of HA based microwave assisted biomedical coatings on surgical grade stainless steel” submitted in fulfillment of the requirement for the reward of degree of **Doctor of Philosophy (Ph.D.)** in the School of Mechanical Engineering, is a research work carried out by Pardeep Singh, Registration No.41900777 is bonafide record of his/her original work carried out under my supervision and that no part of thesis has been submitted for any other degree, diploma or equivalent course.



Signature (Supervisor)

Dr. Hitesh Vasudev (24804)

**School of Mechanical Engineering
(Professor)**

Lovely Professional University, Punjab



Signature (Co-Supervisor)

Dr. Amit Bansal

**Mechanical Engineering (Assistant
Professor)**

IKGPTU, Jalandhar

ABSTRACT

The metallic materials are widely employed as bio-implants in human body for mechanical features and reasonable biocompatibility. However, these materials suffer from corrosion, which is a serious problem. Research and development on metallic biomaterials has shown that surface coating/ modifications of metallic implants by using a suitable bioactive material is a widely accepted alternative to minimize the harmful effects of corrosion.

In the present research work, a microwave assisted surface modifications was performed (SS-31254) by using hydroxyapatite (HA) coatings. Microwave heating is well known for uniform and volumetric heating of materials at molecular level. The attributes associated with microwave heating reduces processing time significantly and resulted in better microstructures and properties of the materials as compared to the conventional processing of materials. SS-31254 is a widely used material in clinical applications. However, it has poor biocompatibility in actually system. Therefore, bioactive HA powder was deposited by using microwave energy. Because the HA coatings is very brittle in nature. Therefore, the study of additions of (Al_2O_3 and ZrO_2 by weight in 10%) in HA in suitable amount has also been discussed. The study of heat-treatment on the samples at all conditions at 700 °C has also been described. The characterization was conducted for the microwave-assisted surface modified samples under each and every circumstance. In order to evaluate the coatings' resistance to corrosion, electrochemical corrosion testing was carried out in a fluid model that was representative to fluids found in biological systems. After conducting corrosion tests on the samples, XRD and SEM/EDS analyses were then performed on them. Experiments using cell culture and Ringers solution were used to investigate the underlying biological pathways.

The clad is predominantly composed of nickel-iron (Ni-Fe) solid solution, together with HA and certain reaction products, primarily in the inter-dendritic areas. According to the findings, the hardness and porosity of the heat-treated surface modified

samples are improved over those of the as-deposited samples. Additionally, the 700 °C heat-treated samples showed the least amount of porosity and the higher hardness.

The in-vitro bioactivity determination of the microwave surface samples was determined by keeping the samples in the solution having ionic compositions matches with plasma in human blood. The microwave surface modified samples were placed in air tight plastic bottles which were filled with 50 mL of SBF for 14 days. After the testing period, the samples were taken from the incubator and studied using SEM. The change in weight of the samples was also taken as criteria to detect the formation of apatite layer on it. The negligible weight gain was observed in the unmodified SS31254 steel indicating non-bioactivity of material. On the other hand, the microwave aided surface modified samples showed increased weight which indicates the formation of apatite layer on it. Furthermore, when the heat-treatment temperature rises, the ability to create an apatite layer decrease. The maximum apatite layer formation was seen on samples at all conditions due to presence of maximum pores/void and amorphous phase in it. The densification of the composite layer by covering pores and voids was seen in heat treated clads. The pore/void act as a nucleating site for apatite to grow onto it. Therefore, the as-deposited surface modified sample exhibited maximum apatite layer formation followed by 700 °C heat-treated sample, and then uncoated samples.

From corrosion analysis, it has been found that the microwave assisted surface modification with HA, HA+10wt%Al₂O₃ and HA+10wt%ZrO₂ better behaviour of the SS-31254 steel, which is required for the implant material in the human body. The microwave modified specimens have low corrosion current density followed by clad specimens and then followed by uncoated base metal. Thus the heat-treated coupons have higher corrosion resistance. The low corrosion rate for the heat-treated microwave assisted surface modified specimens was due to densification of coatings after the application of heat-treatment on the microwave treated specimen's.

ACKNOWLEDGEMENT

First and Foremost, I am very much heartily thankful to my dissertation Supervisor, **Dr. Hitesh Vasudev**, Associate Professor in School of Mechanical Engineering, Lovely Professional University, for his invaluable guidance and support during the present research work.

I wish to express my heartily thanks to co-supervisor, **Dr. Amit Bansal**, Assistant Professor in Mechanical Engineering Department, IKGPTU Kapurthala for giving valuable inputs during every phase of my Ph.D. work.

I wish to thank **Mr. Amrinder Mehta**, in-charge of XRD, CIF cell, LPU, **Mr. Shiv Kumar**, in-charge of FE-SEM, Institute Instrumentation Centre, IIT Roorkee.

I express my profound regards to my parents for their blessings and for being the main source of inspiration to succeed in my endeavours. I would like to express particular thanks to my family, my mother for her advises, care and love.

I would like to thank everyone who supported me for completing this work successfully and I express my apology that I could not mention everyone individually. Above all, I would like to express my sincere gratitude from the core of my heart to **ALMIGHTY** for giving courage, strength and patience to carry out my research out.



(PARDEEP SINGH)

Contents

DECLARATION	i
CERTIFICATE	ii
ABSTRACT.....	iii
ACKNOWLEDGEMENT	v
LIST OF TABLES.....	x
LIST OF FIGURES.....	xi
LIST OF APPENDICES	x iv
CHAPTER 1	1
INTRODUCTION.....	1
1.1 DEMAND OF BIOMATERIAL/IMPLANT	1
1.2 BIOMATERIALS	3
1.3 IMPORTANT ASPECTS OF METALLIC BIOMATERIALS.....	4
1.3.1 MECHANICAL PROPERTIES	5
1.3.2 BIOCOMPATIBILITY	6
1.3.3 WEAR	6
1.3.4 CORROSION.....	8
1.4 METAL IMPLANT MATERIALS WITH MODIFIED SURFACES.....	10
1.5 Limitations of Microwave-Assisted Surface Coating.....	11
1.6 MOTIVATION.....	12
1.7 SUMMARY.....	12
CHAPTER 2	13
LITERATURE REVIEW	13
2.1 REASONS WHY IMPLANTS OFTEN FAIL	13
2.1.1 METAL IMPLANT CORROSION.....	13
2.1.2 WEAR OF IMPLANTS	16
2.2 THE USE OF FAIL-SAFES TO REDUCE IMPLANT LOSSES.....	17
2.2.1 SYSTEMS OF PROTECTION	17

2.3 RESEARCH GAP.....	22
2.4 RESEARCH OBJECTIVES	22
2.5 SUMMARY.....	23
CHAPTER 3	26
EXPERIMENTAL EQUIPMENTS AND METHODOLOGY	26
3.1 SUBSTRATE PREPARTION	26
3.2 CLADDING POWDER.....	27
3.3 SURFACE MODIFICATION THROUGH HYBRID MH	29
3.4 HEAT-TREATMENT OF THE MICROWAVE ASSISTED SURFACE MODIFIED SAMPLES AT ALL CONDITIONS	33
3.5 METALLURGICAL CHARACTERIZATION OF THE CLADS	33
3.5.1 X-RAY DIFFRACTION (XRD).....	34
3.5.2 MICROSTRUCTURAL CHARACTERIZATIONS OF THE MICROWAVE ASSISTED SURFACE MODIFIED SAMPLES WITH OPTICAL MICROSCOPE	34
3.5.3 MICROSTRUCTURAL CHARACTERIZATIONS OF THE MICROWAVE INDUCED CLAD SPECIMENS AT VARIOUS HEAT TREATED CONDITIONS.....	34
3.5.4 MEASUREMENT OF CLADDING THICKNESS	35
3.5.5 POROSITY MEASUREMENT FOR THE CLADS	35
3.6 MECHANICAL CHARACTERIZATIONS OF THE MICROWAVE INDUCED CLAD SPECIMENS AT VARIOUS HEAT TREATED CONDITIONS	36
3.6.1 MEASUREMENT OF MICRO-HARDNESS.....	36
3.7 FUNCTIONAL CHARACTERIZATIONS OF THE MICROWAVE ASSISTED SURFACE MODIFIED SPECIMENS AT AS-DEPOSITED AND HEAT-TREATED CONDITIONS.....	36
3.7.1 IN-VITRO BIOCOMPATIBILITY STUDY.....	37
3.7.2 CORROSION BEHAVIOUR OF THE MICROWAVE INDUCED CLAD SPECIMEN AT VARIOUS HEAT TREATED CONDITIONS	38
3.8 TAFEL PLOT EXPERIMENT.....	40
3.9 SUMMARY.....	41

CHAPTER 4	43
CHARACTERIZATION OF FEED STOCK AND CLADDINGS	43
4.1 SEM/EDS AND XRD ANALYSIS OF FEED STOCK POWDERS.....	43
4.1.1 SEM/EDS AND XRD ANALYSIS OF HA POWDER.....	43
4.1.2 SEM/EDS AND XRD ANALYSIS OF AL ₂ O ₃ POWDER	44
4.1.3 SEM/EDS AND XRD ANALYSIS OF ZrO ₂ POWDER	46
4.1.4 SEM/EDS AND XRD ANALYSIS OF HA10AL POWDER	46
4.1.5 SEM/EDS AND XRD ANALYSIS OF HA10ZR POWDER	48
4.2 SEM/EDS AND XRD ANALYSIS OF AS-DEPOSITED AND HEAT-TREATED SURFACE MODIFIED SPECIMEN AT ALL CONDITIONS	49
4.2.1 MICROSTRUCTURAL/ELEMENTAL STUDY AND XRD ANALYSIS OF AS-DEPOSITED AND HEAT-TREATED SURFACE MODIFIED SPECIMENS WITH PURE HA POWDER.....	49
4.2.2 MICROSTRUCTURAL/ELEMENTAL STUDY AND XRD ANALYSIS OF AS-DEPOSITED AND HEAT-TREATED SURFACE MODIFIED SPECIMENS WITH HA10AL POWDER	54
4.2.3 MICROSTRUCTURAL/ELEMENTAL STUDY AND XRD ANALYSIS OF AS-DEPOSITED AND HEAT-TREATED SURFACE MODIFIED SPECIMENS WITH HA10ZR POWDER	59
4.3 POROSITY MEASUREMENT IN THE AS-DEPOSITED AND HEAT-TREATED SURFACE MODIFIED SAMPLES AT ALL CONDITIONS	61
4.4 MICROHARDNESS MEASUREMENT IN THE AS-DEPOSITED AND HEAT-TREATED SURFACE MODIFIED SAMPLES AT ALL CONDITIONS	63
4.5 SUMMARY.....	65
CHAPTER 5	66
IN-VITRO BIOCOMPATIBILITY STUDY AND CORROSION BEHAVIOUR OF THE BASE METAL (SS-31254) AND SURFACE MODIFIED SPECIMENS AT ALL CONDITIONS.....	66
5.1 IN-VITRO STUDY FOR HA SURFACE MODIFIED SPECIMENS FOR AS-DEPOSITED AND HEAT-TREATED CONDITION.....	66
5.2 IN-VITRO STUDY FOR HA10AL AND HA10ZR SURFACE MODIFIED SPECIMENS FOR AS-DEPOSITED AND HEAT-TREATED CONDITION.....	67

5.3 IN-VITRO CORROSION ANALYSIS.....	70
5.3.1 CORROSION STUDIES	70
5.4 SUMMARY	77
CHAPTER 6	78
CONCLUSIONS AND FUTURE SCOPE.....	78
6.1 CONCLUSIONS.....	78
6.1.1 MAJOR CONCLUSIONS OF THE PRESENT WORK.....	78
6.2 MAJOR CONTRIBUTION OF THE PRESENT WORK	81
6.3 SCOPE FOR THE FUTURE WORK.....	81
BIBLIOGRAPHY	83-93
LIST OF PUBLICATION.....	94

List of Tables

Description	Page No:
Table 1.1 Biomaterials of metallic materials (Bala et al., 2011).....	2
Table 1.2 Important aspects related to implant material and bone (Mudali et al., 2003).....	5
Table 2.1 Consequences for the host organism brought on by corrosion brought on by the presence of metals in a wide variety of biomaterials (Bergant, Z. and Grum, J., 2009).....	13
Table 2.2 Corrosion in implants (Bergant, Z. and Grum, J., 2009).....	14
Table 2.3 TS methods.....	19
Table 3.1 Clads used in the current investigation.....	30
Table 3.2 Effect of exposure time for a fixed set of parameters (power: constant; sample; size; same).....	32
Table 3.3 The optimized parameters for modify the surface layer with pure HA claddings.....	32
Table 3.4 Kroll`s reagent etchant composition.....	34
Table 4.1 The compositions of the γ , interdendritic, and black particle phase in the microwave assisted modified layer.....	58
Table 4.2 Measured porosity (%).....	62
Table 4.3 Microhardness values.....	64
Table 5.1 Weight change of as-deposited and heat-treated surface modified specimens with HA10AL and HA10ZR powder.....	69
Table 5.2 Chemical composition of Ringer`s solution.....	71
Table 5.3 Various Corrosion parameters of the un-coated 254SS and the microwave surface modified samples at all conditions in Ringer`s solution at 37 ± 1 °C temperature.....	75

List of Figures

Description	Page No:
Fig.1.1. Biomaterials in human body parts. (Ahmaniemi et al., 2000).....	1
Fig.1.2. Joints replacement (Awasthi et al., 2021).....	2
Fig.1.3. Various factors influencing the biocompatibility of biomaterial (R. Singh, and N.B. Dahotre., 2007).....	6
Fig.1.4 Application of biopolymer composite coatings into bone	10
Fig.2.1 Stent corrosion in bare metal (Bergant, Z. and Grum, J., 2009).....	15
Fig.2.2 Human joints are an example of congruency. places: (a) hip and (b) shoulder (Bala et al., 2017).....	16
Fig.2.3 Human incongruent (a) artificial knee and ankle joints (b) (Bala et al., 2017)...	16
Fig.2.4 Relationship between wear kinds and operating circumstances presented in a flowchart (Bolelli et al., 2008a).....	17
Fig.2.5 Different coating generations for prosthesis surface modification	17
Fig.2.6 HAp fluorapatite crystal structure (Dooley, R. and Wiertel, E., 2009).....	20
Fig.2.7 Problem formulation outlined in the current research work	23
Fig.2.8 The research plan and research problem.....	25
Fig.3.1 Specimens for various sizes for (a) XRD and SEM analysis, (b) corrosion study, and (c) invitro bioactive study.....	27
Fig.3.2 Mixing of powder (90wt% HA and 10wt% ZrO ₂) on lathe machine.....	29
Fig.3.3 Methodology adopted in the present research work	29
Fig.3.4 Schematic of setup for cladding (Bansal et al. 2017).....	32
Fig.3.5 Sample after Cold Mounting and Polishing.....	34
Fig.3.6 Experimental Setup of Autoclave vertical machine.....	38
Fig.3.7 Experimental Setup of Incubator	38
Fig.3.8 Corrosion testing apparatus	40

Fig.3.9 Schematic illustration of the electric circuit for cathodic polarization measurement.....	42
Fig.4.1 (a) Secondary electron image of HA powder, (b) EDS of HA powder corresponding to point 1 of Fig. 1a.....	44
Fig.4.2 XRD pattern of HA powder	45
Fig.4.3 (a) SEM micrograph and (b) EDS of Al ₂ O ₃	46
Fig.4.4 XRD pattern of alumina Al ₂ O ₃ feedstock	47
Fig.4.5 (a) SEM and (b) EDS of ZrO ₂ powder	48
Fig.4.6 XRD analysis ZrO ₂ powder	48
Fig.4.7 (a) Morphology of HA10AL powder, and (b) element maps of O, Al, P and Ca corresponding to Fig. 4.7a.....	49
Fig.4.8 (a) Morphology of HA10ZR powder, and (b) element maps of O, P, Ca and Zr corresponding to Fig. 4.8a.....	49
Fig.4.9 SEM images of microwave assisted surface modification of SS-31254 alloy at (a) low magnifications showing fused interface with varying microstructure in the modified layer, (b) higher magnification showing the inter-dendritic HA phases in the austenite matrix.....	52
Fig.4.10 (a) SEM image illustrates the line mapping (AB) taken across the inter-dendritic phase of modified SS-316L layer, (b) distribution of elements (Fe, Ca, O, and P) corresponding to line AB.....	53
Fig.4.11 XRD spectra of (a) HA powder, and (b) microwave assisted surface modified SS-31254 layer.....	54
Fig.4.12 SEM image of post heat-treated (at 700°C) HA surface modified layer.....	54
Fig.4.13 XRD analysis of (a) HA powder and (b) HA clad (c) HA post heat-treated clad	55
Fig.4.14 (a) optical macrograph of the HA10AL reinforced 254SS in as-deposited condition. SEM micrographs of microwave surface modified specimens in (b) as-deposited condition, (c) 700 °C heat-treated conditions	56

Fig.4.15 (a) SEM microstructure of interdendritic phase in as-deposited conditions, (b) EDS maps of Fe, O, Ca, and P corresponding to Fig. 6a.....	58
Fig.4.16 (a) HA powder, (b) HA10AL surface modified specimens in as-deposited conditions, and (c) HA10AL surface modified layer in the post heat-treated conditions.....	60
Fig.4.17 SEM image of (a) as-deposited HA10ZR powder, and (b) heat-treated HA10ZR surface modified layer.....	61
Fig.4.18 XRD analysis of (a) as-deposited HA10ZR surface modified layer, and (b) heat-treated HA10ZR surface modified layer.....	62
Fig.4.19 SEM micrographs illustrates the morphology of indents taken on microwave surface modified specimens in (a) unmodified layer (b) as-deposited modified layer, (c) 700 °C heat-treated layer in case of HA10AL specimen.....	65
Fig.5.1 SEM images showing the apatite precipitation after 14 days of the immersion in simulated body fluid of (a) unmodified SS-31254 alloy. (b) microwave assisted modified SS-31254 alloy along with EDS taken at brighter phase (c) microwave assisted modified SS-31254 at heat-treated conditions.....	68
Fig.5.2 SEM images for HA10AL (a) SS-31254 alloy. (b) clad, (c) 700 °C heat-treated layer.....	70
Fig.5.3 SEM images for HA10ZR (a) as-deposited modified layer, (c) 700 °C heat-treated layer.....	71
Fig.5.4 Tafle plot curves for (a) base metal (b) HA As-deposited (c) HA heat-treated (HT) (d) HA10AL As-deposited (e) HA10AL heat-treated (HT) (f) HA10ZR As-deposited (g) HA10ZR heat-treated (HT).....	75
Fig. 5.5 SEM micrograph of corroded base material.....	76
Fig. 5.6 (a) HA in as-deposited condition (b) HA heat-treated (HT) condition (c) HA10AL as-deposited (d) HA10AL heat-treated (HT) (r) HA10ZR as-deposited (f) HA10ZR heat-treated (HT) condition.....	77

List of Appendices

APPENDIX



Model: D8 Advance
Make: Bruker AXS
Instruments,
Germany
Radiation: Cu-K α
Scan rate: 0.5 to 1°
min⁻¹
Scan range: 20° to
100°

Fig. A-1 View of the X-Ray Diffraction Equipment Used for Phase Analysis.



Model: LT 23B
Make: Dewinter,
India
Magnification: 50 x,
100 x, 200 x, 500 x
Display: Large field
Interface: With USB
Digital camera and
Image Analysis
Software (Dewinter
Material Plus,
Version 4.2)

Fig. A-2 View of Optical Microscope.



Model: FEI Quanta
200
Make: FEG-SEM,
Czech Republic
Operating voltage:
2-25 kV
Magnification: 25 x
to 100000 x
Gun: Field Emission
Gun (FEG)

Fig. A-3 Typical View of the Field Emission Scanning Electron Microscope (FE-SEM)
Used for Microstructural Investigation



Model: Economet
VH-1 MD
Make: Chennai
Metco, India
Indenter: Vickers
Test Load: 10 –
1000 gf
Operating Time: 15
s
Min Measuring
Unit: 0.05 μm
Hardness Measuring
Range: 5~2500 HV
Test Microscope
Magnification: 400X
(Measuring), 100X
(Observation).

Data Output: LCD
screen display,
Inside Printer, RS-
232.

Max. Sample
Height: ~100 mm

Fig. A-4 Typical View of the Vicker's Micro-hardness tester



Model:
Metallurgical sample
saw MS-10
Make: Ducom Pvt.
Ltd, Bangalore,
India
Capacity: 240 RPM
Blade Thickness:
200 μ m

Fig. A-5: View of the Diamond Cutter Used for Sample Cu

ABBREVIATIONS

SEM	Scanning Electron Microscopy
EDS	Electron Dispersive Spectroscopy
XRD	X-ray Diffraction
HA	Hydroxyapatite
Al ₂ O ₃	Aluminium oxide
APS	Atmospheric Plasma Spray
SPS	Suspension Plasma Spray
HVOF	High Velocity Oxy fuel
HVFS	High Velocity Flame spray
SS-304	Stainless Steel-304
WCEDM	Wire Cut Electric Discharge Machining
BSE	Back Scattered Electron
MA	Microwave Assisted

Chapter 1

INTRODUCTION

1.1 Demand of biomaterials

The use of bio-implant increases in daily life. Thus, research in this area is very important to reduce costs and improve properties. Until 1860, as illustrated in Fig.1.1, it was possible to successfully implant metallic devices such as bone pins made of iron, or gold in experimental trials. However, after the industry experienced extraordinary growth, the biomaterials are used in knee implants also, as indicated in Fig.1.2. It has been reported that between 2005 and 2030, the anticipated growth in primary TNA operations in the United States is over 673%, whereas the estimated increase in primary THA procedures is approximately 174% . Factors such as the ageing of the baby boomer generation, the rising average human lifespan, and the epidemic of obesity all contribute to the increased stress that is being placed on our weight-bearing joints.

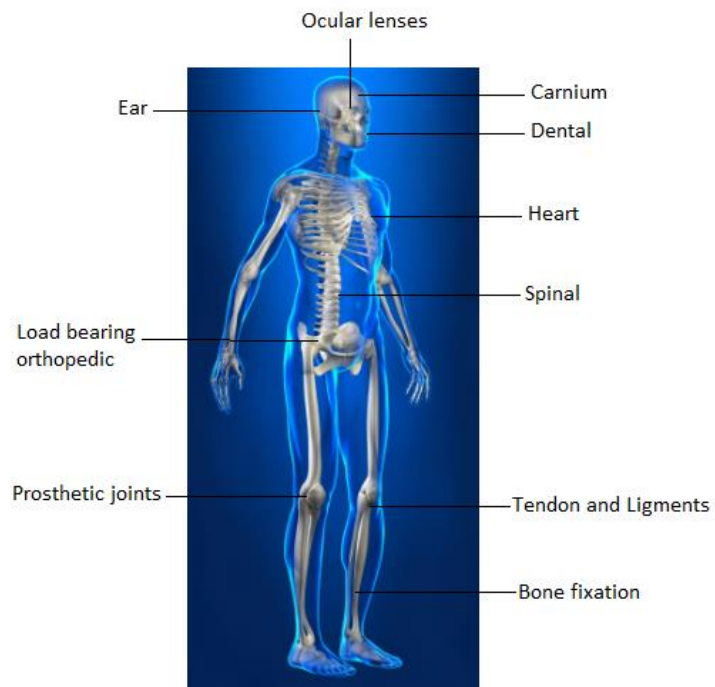


Fig. 1.1 Biomaterials in human body parts.

The joint replacement was mainly done through metallic biometal (SS-316L, Ti-6Al-4V), because they possess adequate strength required to sustain loads in load bearing joints. Table 1.1 illustrates the various metallic materials used as implant material in a number of applications.

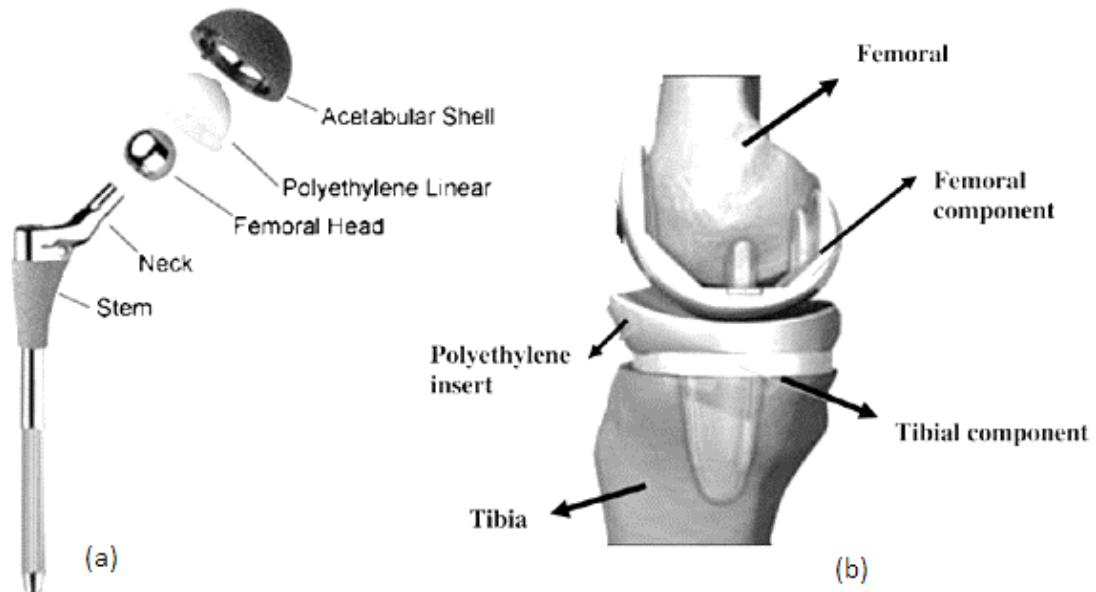


Fig.1.2 Joints replacement (Awasthi et al., 2021).

Table 1.1

Biomaterials of metallic materials

Class	Application	Use and approval
Stainless steels (Fe based biomaterials)	Replacement of the hip joint Temporary implants	
Co-based materials	Joint replacement in surgery for use in dentistry	Applied routinely
Ti-based alloys	Mechanical devices and nails Hip replacement stem and cup	
Others		
NiTi	Scleral stents Surgical anchors Wires used	Approved by FDA

	to guide catheters
	Intracranial aneurysm clips
Mg	Biodegradable orthopedic implants
Ta	To serve as a reference point in radiography
	A plastic surgeon or neurosurgeon may utilise wire sutures.

1.2 BIOMATERIALS

The research is very important to reduce costs and improve properties of biomaterials. The joint replacement was mainly done through metallic biometal because they possess adequate strength required to sustain loads in load bearing joints (Balla et al., 2013; Balamurugan et al., 2002). In biomaterials, the metallic implants are used because they have adequate strength at reasonable cost. The austenitic stainless steels (ASS) are used as implant material for inner joint fixation orthopedic devices (Davis, J.R. ed., 2004). As compared to titanium alloys, the corrosion rate is low in stainless steel. Despite of this, at a very low cost, it has very good mechanical properties, used provisionally for inner parts like bone plates, screws and spine traction. Numerous kinds of stainless steel, including Rex-734, P-558, ASTM-F2581, and UNS.254, have been discovered by the authors for use in orthopaedics (Dehnavi et al., 2017; Tiwari and Mishra., 2021). In recent years, the use of UNS S31254 (254 SS), an austenitic stainless steel with maximal pitting corrosion resistance in chloride and phosphoric environments, outstanding mechanical strength, and toughness, has risen in favour for use as implant material in the medical field.

1.3 IMPORTANT ASPECTS OF BIO-MATERIALS (METALLIC)

The biomaterials must have adequate biocompatibility. It also exhibit excellent corrosion resistant when interact with human body plasma. These materials must have adequate mechanical properties such as high wear resistant for load bearing applications. The implant upon implantation inside a human body must make a balance of all these properties. An implant should have the following features to serve for a longer time without failure in the human body.

Metals are used as biomaterials to harness their superior mechanical properties and thermal conductivity (Bartkowiak et al., 2020). Metallic biomaterials, such as stainless steels, titanium alloys, and cobalt alloys, are extensively used as implanted devices for many medical applications (Baisrun et al., 2018). Furthermore, both scaffolding and scaffolds used in tissue engineering are constructed from metallic materials. This is the underlying cause of the problem (Bastan et al., 2018). Surface Coating Characteristics of Surgical Grade Stainless Steel Implants Coated with a Variety of Materials are as follows (Bodhak et al., 2011; Chai et al., 2021).

- Coverings made of stainless steel.
- Hardness that is superior and consistent.
- Exceptional longevity.
- Extremely effective defence against oxidation caused by wear and pressure.
- Strong resistance to corrosion as a result of the creation of a passive layer of Cr_2O_3 Excellent resistance to oxidation.
- Protection against chemical assault High bonding strength of the coating that is applied using thermal spraying.
- There is a thick covering with little porosity.

The problem with metallic biomaterials is that they are often constructed out of synthetic materials that are devoid of any form of biological activity. The degree of cohesiveness that can be produced between the coating layer and the metal substrate that lies underneath it is the significant problem that has to be investigated. Bad clinical responses

to implants and the tissue that surrounds them are caused by the spalling of the covering away from the substrate (Beig et. al, 2020).

1.3.1. Mechanical Properties

The particular type of biomaterial needed for an application is determined by its mechanical properties. Biomaterials should have adequate strength and longer fatigue life for their excellent performance in the human body. An implant material must exhibit Young's modulus similar to that of the human bone depending on its biomedical applications. Ti6Al4V has modulus matches with that of the human bone whereas 316L stainless steel exhibit an exceedingly higher elastic modulus. Bone resorption at the implant/bone contact can occur if the implant material has a different modulus than the host tissue (M. Wang., 2003). The method employed to create a particular implant also has an impact on its mechanical qualities. Table 1.2 compares the properties of human bone to those of widely used implant materials Kamachimudali et al., 2003).

Table 1.2 Important aspects related to implant material and bone (Kamachimudali et al., 2003).

Material	Strength (Tensile) (MN/m²)	Strength (Yield)(MN/m²)	Hardness value (Vickers) (HV)	Modulus (E) (MN/m²)	Endurance limit (MN/m²)
316L SS	649	279	490	209	0.27
Alloy Co-Cr	1540	1050	450	539	0.47
Cast Co-Cr alloy	689	489	300	239	0.30
Titanium	709	469	-	119	0.29
Ti6Al4V	999	969	-	119	-
Human Bone	140.3	-	26.3	30	-

1.3.2 Biocompatibility

The main prerequisite for any biomaterial is biocompatibility, which is a substance's ability to perform when used in the human body plasma. The biocompatibility is an essential primary requirement of any biomaterial (D.F. Williams., 2003). Biocompatibility of implant devices influenced by a number of parameters as depicted in Fig. 1.3. These factors ultimately affect the performance of implant material and can lead to its failure (Manivasagam et al., 2010). Biocompatible materials, after their implantation in the human body must not release toxic substances, which may induce many complications such as allergies, choronic inflammation and unusual tissue formation (P. Itiravivong., 2001).

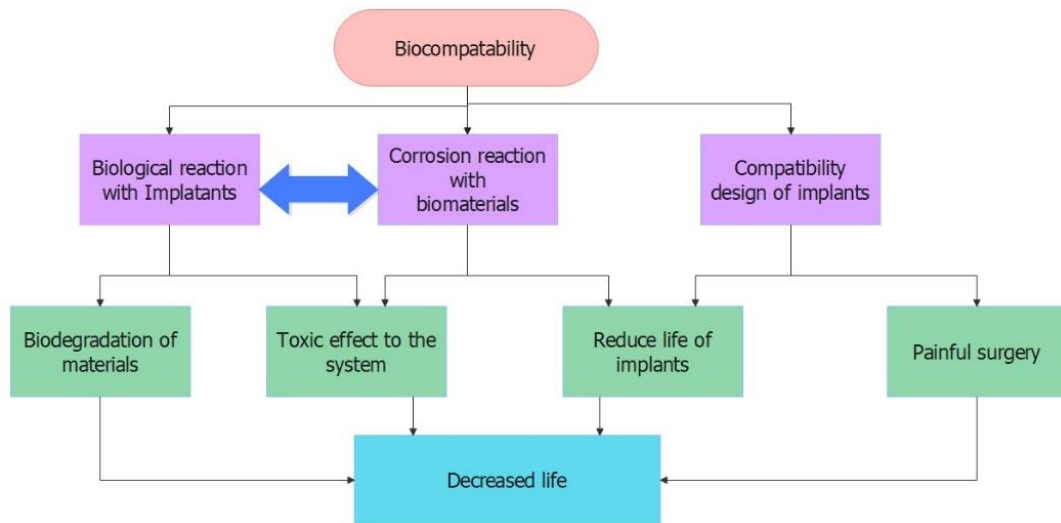


Fig. 1.3 Various factors influencing the biocompatibility of biomaterial (Singh and Dahotre., 2007).

1.3.3 Wear

In the case of knee and hip joint prostheses, wear is the leading cause of implant failure (Roychowdhury et al., 2004). Low wear resistance resulted in the wear debris to build up and cause a variety of tissue reactions. According to Niinomi (2008), these reactions have the potential to result in the premature failure of implants. A primary area of emphasis within orthopaedic research involves the enhancement of fixation and wear

properties pertaining to whole joint components (Geetha et al., 2009). Hence, it is imperative to develop materials that possess elevated levels of hardness and corrosion resistance in order to enhance the longevity of implants within the human body (Eliaz et al., 2002).

Comprehending the Wear Performance of Implants Utilised in Biomedical Procedures

Biomedical implants provide substantial benefits to patients requiring joint replacement, cardiovascular support, and other medical procedures, greatly improving their quality of life. However, the durability of these implants is a crucial factor that directly affects their efficacy and longevity.

The wear performance of biomedical implants is significantly influenced by critical parameters such as surface polish, hardness, toughness, and corrosion resistance. The surface quality of an implant has a direct link with its tribological performance, which subsequently affects how the implant interacts with surrounding tissues and other biomaterials. In order to guarantee the long-term durability of implants, it is crucial to possess characteristics such as hardness and toughness. These features help decrease the rate of wear and prevent fractures of the implants. In order to ensure the long-term effectiveness of a biomaterial for therapeutic purposes, it is crucial to have excellent corrosion resistance. This is important because it helps to reduce the degradation and damage caused by external factors. Corrosion resistance serves to inhibit the occurrence of corrosion. Furthermore, the durability of biomedical implants is mostly influenced by the characteristics of the material used in their fabrication. Key material characteristics that enhance the durability and effectiveness of biomedical implants include robust resistance to wear, a low coefficient of friction, high hardness, exceptional biocompatibility, and great resistance to corrosion. These characteristics are further compounded by their challenging nature to be worn. Due to these characteristics, the implants can effectively withstand the physiological conditions present inside the human body for an extended period, hence reducing wear and friction. Several conventional methods may be used to assess the durability of biomedical implants. Each of these techniques is tailored to a certain group of implants. Procedures such as pin-on-disc

testing, wear testing of polymeric materials, functional and kinematic wear evaluation, in vitro pulsatile durability testing, and wear assessment of full knee-joint and hip-joint prosthesis are included in this category. Various studies, such as gravimetric, volumetric, dimensional, surface roughness, chemical, particle, micro-CT, and custom analyses, along with optical microscopy and scanning electron microscopy, are employed to assess the long-term performance and degradation of the implants. Nevertheless, despite the advancements achieved in biomedical implant technology, there are some notable challenges that must be addressed to enhance their durability. Several obstacles must be addressed, such as fatigue wear in alumina prostheses, implant failures due to infection, mechanical wear, corrosion, tissue rejection, and bacterial invasion during surgical operations. Moreover, inadequate integration of the implant might lead to issues that restrict the durability of the implants. To effectively tackle these problems, it is essential to devise innovative solutions and persist in doing research. Ultimately, having a comprehensive understanding of the wear characteristics of biomedical implants is crucial for developing biomaterials that are reliable, durable, and able to endure the physiological stresses imposed by the human body. Researchers and manufacturers may advance the development of biomedical implants by carefully considering the crucial aspects, material properties, assessment methods, and challenges associated with wear performance. Ultimately, this will lead to enhanced patient outcomes and a better quality of life.

1.3.4 Corrosion

The corrosion response of metallic biomaterials is a significant area of concern. Releasing of metal ions in the body results in the degraded surfaces and implants failure (Wang and Zreiqat., 2010). Therefore, the fabrication of materials with resistance to corrosion is important requirement for the implant (Geetha et al., 2009). Corrosion and its Impact on the Performance of Biomedical Implants

Biomedical implants provide patients with a wide range of therapeutic and functional benefits, making them crucial components of the modern healthcare system. However, the corrosion performance of these implants is a crucial factor that greatly influences

their overall reliability and safety inside the human body in the long run. Various factors contribute to the performance of biomedical implants in corrosion testing. The susceptibility of an implant to corrosion is determined by factors such as the patient's size, shape, and the material composition of the implant. Additional elements that influence the corrosion characteristics of implants include surface properties like as wettability and roughness. The presence of a protective coating on the implant's surface may potentially influence its resistance to corrosion. Corrosion fatigue resistance is a crucial consideration for surgical implants used in applications involving cyclic motion or load-bearing. An implant material must possess the ability to withstand the combined effects of cyclic loading and corrosive environments to ensure its long-term mechanical integrity. Various methodologies are used to assess the corrosion efficacy of biomedical implants. These methods include examining the behaviour of the implants in various scenarios. Electrochemical techniques, such as electrochemical impedance spectroscopy, are often used to assess the corrosion properties of implant materials. In vitro corrosion testing allows researchers to replicate the physiological conditions and assess the ability of materials to resist corrosion. Assessing the effectiveness of implants in specific clinical scenarios may be achieved by conducting personalised tests that adhere to defined assessment protocols.

These evaluation approaches enable the assessment of corrosion potential, metal ion release, breakdown and repassivation potentials, and resistance to several types of corrosion, including crevice corrosion, galvanic corrosion, and fretting corrosion. Moreover, these technologies allow for a full analysis of the microstructure and electrochemical characteristics of implant alloys, yielding crucial insights into their corrosion behaviour. It is crucial to possess a comprehensive comprehension of the corrosion characteristics of biomedical implants to ensure the longevity and safety of implanted medical devices. To enhance the reliability and durability of biomedical implants, researchers and manufacturers can consider the factors that affect corrosion, employ appropriate evaluation methods, and select materials with favourable resistance to corrosion.

1.4 METAL IMPLANT MATERIALS WITH MODIFIED SURFACES

Surface coating is an effective way to protect the metallic biomaterials from various types of degradations such as corrosion and wear. The mechanical properties of the metallic bioimplant such as surgical grade stainless steel are appropriate for material having heavy strength.; however, its lesser biocompatibility curb its adaptation in the medical field (Awasthi et al., 2021). The metallic bioimplant releases harmful ions which are not desired. Further, the surface of the metallic implant consists of surgical grade stainless steel does not have bioactivity and conductivity (Azarmi et al., 2008). Thus, to provide protection against harmful effect of metallic bioimplant and to increase its bioactivity; the biocompatible coatings have been deposited on the surfaces of surgical grade stainless steel. The metallic biomaterials can be effectively shielded against various sorts of degradations like corrosion and wear by applying a biocompatible coating. The usage of bioceramic-based hydroxyapatite (HA) has been discovered. Because of its similarity to the primary phase found in bone and its ability to generate a strong interfacial contact between implant and bone, HA is utilised due to its application as biocompatible coatings, allowing for improved prosthesis attachment.

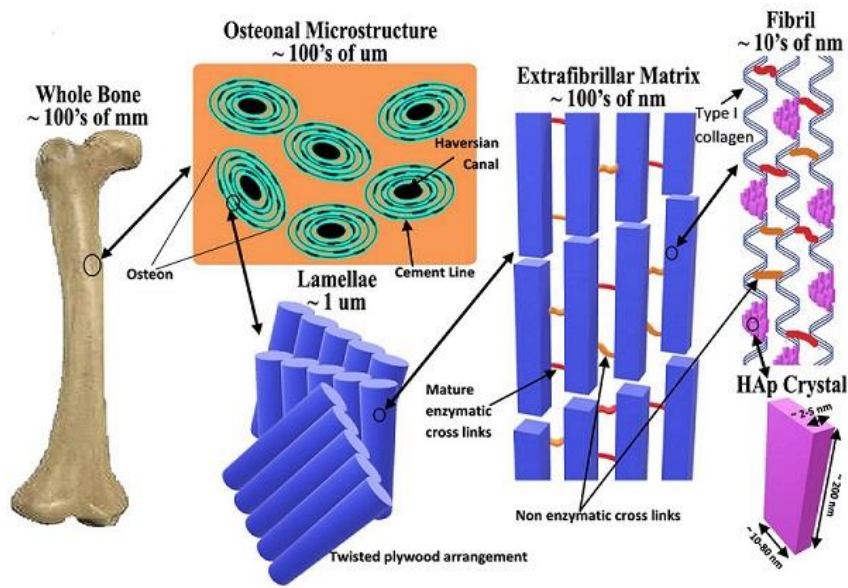


Fig 1.4 Application of biopolymer composite coatings into bone

Further, HA having chemical formula $\text{Ca}(\text{PO}_4)_6(\text{OH})_2$ is the frequently used material in the dentistry and prosthesis area of applications due to its excellent biocompatibility and tissue regeneration property (Tiwari and Mishra., 2021). Thus, the biocompatibility of metallic implant surface can be improved with pure biometal such as HA or its composite material. The main function of HA implant coatings is its participation in human tissues on the implant surface (Bergant and Grum., 2009; Bergant et al., 2014). The application of biopolymer HA based composite coatings on a particular bone is shown in Fig. 1.4.

The coating of HA on the metal substrates are introduced on the surfaces by using various well established surface modifications techniques like sol-gel, biomimetry, chemical vapour deposition, sputtering, dip coating, immersion coatings, ion beam assisted deposition, plasma sintering, electrophoretic deposition, electro hydrodynamic spraying, pulsed laser deposition based surface modification of metallic implant with reinforced HA material, thermal spray methods, and flame spray etc. (Bergmann and Vicenzi., 2011; Birks et al., 2006; Bolelli et al., 2008a; Bolelli et al. 2008b; Boulos et al., 2021; Calvarin et al., 2000; Campo et al., 2009; Chatha et al., 2013; Chatha et al., 2016; Chatterjee et al., 2001; Ctibor et al., 2006; Daram and Banjongprasert., 2020.) Each of these coatings have significant advantages and limitations with respect to a particular fields/ applications. For example the plasma spraying is a complex process for performing HA based coating on the metallic implant because a lot of factors were involved in its coatings. The laser assisted surface modifications is a costly process on the other hand.

1.5 LIMITATIONS OF MICROWAVE-ASSISTED SURFACE COATING

Microwave-assisted surface coating has several benefits, including reduced weight, improved resistance to corrosion, and increased efficiency. Nevertheless, there are limitations to this technique. Research examined three drawbacks of microwave technology, including its lack of scalability, restricted range of applications, and potential health concerns. The number 3. The scalability problem pertains to the difficulties of using this technology in bigger industrial operations. Moreover, the restricted use of microwave technology indicates certain limitations on the suitable areas for its successful

implementation. Furthermore, the possible drawbacks of microwave technology in terms of health dangers have been acknowledged. The presence of these restrictions underscores the need for more investigation and advancement to tackle the difficulties encountered in microwave-assisted surface coating procedures.

1.6 MOTIVATION

There is a huge demand for biomaterials in future. The metallic biomaterial is commonly used for the fabrication of implant because they exhibit better mechanical properties at reasonable cost. However, the metallic implant lacks in providing the required biocompatibility when they are come in contact with human body plasma. Therefore, a suitable coating has been done on these implant material. The metallic biomaterials can be effectively shielded against various sorts of degradations like corrosion and wear by applying a biocompatible coating. There are number of coatings methods were available as discussed above. However, there are limitations associated with these processes. To overcome the limitation of the existing methods, a new process microwave assisted surface modifications has been utilized in the present work to on stainless steel such as SS-31254. In one combination HA has been used as a standalone coating on the given biomedical materials. In another combination, a composite coating of HA with 10wt% of Al_2O_3 and ZrO_2 has been investigated. The coatings were further post-processed with heat-treating these coatings at 700 °C for 1 hour to optimised their mechanical and biological properties.

1.7 SUMMARY

The need of biomaterials has been discussed in this chapter Surface engineering offers a wide range of technologies to improve surface features of the implants to be used in human body applications. A brief overview of various surface engineering methods has been illustrated. The significance of HA based coatings in the domain of surface engineering has been highlighted; potentials of using microwave energy for material processing have been introduced

Chapter 2

LITERATURE REVIEW

This encompasses studies on implant corrosion and various surface modification techniques used for biomedical implants. The more emphasis is given on application of microwave energy for processing of various engineering materials.

2.1 REASONS WHY IMPLANTS OFTEN FAIL

2.1.1 Metal implant corrosion


Corrosion is the major problem in the metallic implant material when they are subjected in human body plasma. Almost all metals experienced corrosion while in contact with the biological systems. The effects of various important elements (present in metallic bioimplant) on the human body when they are in contact with the biological systems is illustrated in Table 2.1. The various types of corrosion in bioimplant for various metal based materials is given in Table 2.2. Corrosion of a cardiac stent is seen in Fig. 2.1. Theoretically, a metallic implant's performance can be improved only if the discharge of metal ions is reduced in the most extreme environments of the body. This can be fulfilled by performing a suitable coating on the bioimplant by using suitable surface modification technique.

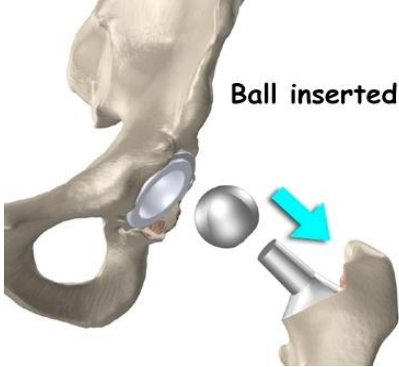


Table 2.1 Consequences for the host organism brought on by corrosion in the presence of metals in a wide variety of biomaterials (Bergant and Grum., 2009).

Various elements in biomaterials	Effects on the human body
Ni	Affects on the skin, such as dermatitis.
Co	Anemia B, a condition that prevents iron from being absorbed into the bloodstream.
Cr	It causes ulcers and neurological system problems.
Al	Effects on Epilepsy and Alzheimer's

Va Harmful even in its purest form

Table 2.2 Corrosion in implants (Bergant and Grum., 2009).

Corrosion type	Material	Location	shape
Pitting	304SS and Co- alloys	Ortho/ Dental-alloy	
Crevice	316 L-SS	Bone Plates in bones and Screws	
Stress corrosion cracking	316 L-SS and CoCrMo	<i>in vivo</i>	
Corrosion fatigue	316 L-SS and CoCrNiFe	Bone cement	

Fretting	Ti-Alloys	Ball joints	
Galvanic	304SS/316SS, Ti-Alloys or CoCrMo	Screws and nuts	
Selective Leaching	Mercury from gold	oral implants	

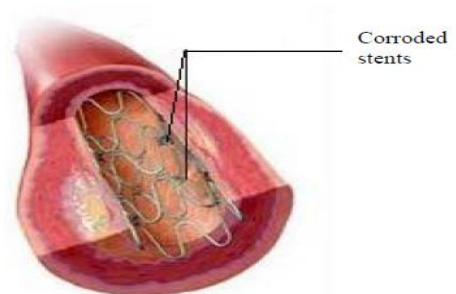
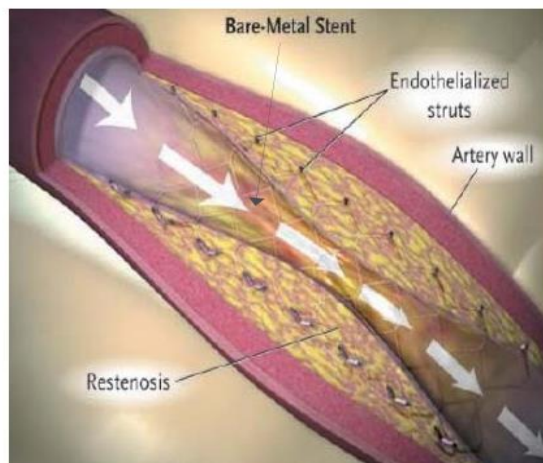


Fig. 2.1 Stent corrosion in bare metal (Bergant and Grum., 2009).

2.1.2 Wear of implants

There is the possibility of congruent and incongruent motion at mobile joints. The spherical head fits snugly within the cup-shaped socket is shown in Fig. 2.2. The incongruent type of joints (like the knee and ankle joints depicted in Fig. 2.3) created heterogeneous strains because of the contact of two hard incongruent surfaces. Fig. 2.4 is a flowchart depicting the connection between wear types and operation environments.

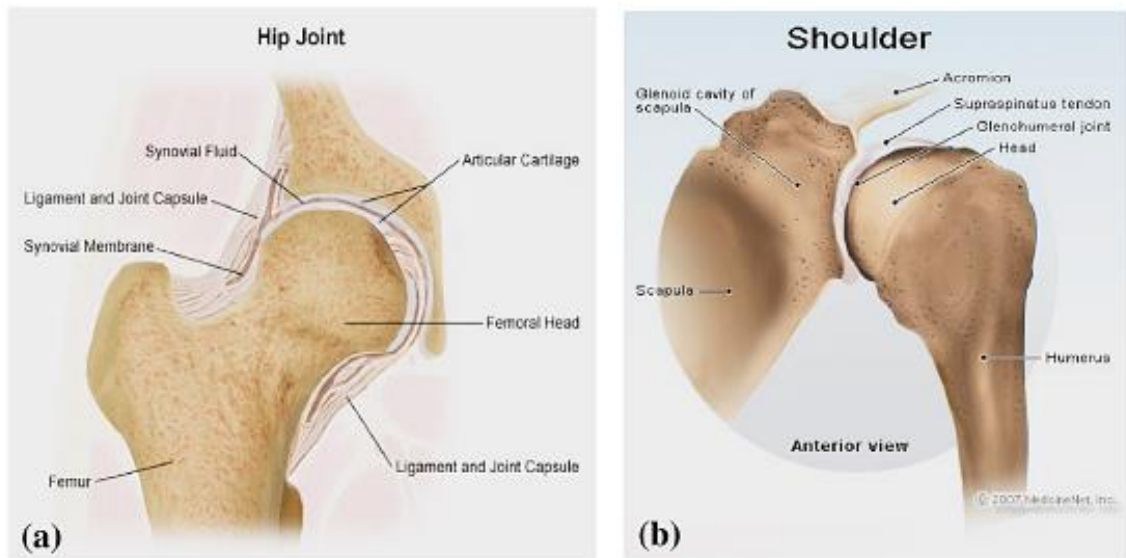


Fig. 2.2 Human joints are an example of congruency. places: (a) hip and (b) shoulder



Fig. 2.3 Human incongruent (a) artificial knee and ankle joints (b)

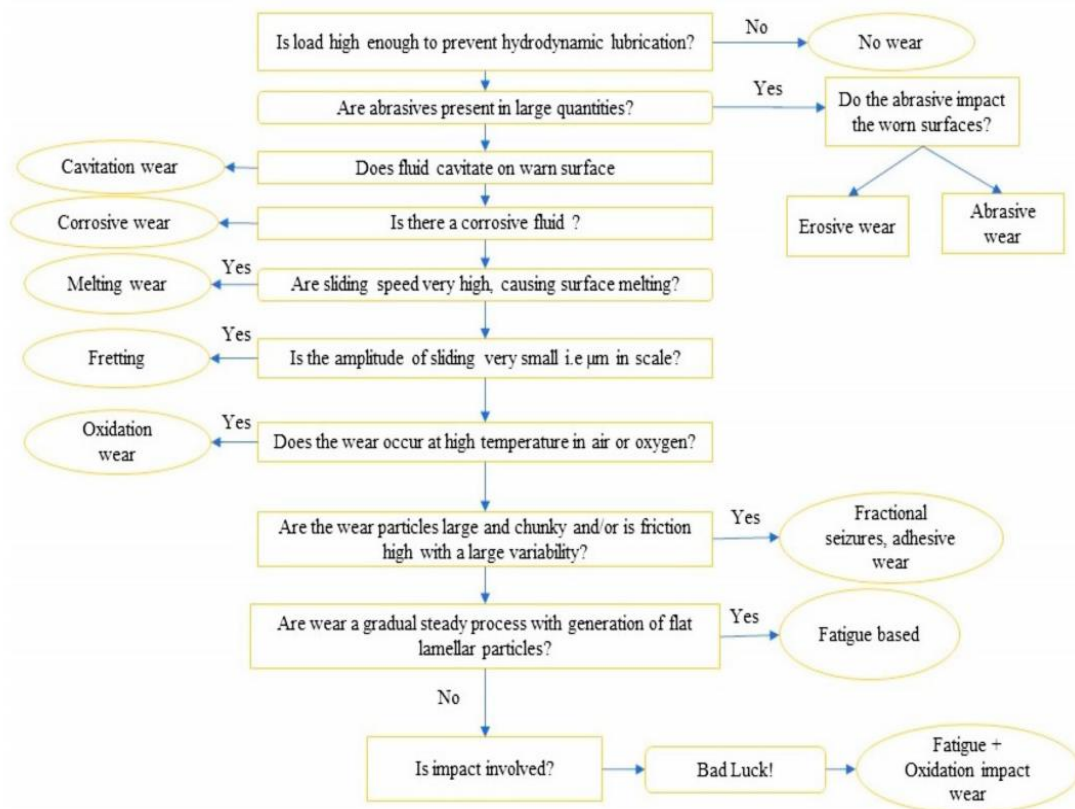


Fig.2.4 Relationship between wear kinds and operating circumstances presented in a flowchart (Bolelli et al., 2008a).

2.2 THE USE OF FAIL-SAFES TO REDUCE IMPLANT LOSSES

2.2.1 Systems of protection

Fig. 2.5 depicts the four main generations of prosthetic surface modifications throughout history. But scientists and doctors are looking for coating that promotes more robust bone growth or bio-function beyond that of HA with thermal spray.

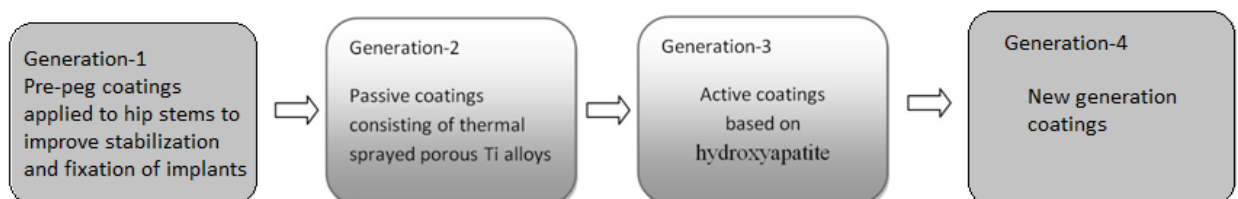


Fig. 2.5 Different coating generations for prosthesis surface modification.

Nonetheless, as shown in Table 2.2, various compositions of powders that may be deposited on surfaces using a number of thermal spray (TS) methods. As seen in Fig. 2.6,

HA has a crystal structure that is similar to that of other compounds in the same family. The structure of apatite is shown in Fig. 2.6. Although many surface modifications techniques used to process the HA on the metal based implant material. Currently, the Plasma spraying is well accepted commercially available procedures for fabricating HA based coatings on the implant devices because it delivers a homogeneous and relatively high density when compared to other coating processes as discussed above. In this technique, the bonding between particles was occurred by the impact of high velocity particles and rapid quenching of the partially-melted/ melted powder particles during the process. However, the coating produced by this method exhibited poor substrate/coatings adherence, and are a candidate to easy tear and wear. The easy wear and tear causes undesirable debris formation, which is generally not required for long term application of this coatings in biological environment. Further, this technique produces coating having irregular morphology with poor control of coating thickness. The other most widely used technique to produce bioactive coating on metallic bioimplant material is laser surface cladding. In metallurgic field, this technique has various advantageous like flexibility in the process, minimum surface preparation, good diffusion bonding with the substrate, and accuracy in the deposited coatings. However, the major limitations associated with this process is the high cost of operation associated with it (Vasudev et al., 2019). Recently the microwave cladding technique has been successfully utilized for surface modifications of various engineering components used for various applications. The ability of a material to absorb microwaves is dependent upon its loss tangent value. The internal heat generation inside the material due to absorption of microwave at atomic level causes significant improvement in mechanical properties of the engineering materials. The advantages associated with this technique is the low processing time and environment friendly phenomenon associated with this heating. Earlier, there is a misconception that bulk metallic materials cannot be processed using microwave energy because they are opaque to microwaves at room temperature due to the presence of electron cloud. Later, it has been reported that metal in powder form or bulk metal at a high temperature can be processed by utilizing microwave energy. This phenomenon has

led to the development of hybrid MH technique. The hybrid heating can be achieved either by employing an independent heat source such as an electric furnace or with the help of external susceptor. Later, this heat is transferred to material to be processed through a conventional way. This heating is a classical example of two-way directional microwave heating. In this heating, the specimen is heated by both mode of heating i.e. microwave-coupled external heating source and microwave heating. The research group at IIT Rookree first reported the feasibility of performing microwave cladding on the metallic material through hybrid MH technique by utilizing a micron-based powder in pure and composite form. Later, this technique was utilized for depositing the nano-based powder on the metallic material (Vasudev et al., 2019). Afterwards, the work involves the development of functionally graded cladding on metallic materials by utilizing this novel technique. The microwave induced clads exhibited improvement in tribological and mechanical properties.

Table 2.3 TS methods:

Material	Method	Thickness (μm)	Reference
Glass (bioactive)	HVSFS	10-15	(Bolelli et al., 2008b)
Hydroxyapatite	HVSFS	14-23	(Boulos et al., 2021)
Hardystonite	APS	15-18	(Calvarin et al., 2000)
Bioactive glass	HVSFS	20-50	(Campo et al., 2009)
Tricalcium phosphate	HVSFS	20-25	(Bolelli et al., 2008b)
Hydroxyapatite	HVSFS	27-37	(Chatha et al., 2013)
Hydroxyapatite	APS	30-40	(Chatha et al., 2016)
Bioactive glass	SPS	<50	(Campo et al., 2009)
Hydroxyapatite	APS	50	(Chatterjee et al., 2001)
Hydroxyapatite/titanium composite	APS	80	(Ctibor et al., 2006)

HA/ β TCP composite	APS	80-90	(Daram, P. and Banjongprasert, C.,2020)
Wollastonite	FS	100-150	(Davis, J.R. ed., 2004)
Baghdadite	APS	120	(Deb et al., 1996)
Diopside	APS	200-300	(Dehnavi et al., 2017)
Dicalcium silicate	APS	380	(Delaunay et al.,2000)
HA and HA/TiO ₂	HVFS	135 for HA, 140for HA/TiO ₂	(Deng et al., 2012a)
HA + 10 wt% Al ₂ O ₃ HA + 10 wt% ZrO ₂	VPS	-	(Deng et al., 2012b)

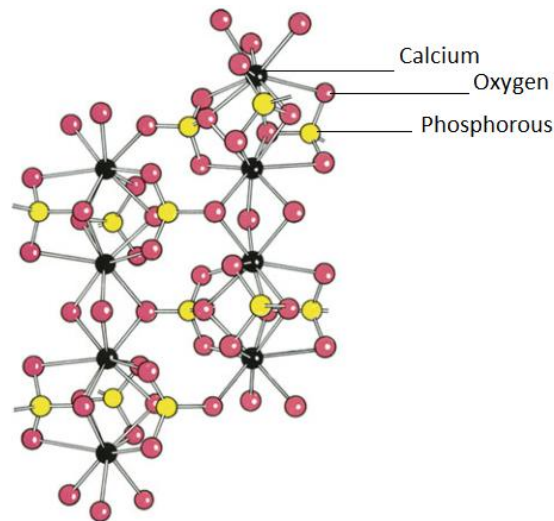


Fig. 2.6 HA fluorapatite crystal structure (Dooley and Wiertel., 2009).

A common practice in the field of biomaterials is to use austenitic stainless steels (SS), specifically for the construction of internal fixation devices used in orthopaedic procedures (Disegi et al., 2001). Reports indicate that the corrosion resistance of stainless steel is much inferior than that of titanium and titanium alloys. Its low cost and excellent mechanical properties make it ideal for temporary applications such bone plates, screws, spinal traction, and related medical procedures (Afonso at al., 2008; Chen et al., 2015). Researchers have investigated many types of stainless steels, such as Rex-734, P558,

ASTM F2581, and UNS S31254, to determine their suitability for orthopaedic applications (Afonso et al., 2015; Dziubinska et al., 2018; Salahinejad et al., 2013; Jaimes et al., 2010). The austenitic stainless steel, UNS S31254 (254 SS), is a medical-grade material that exhibits non-cytotoxic properties, exceptional mechanical strength, and toughness (Micheli et al., 1999; Meguid et al., 2007; Das et al., 2017). Furthermore, it exhibits a robust resistance to pitting corrosion when exposed to chloride and phosphoric conditions.

Then the functionality of the stainless-steel surgical grades and other materials such as Mg and Ti-based alloys have been modified by using HA and HA-based coatings. Due to their limited capacity to endure load-bearing functions, metallic biomaterials with inadequate adhesion between the coating and the substrate are unsuitable for use in such applications. In the past, many methods have been used to apply bioactive coatings onto metallic biomaterials. One of these procedures involves the application of a HA coating. Over time, several procedures were developed to enhance the adhesive strength of the substrates and increase their dependability. The insufficient bonding strength between the coating and the metallic biocompatible substrate is often seen as a significant concern because of their interconnection (Subash et al., 2022; Sun et al., 2002). The range of numbers is from 41 to 43. If the covering fails to adhere to the implant properly, the implant and the surrounding tissues may be exposed to the detrimental effects induced by the loose particles. Infectious illness is a possible result. HA coatings are placed on metallic biocompatible substrates to maintain the mechanical behaviour of the substrate, namely its load-bearing capacity. This is done to ensure the ongoing biocompatibility of HA (Thompson et al., 2015).

Furthermore, HA is also compatible with living organisms. The mechanical properties of metallic biocompatible substrates, including their ability to endure stresses, remain intact after the application of a hydroxyapatite (HA) coating onto the substrate. To guarantee HA's biocompatibility is maintained, this action is taken. HA's biocompatibility stems from its chemical composition, which closely resembles that of human bone, including substantial amounts of calcium and phosphorus (Vladescu et al., 2018; Vladislavic et al.,

2021). This may confer certain advantages to metallic implants, such as improving their ability to adhere to the surrounding tissue and maybe offering additional benefits.

2.3 RESEARCH GAP

The following conclusions have been made after doing an exhaustive review on the biomedical implants developed using different surface modification techniques:

1. From above discussion, it has been found that the microwave energy has extensively utilized for processing of metallic materials. The basic reason behind the selection of microwave cladding process for modify the surface properties of metallic materials is that development of bio-implant coating using a thermal spray process has its own limitations such as high porosity, poor mechanical anchorage between splats, residual stresses and non-uniform coating microstructure.
2. On the other hand, the potential of microwave heating for the deposition of the pure HA coatings on metallic bio-implant has not been investigated till now.
3. From the above literature study, it has been found that the microwave was explored sufficiently as discussed in the above section.
4. Further, as per the detailed literature study, it has been found that microwave clad specimen exhibits superior mechanical properties than thermal spray and laser clad specimens (Vasudev et al., 2019). The pure HA and reinforced HA (HA+10wt%Al₂O₃ and HA+10wt%Zr₂O₃) coatings on the metallic bio-implant is an advanced area.
5. The detailed data on the structure-property-correlation of bio-implant coatings provide the new solution to provide superior mechanical and biocompatibility properties to the metallic bio-implant.

2.4 RESEARCH OBJECTIVES

1. To develop Hydroxyapatite (HA), (HA+10wt%Al₂O₃ and HA+10wt%Zr₂O₃) coatings on the surgical grade stainless steel using the principles of microwave hybrid heating (MHH) technique.

2. To examine the as-cladded and post treated composite claddings for comparison in terms of mechanical and micro-structural characteristics.
3. To understand the physics of the microwave cladding process using a detailed study of the microstructure, temperature profiles and mechanical properties of the clad and relating with other process parameters.
4. To characterize the as-sprayed and post heat-treated coatings through Mechanical, Metallurgical and Functional techniques that involve in-vitro corrosion analysis and in-vitro bioactivity analysis of the deposited cladding in Hank's balanced salt solution (HBSS).

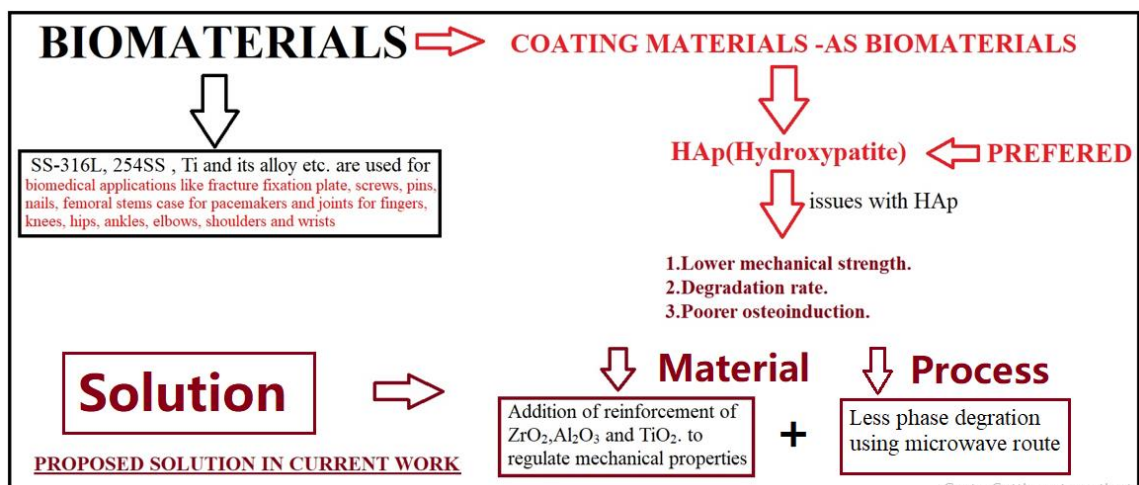


Fig.2.7 Problem formulation outlined in the current research work.

2.5 SUMMARY

A brief discussion on the implant corrosion has been presented. The capabilities of different existing cladding/coating techniques based on the requirements was elaborated and the limitations of such techniques have also been discussed. The use of microwave cladding has several benefits in the field of surface engineering. An important advantage is the decreased manufacturing cost and shorter processing duration in comparison to other cladding methods. In addition, it generates cladding materials without any porosity and thermal distortion at the molecular level, leading to enhanced tribological and mechanical characteristics in the produced clads. Brief discussions on

microwaves, interaction of microwave with materials and hybrid heating technique have been discussed. Experts provide comprehensive reports on the use of microwaves in the treatment of metals. It has been investigated there is a lack of literature on the application of microwave in biomedical field. It was observed that many major limitations of existing cladding/ coating processes can be overcome by using microwave as a heating source. The gaps observed in the literature indicate that the potential of microwave heating for the deposition of the pure HA and reinforced HA (HA+10wt%Al₂O₃ and HA+10wt%ZrO₂) coatings on metallic bio-implant has not been investigated till now. The problem formulated and research plan is presented in **Fig. 2.7.** and **Fig.2.8,** respectively.

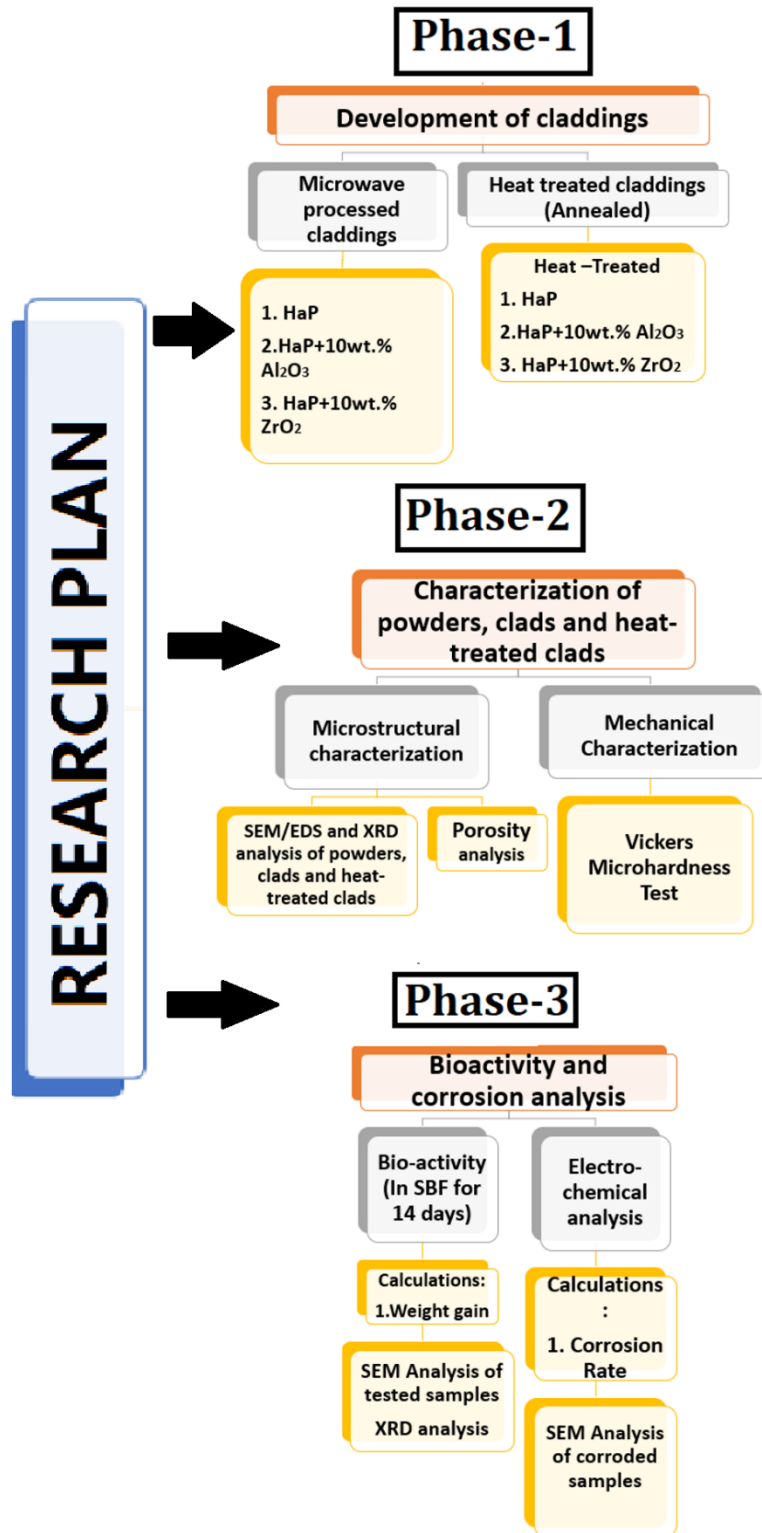


Fig. 2.7 The research plan and Research problem.

Chapter 3

EXPERIMENTAL EQUIPMENTS AND METHODOLOGY

The method of surface modifications, as well as the process parameters of the apparatus employed to modify the surface layer of SS-31254 with HA, HA+10wt% Al₂O₃, and HA+10wt% ZrO₂ are described in this chapter. The procedure for performing the different heat treatment of the as-deposited surface modified specimens has been discussed. The instruments/tools utilized to characterize uncoated and coated samples at different stages of the research effort have been detailed. Microstructures were characterised with scanning electron microscopy/energy dispersive X-ray spectroscopy. X-ray diffraction apparatus was used for the samples to characterize the products formed on the surface during studies. The various characterization techniques used to evaluate the performance of the cladding for the analysis of in-vitro and corrosion products formed during various tests have also been explained in this chapter.

3.1 SUBSTRATE PREPARATION

Commercially available stainless-steel surgical grade (254SS) procured from Amigo Impex, Mumbai, India was utilized as a substrate material for modifying its surface layer in this research work. The chemical compositions (wt%) of 254SS as measured by spark emission spectrometer is given as: 17.71Ni, 19.39Cr, 6.24Mo, 0.207N, 0.52Si, 0.018C, 0.004S, 0.017P, bal Fe. For the surface modifications of the SS-31254, there is a requirement of specimens having various sizes like 20×20×3 mm³ for XRD and SEM analysis, 25×25×3 mm³ for corrosion investigations, and 10×15×3 mm³ for in-vitro biocompatible study. The specimens of required dimensions were cut through by utilizing a wire electric discharge machining apparatus as illustrated in Fig. 3.1 from the SS-254 sheet having dimensions approximately 180 × 200 mm² with 3 mm thickness. Then the smoothing of the cut specimens was done by using an emery paper of different grades like 200, 400, 600, 800, 1000, 2000 etc. The specimens having dimensions 20

mm×20 mm× 3mm were used for modifying its surface layer by hybrid MH technique. Before performing experiments, the SS-31254 substrates were ultrasonically cleaned in acetone for about 30 min and further hot air dried. HA powder having purity > 95% was supplied by Plasma Biotel Pvt. Ltd. The Al₂O₃ powder was procured from the H C starck, Germany. The ZrO₂ powder was purchased from the Intelligent Materials Pvt. Ltd., India.

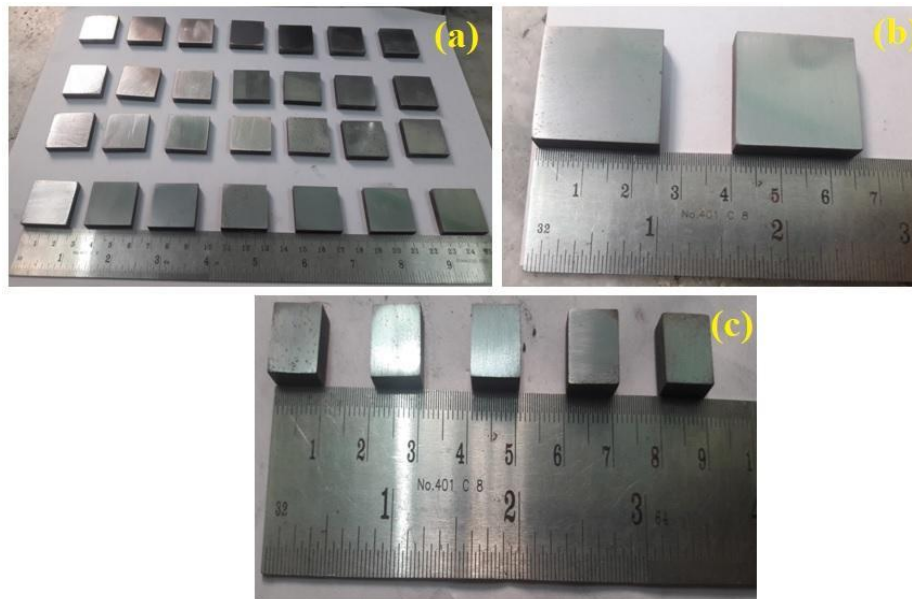


Fig. 3.1 Specimens for various sizes for (a) XRD and SEM analysis, (b) corrosion study, and (c) invitro bioactive study.

3.2. CLADDING POWDER

Three distinct powder combinations containing HA, aluminium oxide (Al₂O₃) and zirconium oxide (ZrO₂) were fabricated on SS-31254 substrate with hybrid MH technique. The first combination is pure HA, then 10 wt% of Al₂O₃ as blended with HA in the second combination, which is termed as HA10AL. A 10 wt% of ZrO₂ as blended with HA, which is termed as HA10ZR. The 10% weight proportions of the hard particles are considered as optimum proportions of the reinforcement in the HA powder. The mixing was performed by using a conventional lathe apparatus as shown in Fig. 3.2. The powder was weighted initially to mix in a defined proportion and then mixed in a

container for 6 hours for uniform mixing. The HA powder was kept 90 wt.% and 10wt.% of Al_2O_3 and another coating composition was composed of 90 wt.% HA and 10wt.% of ZrO_2 . The selection of this 10 wt% combination is based on previous study findings by Li et al. 2002 and Morks et al. 2008, which indicate that increasing the reinforcement content in HA coatings beyond 10 wt% adversely affects certain mechanical characteristics. In addition, Chang et al. 1997, conducted a study on the impact of adding ZrO_2 -8mol % yttria as a secondary component in plasma sprayed HA coatings with varying weight percentages. They discovered that introducing 10 wt% ZrO_2 in HA resulted in a substantial enhancement in bond strength.



Fig. 3.2 Mixing of powder (90wt% HA and 10wt% ZrO_2) on lathe machine.

The methodology adopted in the present research work has been mentioned in Fig.3.3. The work was divided into three phases, where the claddings were developed in the first phase followed by post-treatment of claddings. In the second phase, the powders, claddings and post-treated claddings were characterized for micro-structural and mechanical analysis. In the last phase of the work, the developed claddings and post-treated claddings were subjected to bio-activity and corrosion analysis followed by micro-structural characterization and phase-identification using XRD analysis.

Methodology adopted in the present research work.

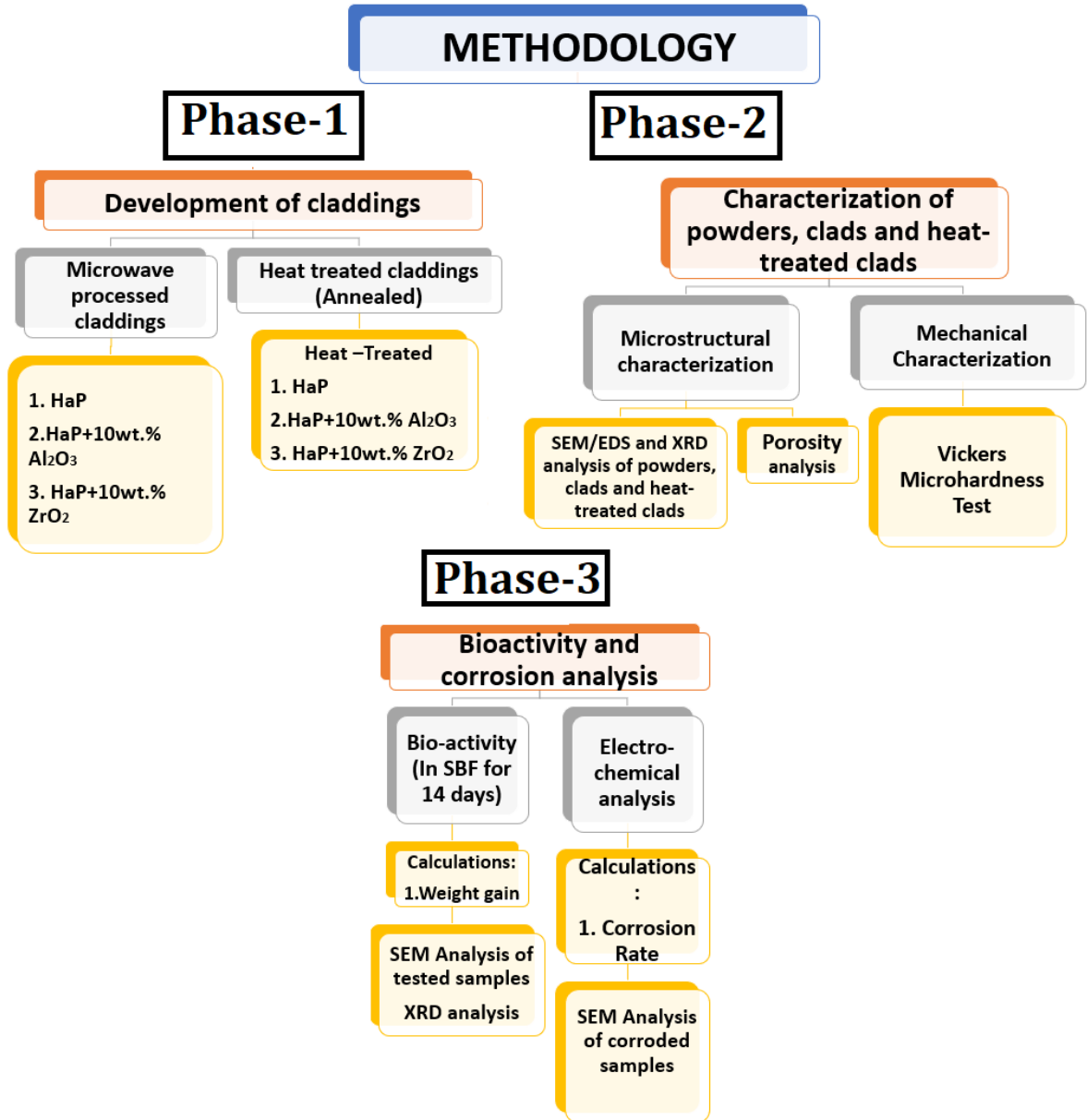


Fig.3.3. Methodology adopted in the research work

3.3 SURFACE MODIFICATION THROUGH HYBRID MH

The microwave source utilized in this work for surface modification of the SS-31254 through pure HA, HA10AL and HA10ZR was an industrial microwave oven

(make: VB-ceramics, Chennai). The following claddings were developed in the current investigation as mentioned in Table.3.1.

Table 3.1 Clads used in the current investigation

S.No	Coatings	Designation System
1.	HA	HA
2.	HA +Al ₂ O ₃	HA10AL
3.	HA +ZrO ₂	HA10ZR
4.	HA	HA at 700 °C heat-treated condition
5.	HA +Al ₂ O ₃	HA10AL at 700 °C heat-treated condition
6.	HA +ZrO ₂	HA10ZR at 700 °C heat-treated condition

The equipment was equipped with an infrared pyrometer (Make: Raytek; Model: RAYXRTG%SFA) for the online temperature control measurement of the susceptor during trials. The oven operates at a fixed frequency of 2.45GHz and power of 1.1 kW. The HA powder was manually preplaced on the polished and clean SS-31254 coupons maintaining a uniform thickness of the precursor around 400 µm. To obtain a uniform thickness on the substrate material, a computer-controlled spindle along with a glass slide was used. The HA powder being a ceramic material cannot be directly deposited on SS-31254 with microwave heating, because it is transparent to microwave at room temperature. The material behaviour with microwave can be predicted by knowing its dielectric properties. The radiation enters these objects and exits with the same incident energy as when it entered. When the incident power is decreased by half due to absorption, that's the depth into the material in known as penetration depth. The details about the penetration depth for transparent material (ceramics) is explained elsewhere (Kaushal et al. 2018 and Marcelo et al. 2010). At room temperature and 2.45 GHz, the HA powder used in this research is microwave-transparent (Marcelo et al. 2010). It has been reported, though, that at some critical temperature, owing to an increase in loss tangent value with temperature, transparent materials will begin absorbing microwave

radiation. Therefore, the SS-31254 alloy base material was modified on its surface using the concept of hybrid MH as described by many authors. Using the concept of the hybrid MH technique, Fig. 3.4 depicts the setup used to modify the SS-31254 alloy's surface (Bansal et al. 2017). The boron carbide was used as susceptor material to provide initial heating to the HA powder by direct coupling with microwave radiation at room temperature. In order to keep the HA powder from coming into touch with the susceptor, a zirconia plate of around 500 μm thickness was introduced between them. The microwave radiation emitted from the waveguide is directly absorbed by susceptor and the susceptor uses conventional heat transmission to bring the bioactive HA powder to its critical temperature. Afterwards, the HA powder itself starts absorbing microwave radiation because of its increase in loss tangent value with an increase in temperature. The HA powder temperature rises and the base material (SS31254) in the vicinity with HA powder was also heated up and consequently the substrate surface layer is also melted. A molten pool is created on the metallic substrate surface and melted HA powders were mixed in the molten substrate layer. The melting temperature of HA was around 1670 $^{\circ}\text{C}$ and the melting point of the base material was in the range of (1375-1400 $^{\circ}\text{C}$). As a result, the substrate's top layer melted completely alongside the HA powder. At elevated temperatures, the substrate components and the bioactive HA granules diffuse together. Rapid quenching of the melted composite mixture was occurred as the power is switched off. The base metal having high thermal conductivity act as a heat sink for the deposition of the composite clad layer on it. Therefore, the composite layer having diffusion bonding with the substrate is achieved. The microwave cladding is Based on trial and run-based approach. Initially, the samples were tried with various trails and time was noticed for the each change occurred in the cladded samples. The observation noticed during the cladding process has been mentioned in the remarks as shown in Table.3.2. The microwave processing parameters were optimized by varying the exposure time for a fixed power 1.1 kW and sample size ($10\times 10\times 3\text{ mm}^3$). The effect of exposure time for a fixed set of parameters (power: constant; sample size: same) on the microwave surface modification of SS31254 alloy is illustrated in Table 3.2. The final

optimized parameters were depicted in Table. 3.3. Since it is currently not feasible to precisely measure the temperature at the molten composite layer, an infrared pyrometer was used to track the temperature of the boron carbide's upper surface (susceptor) throughout the experiment. However, owing to process, the temperature at the molten composite layer was higher than the observed temperature. The same procedure is adopted for the other two combination of claddings.

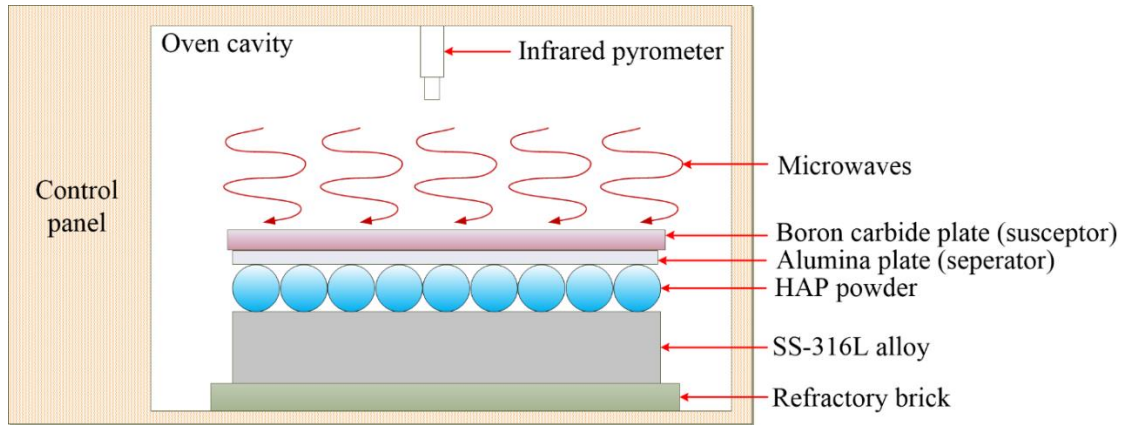


Fig. 3.4 Schematic of setup for cladding (Bansal et al. 2017).

Table 3.2 Effect of exposure time for a fixed set of parameters (power: constant; sample size: same).

Sample No.	Exposure time (Min)	Observed temp (°C)	Remarks
01	10	800	There was no evidence of the clad substance melting.
02	13	900	It was noticed that the clad powder partially melted, but no bonding occurred with the base.
03	15	1050	Through a diffusion process, bioactive HA was effectively incorporated into the SS-31254 alloy layer.
04	18	1110	There is a complete melting of the substrate along with powder was observed. A deformed specimen was formed.

Table 3.3 The optimized parameters for modify the surface layer with pure HA claddings.

Parameters	Range
------------	-------

Power	1.1 kW
Exposure time	15 min
Frequency	2.45 GHz

3.4 HEAT-TREATMENT OF CLADS

Large-scale breakdown of the phases within the body leads to a loss of structural integrity, mechanical strength, and adhesion strength. Concrete annealing, a sort of heat treatment, has been backed as an effective way to improve cladding performance by a number of studies (He et al., 2001). Therefore, the surface modified samples at all conditions were exposed to post heat-treatment in a muffle furnace for 2 hours (heating rate 20°C/min) at 700°C to study how heat treatment affects the changed layer's microstructure, mechanical properties, and bioactivity.

3.5 METALLURGICAL CHARACTERIZATIONS OF THE CLADS

Low speed diamond saw sections were used to cut through the thickness of the microwave generated clad specimens, and the specimens were then cold mounted in epoxy to compare the differences between the as-deposited and heat-treated conditions. Cold mounting or embedding is the process of combining a resin with a hardener (or accelerator) to create the mounting compound, followed by the polymerization process to form the block. The specimen which are sensitive to heat as well as pressure are generally prefer cold mounting. Emery sheets of varying grits were used to smooth and shine the cold-mounted specimens. Figure 3.5 displays optical images of the cold mounted polished samples.



Fig. 3.5 Sample after Cold Mounting and Polishing

Microwave-included clads specimens were characterised by using number of characterisation tools. The following section briefly explains the procedures and equipment used in the metallurgical characterization of microwave clad and heat-treated specimens.

3.5.1 X-Ray Diffraction (XRD) Analysis

The XRD were used to determine the various phases present in both the clad powder and the microwave-induced clad specimens under as-deposited and different heat treatment scenarios. Analysis of the phases generated on the surface of the clad and heat-treated specimens, as well as the feedstock power, was performed using the XRD patterns acquired by the XRD machine. The X-ray diffraction (XRD) measurements were taken using a Bruker AXS diffractometer with $1^\circ/\text{min}$ and a step range (2θ range) of 10° - 100° . Cu-K α radiation at 40 mA and 40 kV was used to perform the XRD. Appendix A provides information about the X-ray diffraction (XRD) facility that was used for the present research work (Fig. A-1).

3.5.2 Microstructural characterizations of clads

The microstructural features in the surface modified samples such as grain boundaries, and grain size were revealed by analysing images taken on the optical microscope. Kroll's reagent was used to etch the polished samples for taking images in optical microscopes supported with imaging software. The composition of the typical Kroll's reagent used in the present study is illustrated in Table 3.4.

Table 3.4 Kroll's reagent etchant composition.

Composition	In mL
Distilled water	92
HNO ₃	6
HF	2

3.5.3 Microstructural characterizations of the microwave induced clad specimens at various heat treated conditions

Morphologies of both as-deposited and heat-treated specimens were examined with a 15kV field emission scanning electron microscopy (FE-SEM). All specimens were initially silver pasted between the samples and stub for having conductivity thereafter, gold coated for obtaining elemental-maps for the top of the surface (as-deposited and heat-treated) and across the cross-section of the cladding. The energy dispersive spectroscopy (EDS) analysis provides the elemental compositions (weight %) at the selected region. Samples were prepared as per procedure given in section 3.4 for the cross-section analysis of the samples before and after the testing. The SEM micrographs at different magnifications were taken along with the point and line scans. EDS analysis was performed for the elemental composition at different regions of substrate, as clad, and heat treated samples. SEM/EDS analysis of the substrate, as clad, and heat treated specimens has been reported in Chapter 4 of the current research work study.

3.5.4 Measurement of Cladding Thickness

During the microwave assisted surface modification process, the thickness was measured with a thickness gauge designed for thin films (Version: Minitest 2000; Manufacturer: Elektro-Physik Koln Company, Germany) with a precision of $\pm 1\mu\text{m}$. The thickness measurements were further confirmed by mounting and sectioning the deposited claddings according to the process outlined in section 3.5. The SEM/EDAX techniques was used for obtaining the cross-sectional back scattered electron (BSE) images by which the approximate thickness of the modify layer can be determined.

Appendix-A contains a detailed description of the SEM apparatus (Fig. A-3). The average thickness of the deposited coating was calculated and observed using BSE images and same is presented in detailed in chapter 4 of the present research work.

3.5.5 Porosity measurement for the clads.

The as-deposited and heat-treated surface modified samples were polished prior to the measurement of porosity. The both samples were polished down to emery papers of 1200 grit size for porosity measurement. This involved the measurement of porosity on Dewinter inverted optical microscope (Model: LT-2B, Make: Chennai Metco Pvt. Ltd, Chennai, India) using STM B276 imaging software (Dewinter Material Plus, Version 4.2). The detail of the Dewinter inverted optical microscope is presented in Appendix A (Fig. A-2). Ten values of porosity were taken and their averages have been reported. The porosity values of the deposited coatings in both conditions (as-deposited and heat-treated) for all the samples are the average of the ten measurements and are given in Chapter 4 of the current research study.

3.6 MECHANICAL CHARACTERIZATIONS OF THE MICROWAVE INDUCED CLAD SPECIMENS AT VARIOUS HEAT TREATED CONDITIONS.

The evaluation of mechanical properties was carried out in terms of microhardness. Details are explained in the following subsections.

3.6.1 Measurement of Micro-hardness

The micro-hardness of the both (as-deposited and heat-treated surface modified specimens) samples were obtained by utilizing a Vickers's micro-hardness tester at 50 g load with load with a dwell period of 10 s. The detail of Vickers's micro-hardness tester used in the present investigation is presented in Appendix A (Fig. A-4). Micro-hardness was measured in layers of both as-deposited and heat-treated clad specimens. Ten indentations were made over the coating's cross-section at two separate points; five indentations were made along the layer thickness at each point (primary matrix as well as other secondary phases). Finally, their average values are reported and the distribution of

micro-hardness values for clad specimens at various conditions is presented in chapter 4 of the current study.

3.7 FUNCTIONAL CHARACTERIZATIONS OF THE SPECIMENS

The functional evaluation is what ultimately establishes the sample's functional performance after being processed. Accordingly, aspects of specimens were evaluated using in-vitro biocompatibility study and corrosion testing. The procedure and details of functional characterizations of the specimens are explained in the following sections.

3.7.1 In-vitro biocompatibility study

The as-sprayed and heat-treated surface modified samples were tested for bioactivity in vitro with a synthetic body fluid (SBF) model (Tiwari et al., 2021). The SBF had an electrical profile that was very close to that of human plasma. Used SBF had characteristics not dissimilar from human plasma. The SBF solution was prepared by dissolving the reagent grade ingredients in distilled water (700 ml) according to the following proportions: NaHCO_3 (0.35g), NaCl (8.03g), KCl (0.26g), $\text{MgCl}_2 \cdot 6\text{H}_2\text{O}$ (0.32 g), $\text{K}_2\text{HPO}_4 \cdot 3\text{H}_2\text{O}$ (0.23g), CaCl_2 (0.3 g) and Na_2SO_4 (0.07g). The microwave induced modified SS-31254 alloy samples along with unmodified SS-31254 alloy were thoroughly cleaned in acetone and dried in hot air, before carrying out the immersion test. The in-vitro assays were carried out by soaking the samples in the 40 mL SBF solution in plastic containers. The plastic receptacles underwent a 24-hour cycle of sterilisation in an autoclave at 100 degrees Celsius and 10 atmospheres of pressure. This process helps to remove the bacteria and other living microorganisms. The experimental setup of autoclave machine established at NIT, Jalandhar as shown in Fig. 3.6. The plastic flasks were then placed in a rotating incubator set to 72 rpm, where they remained without any solution changes. The container was maintained at 37 degrees Celsius throughout the soaking period. The samples following the completion of the soaking periods were dried in a vacuum desiccator for 15 h. The experimental setup of incubator machine established

at NIT, Jalandhar as shown in Fig. 3.7. Any weight loss or increase caused by soaking in the SBF solution was analysed by comparing the subjects' starting and ending weights. The FESEM equipped with EDS at LPU Phagwara was utilized to observe the formation of apatite on modified and unmodified SS-31254 alloy samples. The results are illustrated in Chapter 5.



Fig. 3.6 Experimental Setup of Autoclave vertical machine



Fig. 3.7: Experimental Setup of Incubator

3.7.2 Corrosion behaviour the microwave induced clad specimens at various heat treated conditions

Corrosion is generally initiated from the surface of material by the interaction of environment at the surface. The electrochemical reactions act as a catalyst for a corrosion to occur on the surface/ sub-surface of the material. Thus, the electrochemical testing is best for investigation of the corrosion mechanism.

For performing electrochemical study, the main requirement of the tested sample is that it must be electrical conductors and further size of the sample is small enough (few square centimeters) to be properly fitted in the Gamry instrument for the metal in a corrosive environment. There are three electrode configuration used in Gamry instrument for performing the corrosion testing. The all electrodes used for studying the corrosion behaviour are immersed into the solution, and they are joined to an appliance called potentiostat. The electrolytic solution used in the study has closely resembles with the actual application environment of the specimen being tested. As an added bonus, a potentiostat may be used by adjusting the potential of the metal sample to the required level. The density of the corrosion current (I_{corr}) at the corrosion potential may be calculated using this setup (E_{corr}). Electrochemistry allows for the assessment of several corrosion occurrences. Both base metal and as-deposited clad specimens and specimens treated through various heat treatment conditions were subjected to an electrochemical corrosion test in the current investigation. The corrosion behaviour of the microwave-assisted surface-modified specimens was studied using an electrochemical test, and its schematic construction is depicted in Figure 3.8. The standard calomel electrode (SCE) was used as a primary reference electrode against which all other potentials were measured. A rod of pure graphite served as the counter electrode. In this investigation, a functional electrode with a corrosive area of 1.5836 cm^2 was constructed using microwave aided surface modified specimens under both as-deposited and heat-treated circumstances. The epoxy insulation ensured that only the working portion of the clad specimen was exposed to the corrosive conditions of the electrochemical research. The clad specimen was prepared for electrochemical testing by first being polished with emery sheets ranging in grit size from 200 to 1000, then being cleaned with an ultrasonic cleaner, and lastly being hot-dried with air. For the purpose of studying specimens under

various settings, a potentiodynamic polarisation curve was drawn while the experiments were conducted in a 3.5 wt% NaCl solution at room temperature. The potentiodynamic polarisations test is conducted using a computer running the DC105 Gamry electrochemical programme and a Potentiostat/ Galvanostat (Series G-750; Gamry Instruments, War-Minster, PA). During the electrochemical tests, the potential was varied from -500 mV to 1500 mV against E_{corr} . Using a potentiostat with a scan rate of 1 mV/sec, the electrode potential was maintained within 1 mV of a preset value over a broad range of applied current. The experiments were performed using a fresh solution for each experiment and testing were carried out at ambient temperature. The procedure for performing experiments using Gamry Instrument is as follows:

- a) Green–Blue: Working and Working Sense, connected together. A black cable was attached to the connection point, referred to from here on as Black. This is the conventional-positive electrode. The black cable was connected to the counter electrode (i.e. the anode in the electrochemical test set up).
- b) Red–White: Counter and reference electrodes were also connected together. A red cable was attached to the connection point, referred to from here on as Red. This is the conventional —counter|| or —negativell electrode.

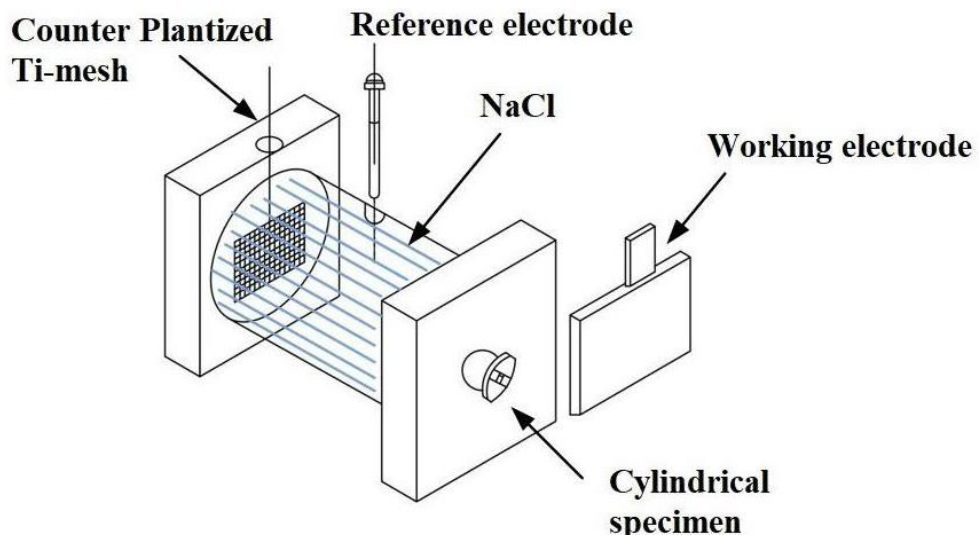


Fig 3.8: Corrosion testing apparatus.

3.8 TAFEL PLOT EXPERIMENT

The electrochemical study was performed by utilizing a Tafel extrapolation method. To ensure the repeatability of the test results, the electrochemical corrosion study was done on three clad samples for each condition (as-deposited and heat-treated). The Tafel extrapolation method is based on mixed-potential theory for determining the corrosion rate of samples. The data captured from anodic or cathodic polarization measurement were used in a mixed-potential theory. Further, during electrochemical study, the cathodic polarization data are generally taken because these data are easier to assess using an experimental method. A schematic construction for performing a cathodic polarization measurement is shown in Fig. 3.9. The sample, whose corrosion rate is to be measured served as a working electrode (W.E.), and cathodic current was provided to it by means of an auxiliary electrode which is generally made from inert material such as platinum or graphite. The current in the experimental process was measured by means of an ammeter *A*, and the potential of the clad specimens was measured with respect to a reference electrode by a potentiometer-electrometer circuit. The results obtained during the cathodic polarization of clad specimens in an SBF solution. An indicator voltmeter shows the corrosion potential of the clad specimen being tested in relation to the reference calomel electrode before the cathodic current is applied. It is possible to plot the electrode's potential vs the logarithm of the applied current by doing the following: E vs $\log i$. Extrapolating to the corrosion potential (E_{corr}), tangents were drawn on the $\log i$ versus E graph, meeting at a single point. This X-axis value represents the current corrosion (I_{corr}). Log axes are used in corrosion experiments to show a wide range of current values. Passivity causes a six-fold shift in corrosion experiment current. After electrochemical analysis, the microstructure was analysed.

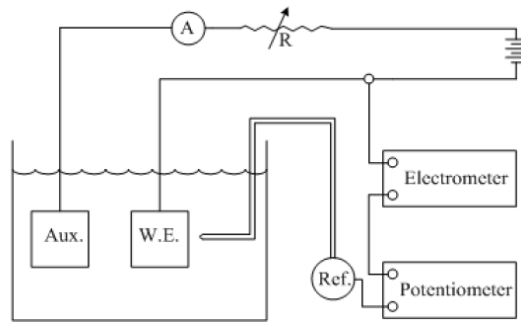


Fig. 3.9 Schematic illustration of the electric circuit for cathodic polarization measurement.

3.9 SUMMARY

A detailed description of the various steps in the microwave assisted surface modifications by using hybrid MH was discussed. Heating the samples that have had their surfaces treated by a microwave has been characterised as being crucial under all circumstances. The properties of clad and heat-treated specimens are determined with the use of a variety of metallurgical and mechanical characterization instruments and techniques, which are discussed in detail in this chapter. Samples with their surfaces transformed by microwaves have had their corrosion resistance and in-vitro properties reviewed at length, along with the methods and conditions used to evaluate these attributes.

Chapter 4

Characterization of Feed stock and claddings

In the present work, the concept of hybrid MH was utilized as a heat source for depositing HA, HA10AL, and HA10ZR based cladding on the SS-31254 substrate surfaces. The inherent attributes of hybrid MH are uniform and volumetric heating which resulted in the reduced thermal gradient, and less residual stresses in the surface modified clad microstructure while compared to the other thermal processes. To further enhance its microstructural and mechanical capabilities, the as-deposited samples were subjected to various heat treatment to decrease porosity and densify the clad microstructure. The as-deposited and heat-treated surface modified specimens are characterised (metallurgical and mechanical characteristics) using a variety of characterisation techniques discussed in this chapter. SEM/EDS tools were used for the microstructural and elemental analysis of the as-deposited and heat-treated clad microstructure. The micro-hardness of all the specimens at all conditions was evaluated along the cross-sectional direction and porosity along the cross-sectional direction is also reported in the present chapter. The presented results are discussed with regard to the available literature.

4.1 SEM/EDS AND XRD ANALYSIS OF FEED STOCK POWDERS

The feedstock powders (HA, Al₂O₃ and ZrO₂) were characterized by examining X-ray diffraction, and SEM/EDS analysis.

4.1.1 SEM/EDS and XRD analysis of HA powder

The SEM-EDS and XRD analysis techniques were adopted for the characterization of feedstock, cladding and Heat-treated cladding (Tiwari et al., 2021). The HA powders had a typical spherical morphology with an average particle size was close to 35 μm as illustrated in SEM micrograph in Fig. 4.1 (a). Secondary electron SEM pictures of powder particles were examined in Image J analysis software to measure the average diameter of the HA powder. As can be seen in Fig. 4.1, the bioactive HA powder

contains significant amounts of Ca, P, and O, as shown by the elemental study of the powder performed by using EDS equipped with SEM as seen in Fig. 4.1 (b). Fig. 4.2 illustrates the XRD spectrum of HA powder. The HA powder's XRD spectrum clearly shows HA peaks and no other phases, suggesting it is mostly pure without any impurity.

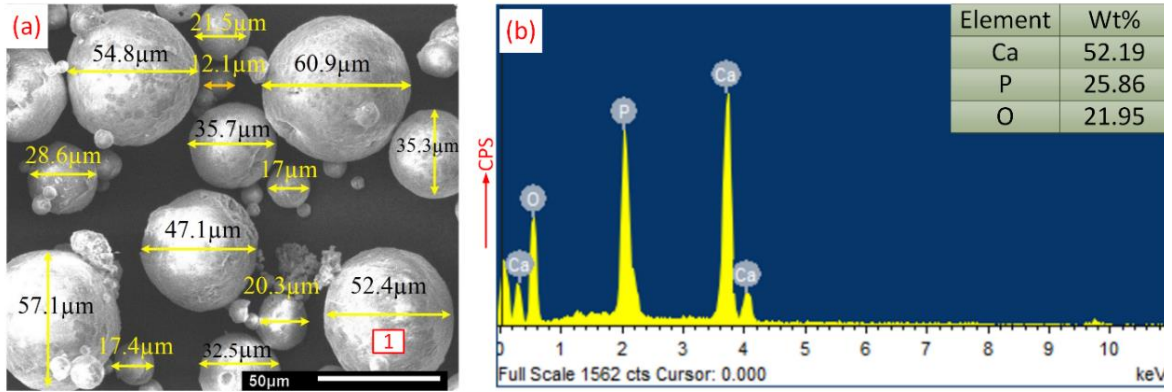


Fig.4.1 (a) Secondary electron image of HA powder, (b) EDS of HA powder corresponding to point 1 of Fig. 4.1a.

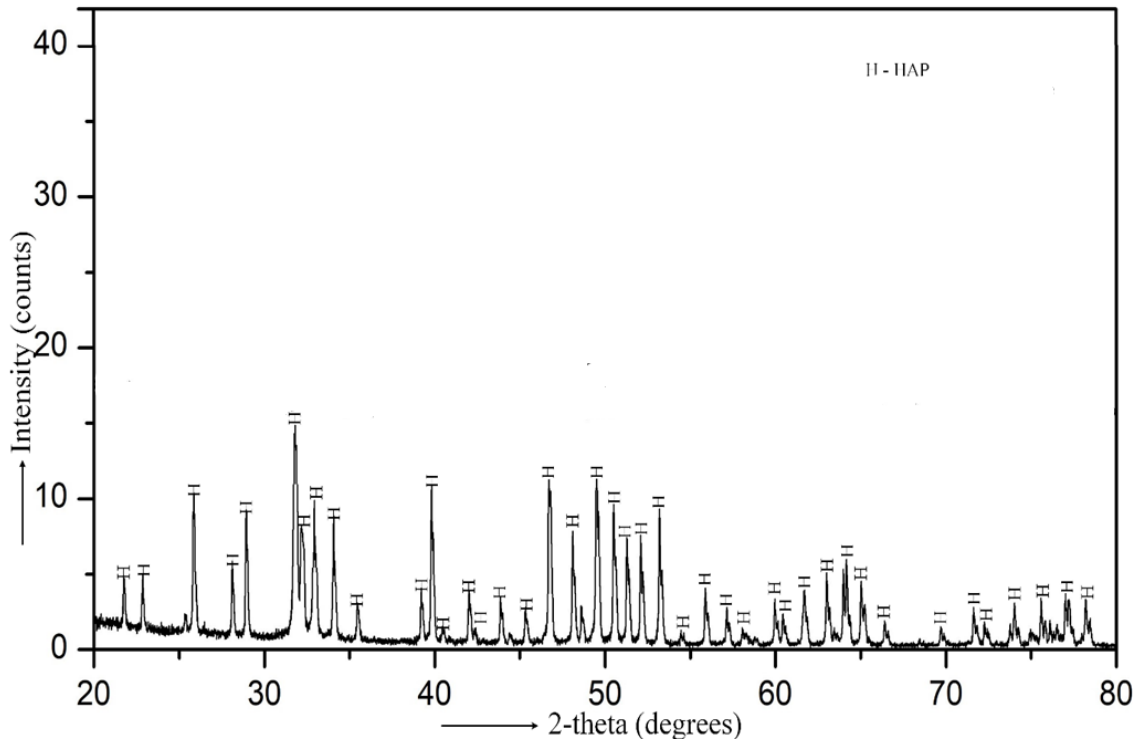


Fig. 4.2 XRD pattern of HA powder

4.1.2 SEM/EDS and XRD analysis of Al₂O₃ powder

Fig. 4.3 displays the results of a SEM/EDS investigation performed on some Al_2O_3 powder. Fig.4.3(a) represents the SEM micrograph and Fig 4.3(b) shows the EDS of Al_2O_3 powder. The scanning electron micrograph displays the angular morphology of Al_2O_3 powder with an average powder particle size of roughly 40 microns.

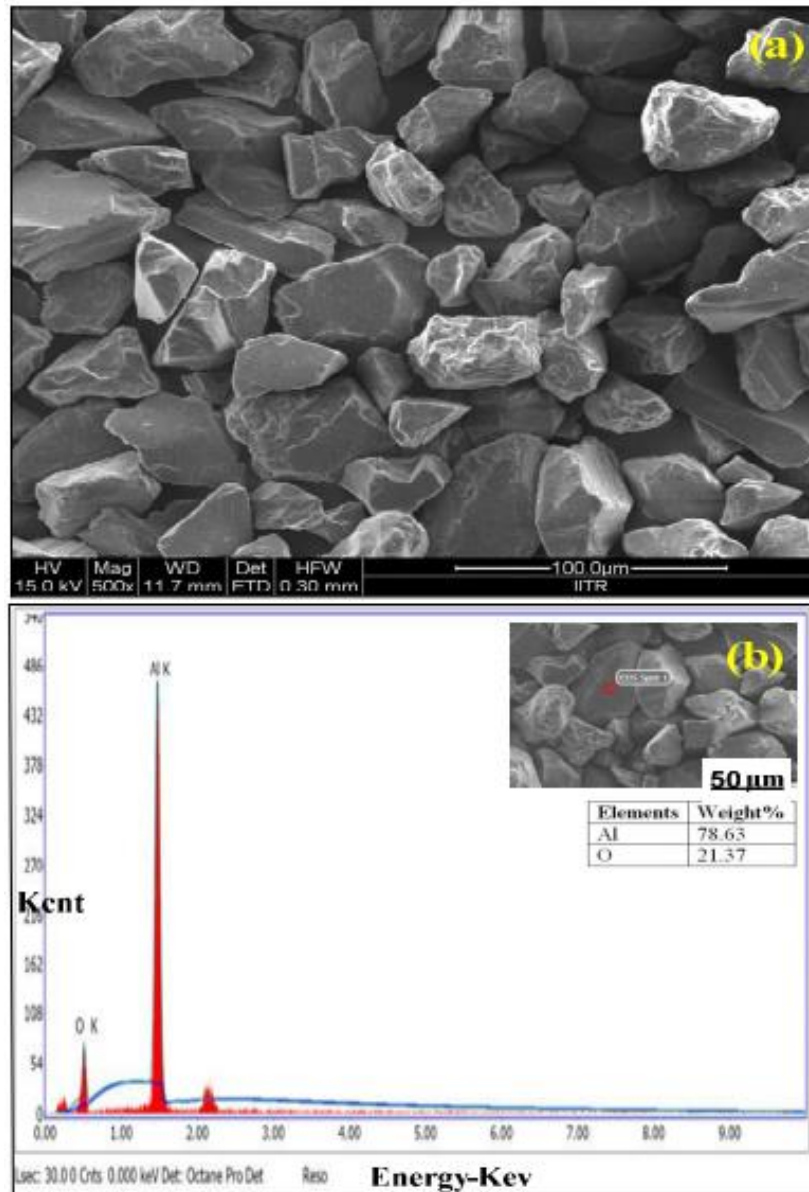


Fig 4.3 (a) SEM micrograph and (b)EDS of Al_2O_3 .

The XRD spectra of Al_2O_3 powder are shown in Fig. 4.4. At various diffraction angles, the XRD results also corroborate the presence of Al_2O_3 .

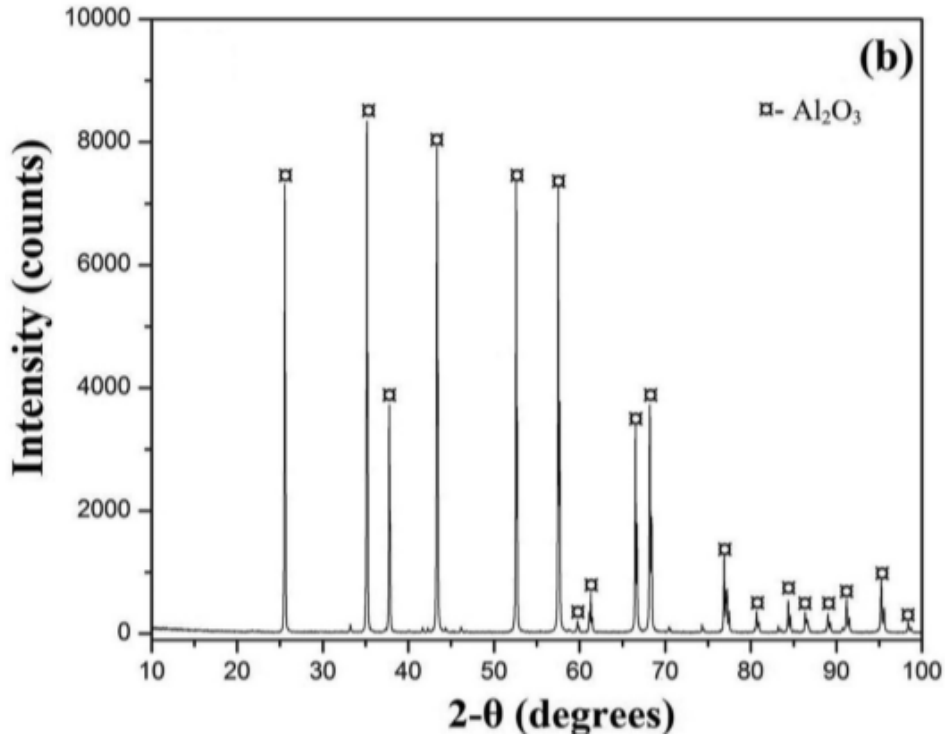


Fig. 4.4 XRD pattern of alumina Al_2O_3 feedstock

4.1.3 SEM/EDS and XRD analysis of ZrO_2 powder

The SEM and EDS analysis of ZrO_2 powder is shown in Fig. 4.5a and Fig.4.5b, respectively. indicates the spherical morphology of the ZrO_2 powder. The average powder particle size of the ZrO_2 was nearly about 2-10 μm . The XRD analysis (Fig. 4.6) of the ZrO_2 powder reveals the presence of peaks corresponding to ZrO_2 phase.

4.1.4 SEM/EDS analysis of HA10AL powder

The clad powders HA-10wt% Al_2O_3 (HA10AL) were prepared through mechanical mixing of both powders in a ceramic pot for 2h. This 10wt% reinforcement was chosen since it has been reported that by adding reinforcement to HA coatings in amounts greater than 10% resulted in deterioration of some of its mechanical properties

(Davis, J.R. ed., 2004). The SEM micrograph illustrates the morphology of HA10AL is shown in Fig. 4.7a. Fig. 4.7b depicts the elemental mapping of major elements (Ca, P, O, and Al) present in the HA10AL powder, which indicates that where Ca, and P is present, the Al is absent and vice versa. This confirms that both powders have maintained their identity during their mechanical mixing in a ceramic pot.

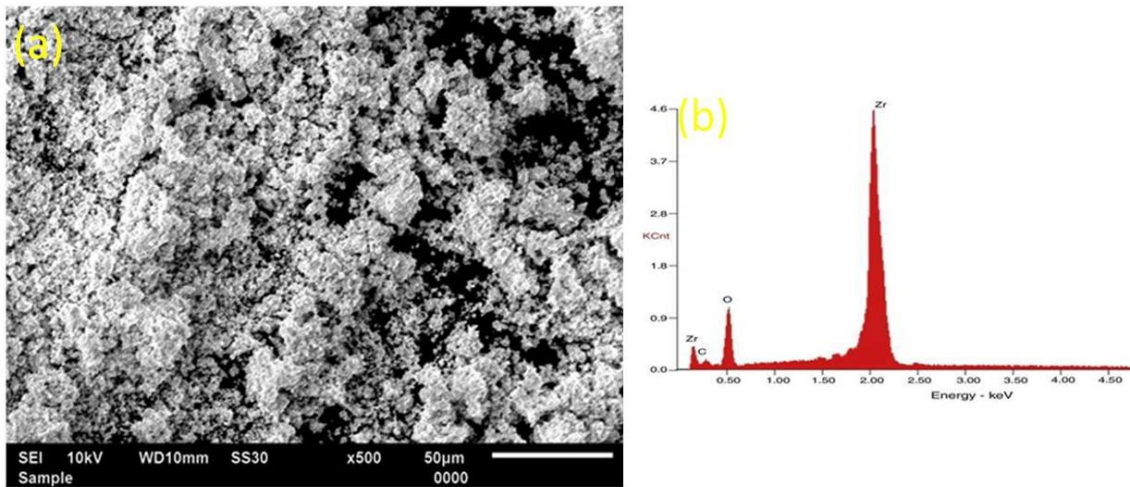


Fig 4.5 (a) SEM and (b) EDS of ZrO₂ powder

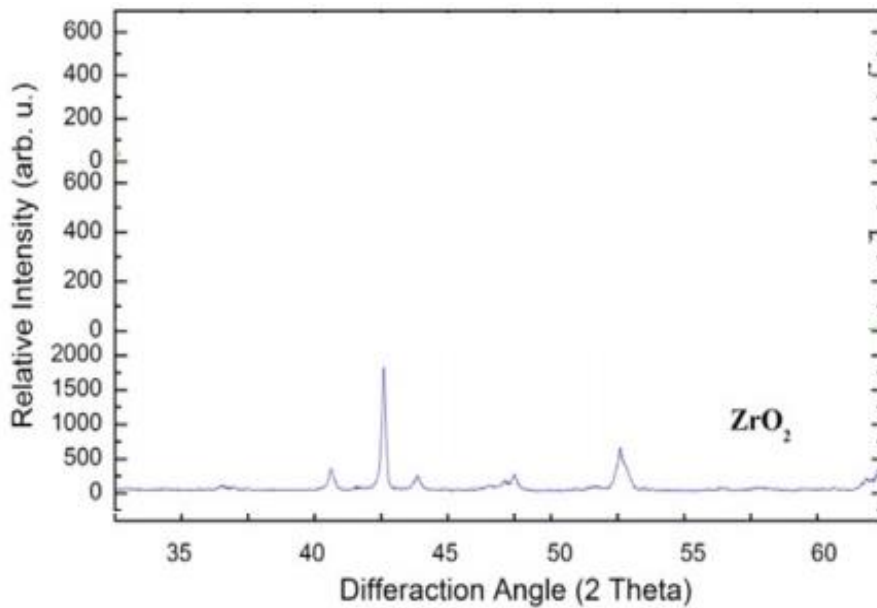


Fig. 4.6 XRD analysis ZrO₂ powder

4.1.5 SEM/EDS analysis of HA10ZR powder

The SEM micrograph illustrates the morphology of HA10ZR is shown in Fig. 4.8. The ZrO_2 powder covering the HA powders were clearly seen in the SEM micrograph as shown in Fig. 4.8.

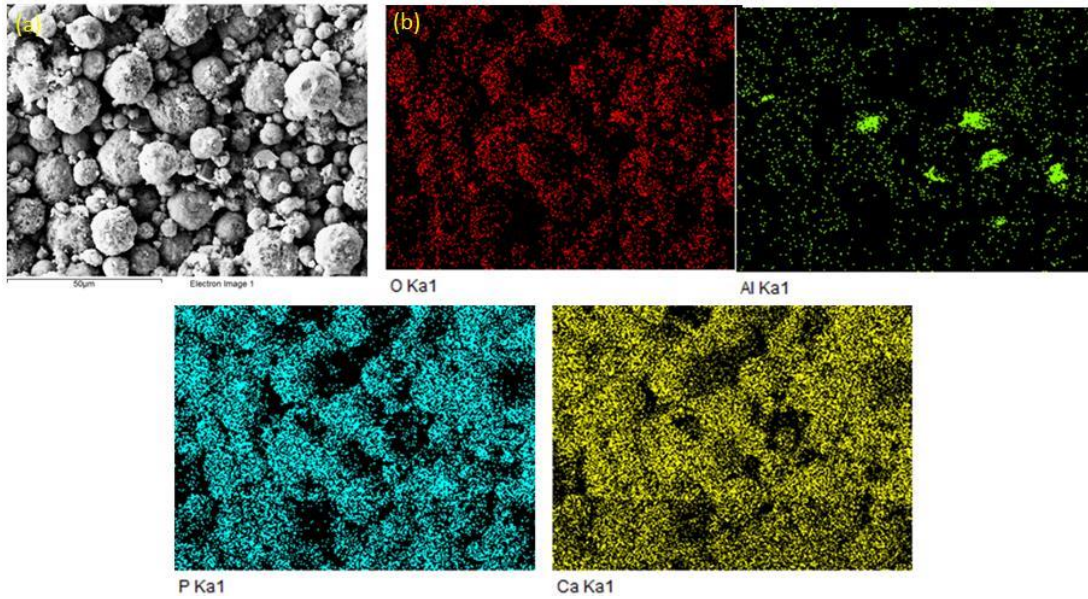


Fig. 4.7 (a) Morphology of HA10AL powder, and (b) element maps of O, Al, P and Ca corresponding to Fig. 4.7a.

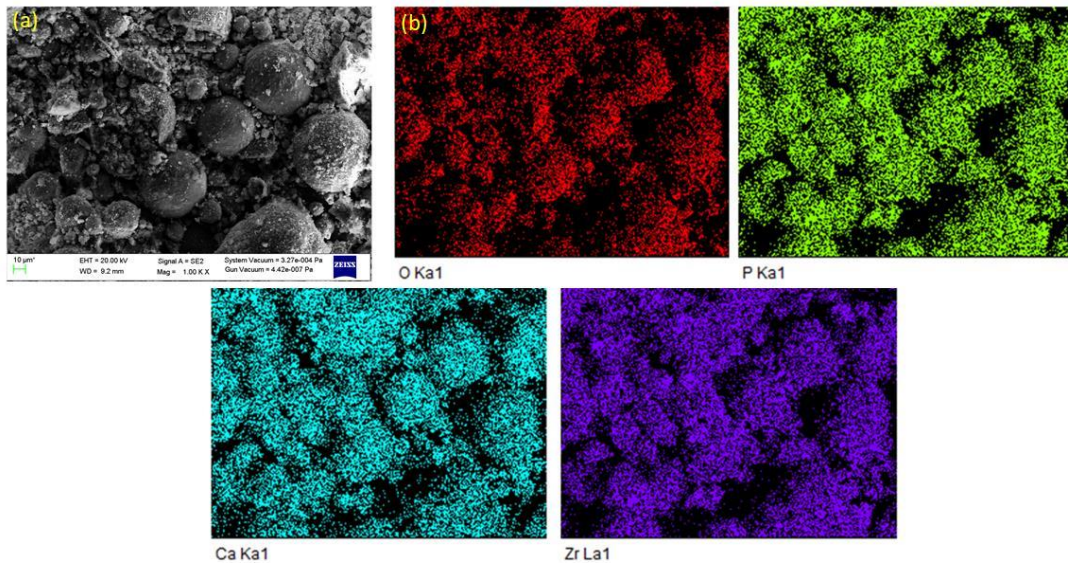


Fig. 4.8 (a) Morphology of HA10ZR powder, and (b) element maps of O, P, Ca and Zr corresponding to Fig. 4.8a.

4.2 SEM/EDS AND XRD ANALYSIS OF AS-DEPOSITED AND HEAT-TREATED SURFACE MODIFIED SPECIMENS AT ALL CONDITIONS.

The following parts provide an explanation of the results of the characterizations of as-deposited and heat-treated surface modified specimens at all conditions along with their results.

4.2.1 Microstructural/ elemental study and XRD analysis of as-deposited and heat-treated surface modified specimens with pure HA powder

As-deposited results: The cross-sectional microstructures of the microwave assisted surface modified SS-31254 alloy layer in the as-deposited condition is shown in Fig. 4.9a. The higher magnification SEM image illustrating the modified microstructure is shown in Fig. 4.9b. There are no any gross defects such as cracks were observed in the modified clad microstructure. During microwave exposure, the bioactive HA powder was melted by absorbing heat at high temperatures. Subsequently, the upper surfaces of the base material (around 200-300 μm thickness) were also melted. There is a diffusion occurred between the HA powder and melted base material at high temperatures. The intermixing of the elements at high temperatures was occurred due to localized melt pool current in the molten bioactive HA powder layer and the melted substrate layer. The intermixing of the elements at high temperature during the microwave cladding process was reported by earlier work also (Deng et al., 2012b). After the completion of experiment, the diffused layer consisting of a mixture of melted base material and HA powder was deposited on the base material. Therefore, the as-deposited clad microstructure exhibited an as-cast microstructure having austenite dendrite with some inter-dendrite phases. The interface between the substrate and the deposited clad layer is not perfect and rather diffuse as shown in Fig. 4.9a. The diffused zone indicates the mutual mixing (from substrate to clad powder and vice-versa) of elements during hybrid MH process. Furthermore, the microwave surface modified layer of SS-31254 alloy by injecting HA powder into it showed distinctive microstructure dependent on the cooling

rate experienced by the melted composite layer. The microstructure of the composite layer's topmost layer was equiaxed. The changed layer showed a typical cellular microstructure in the centre. Yet, the composite layer's connection to the substrate is consistent with epitaxial planar growth. During the hybrid MH process, a temperature gradient to solidification rate (G/R) is created, which can be used to describe the evolution of the composite layer's microstructure. Dendrite growth gives way to cellular dendrite structure and subsequently to the planar front when the ratio of G/R grows, as has already been observed. In the bottom of the melt pool, G has the biggest value by a wide margin, whereas R is close to zero. G/R has a high value, indicating that epitaxial plane growth predominated during the solidification process. The value of R rises gradually in the middle of the composite layer, while the ratio of G/R falls, leading to the creation of cellular crystal. The value of R is relatively high and the value of G is relatively low at the composite layer's surface. As a result, an equiaxed crystal formed near the surface of the composite layer because the ratio G/R was low. The results are in agreement with the in-situ production of bio-ceramic composite coatings of HA on SS-31254 alloy by utilising a laser as a heat source for the production of cladding (Deurling et al., 2009). From the above discussion, it has been observed that the microwave and laser surface modified bio-implant layer consisted of mixture of molten bioactive powder along with substrate surface layer. This composite layer bonds mechanically to the substrate. In contrast, the bond between the deposited coatings and the substrate surface is mostly mechanical in the thermal spray process (high velocity oxy fuel, and plasma-spray). The sharp interface between the coating and the substrate surface is not ideal for long-term use in case of thermal spray process (Doleker et al., 2019). Element line mapping was used to quantitatively map element distribution over the inter-dendritic phase of the modified SS-31254 alloy layer (see Fig. 4.10a). In Fig. 4.10b, the corresponding element distribution superimposed on the line AB is depicted. Inter-dendritic space is that where elemental enrichment of Ca, P, O and depletion of element Fe occur, as seen in Fig. 4.10b. This proves that bioactive HA material is predominantly found in the inter-dendritic phase. The microwave-aided SS-31254 modified layer has a

porosity content (%) ranging from 2% to 3%. The success of bio-implants within the human body is significantly impacted by their porosity (in percent). Because of the porosity, the material's mechanical qualities suffer. However, the development of apatite on the microwave-modified layer of SS-31254 alloy requires a small amount of porosity. When considering the needed mechanical strength and the changed layer's ability to form apatite, the measured porosity in the microwave-surface modified layer of SS-31254 alloy is optimal.

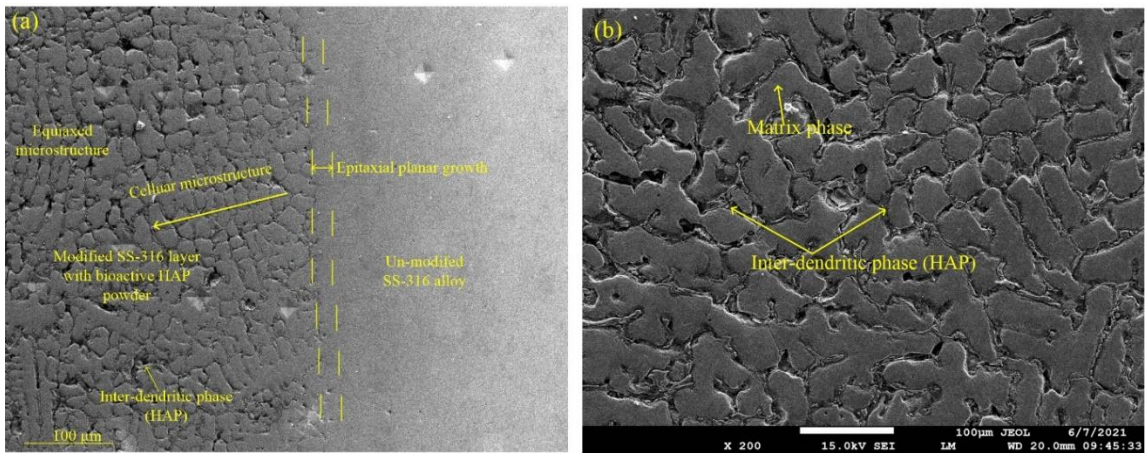


Fig. 4.9 SEM images of microwave assisted surface modification of SS-31254 alloy at (a) low magnifications showing fused interface with varying microstructure in the modified layer, (b) higher magnification showing the inter-dendritic HA phases in the austenite matrix.

The XRD spectrum of the HA powder and microwave-assisted surface-modified samples in the as-deposited conditions are shown in Fig. 4.11. The results showed the presence of Fe-Ni based matrix with HA along with other reaction products phases like Fe_3P , Fe_2P , and FeP , $\text{Ca}_9\text{Fe}(\text{PO}_4)_7$, αTCP (Tricalcium phosphate) in the XRD spectrum. The presence of Fe_3P , Fe_2P , FeP , and $\text{Ca}_9\text{Fe}(\text{PO}_4)_7$ was due to reaction of Fe with HA powder at high temperature and subsequently formation of these phases were occurred. The decomposition of HA powder was occurred due to the high temperature involved in microwave assisted surface modifications process and the formation of amorphous tricalcium phosphate ($\alpha\text{-TCP}$) phase was occurred (Dooley and Wiertel., 2009). From SEM micrographs, it has been observed that these phases were mainly formed in the inter-dendritic regions. This further endorse that in the present work there

is a complete melting of clad powder (HA) along with the substrate material (mainly from the surface in the 200 to 300 μm range) was occurred during microwave exposure at high temperature. After the completion of experiment, the melt starts to solidify in a dendritic mode with the formation of austenite.

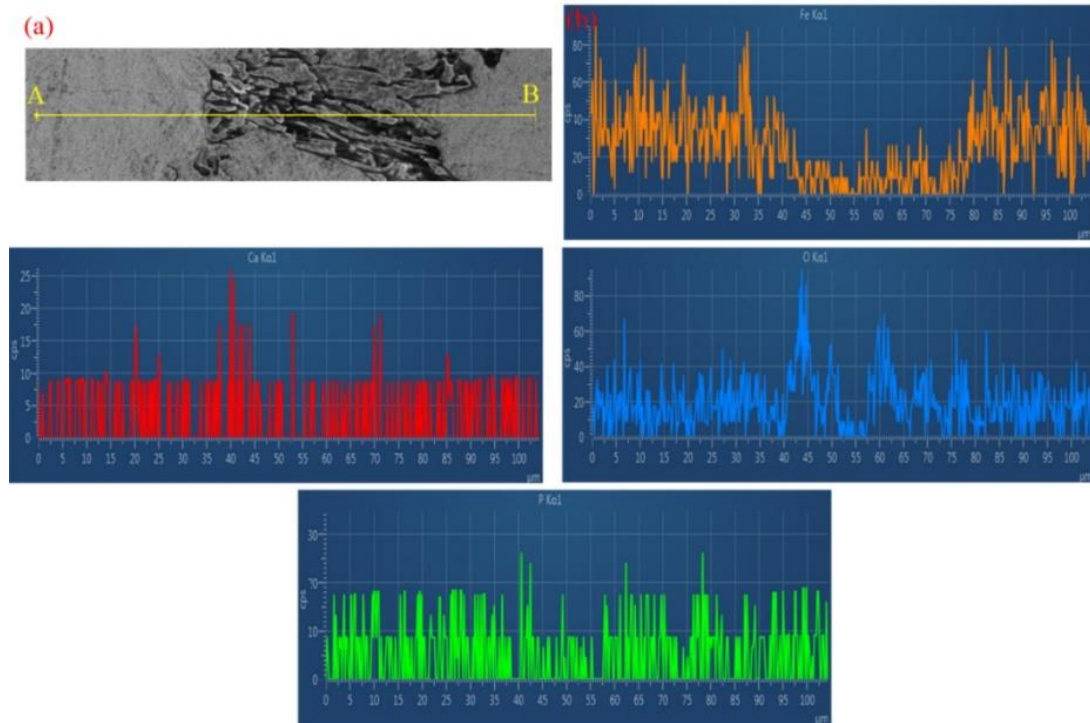


Fig. 4.10 (a) SEM image illustrates the line mapping (AB) taken across the inter-dendritic phase of modified SS-31254 layer, (b) distribution of elements (Fe, Ca, O, and P) corresponding to line AB.

However, due to the low solubility of Ca and P in the austenite matrix, there is an enrichment of these elements (Ca, and P) was occurred in the remaining liquid, as more and more austenite forms. Subsequently, at the end of solidification process, there is a formation of HA along with small amount of other reaction products phases (Fe_3P , Fe_2P , FeP , and $\text{Ca}_9\text{Fe}(\text{PO}_4)_7$) were occurred mainly in the inter-dendritic regions. The presence of Fe_3P traces along with HA in the interdendritic region was also reported by (Balla et al.2013; Chatterjee et al., 2001) for the surface modification of SS-31254 alloy with HA through laser as a source of energy.

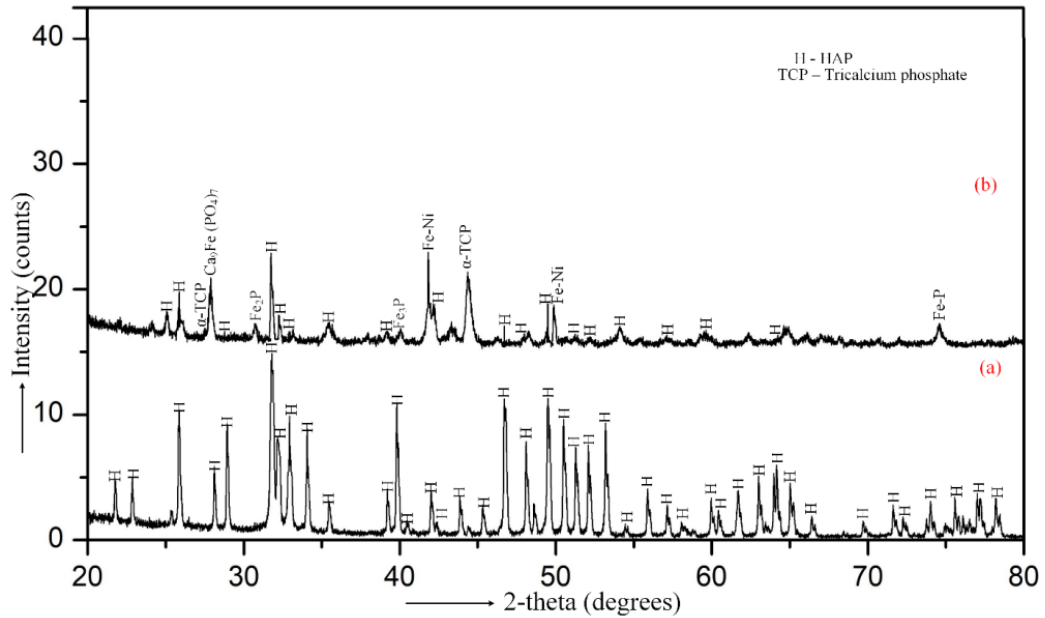


Fig. 4.11 XRD spectra of (a) HA powder, and (b) microwave assisted surface modified SS-31254 layer.

Heat-treated results: The SEM and XRD analysis of the HA surface modified specimen heat-treated at 700 °C is shown in Fig. 4.12 and 4.13 respectively. The SEM micrograph as compared to as-deposited surface modified specimens in case of pure HA except with minor densification through reduction of pores in the heat-treated surface modified layer. The surface modified specimens' reveals the absence of secondary phases (α , β) in the modified layer.

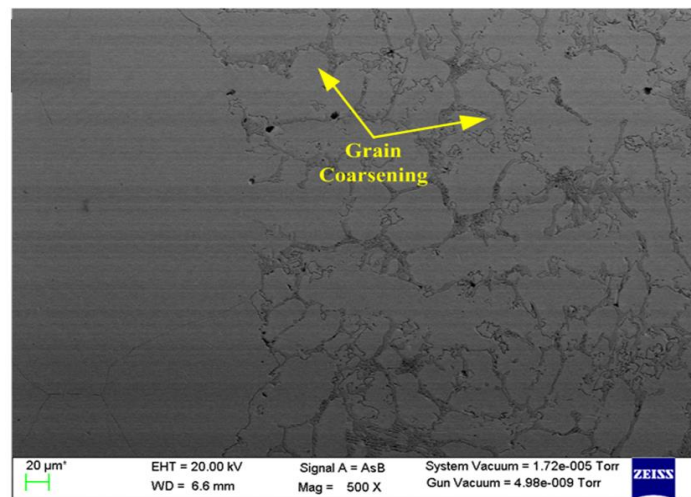


Fig. 4.12 SEM image of post heat-treated (at 700°C) HA surface modified layer .

4.2.2 Microstructural/ elemental study and XRD analysis of as-deposited and heat-treated surface modified specimens with HA10AL powder

Microstructural analysis:

In this study, the surface layer of 254SS was changed to behave as a biocompatible material while the interior section operated as an anchor for the implant. Figure 4.14a shows an optical micrograph of the microwave surface modified sample's cross-sectional microstructures (as-deposited condition). From Fig. 4.14 a, it has been observed that the modified substrate layer is well metallurgical bounded with the unmodified substrate. Between the surface modified layer and the unchanged substrate, the microwave cladding method creates a sound and dispersed interface. Other thermal spray techniques, on the other hand, provide HA coatings with a sharp interface, which are often unsuitable for long-term application (Delaunay et al., 2000).

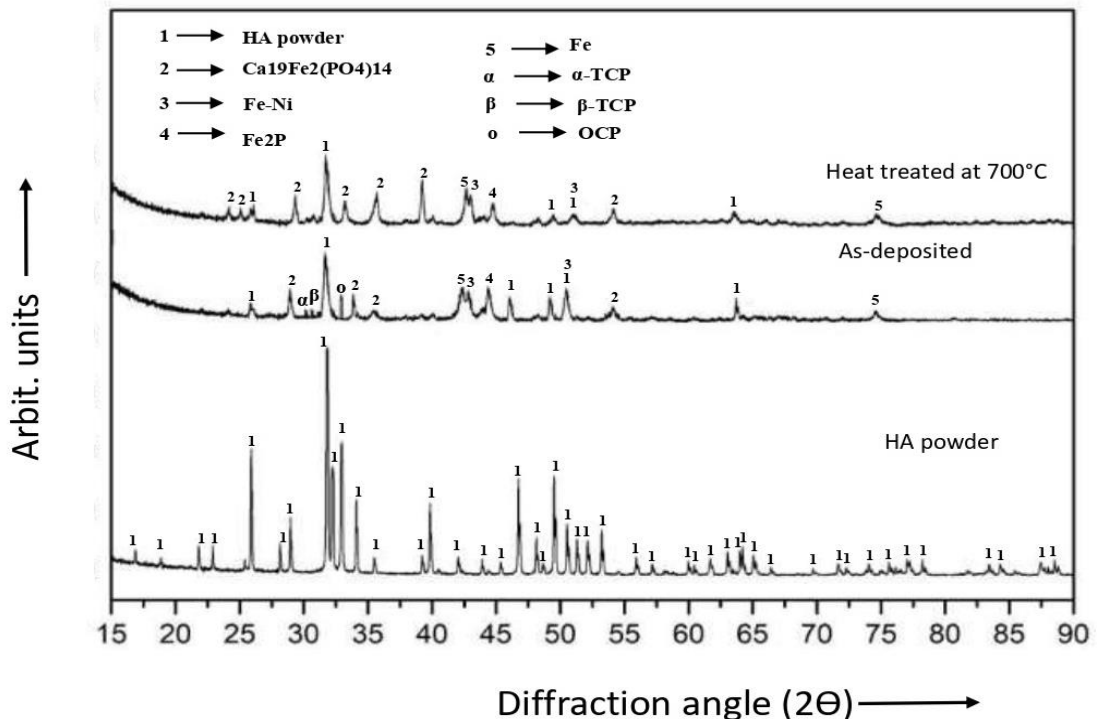


Fig. 4.13 XRD analysis of (a) HA powder, (b) HA clad, and (c) HA post heat-treated clad.

There is no any cracks or mechanical discontinuity was observed in the solidified composite layer and at the solid/liquid interface. The entire changed solidified layer has a comparable microstructure (mainly cellular). As soon as, the irradiation was stopped, there is no further conversion of microwave energy into heat energy in the molten composite layer occurred, rather it starts losing heat (cooling). The rapid quenching of molten composite layer occurred via heat transfer to the unmodified substrate. Because the unaltered substrate has a higher thermal conductivity, it works as a heat sink for the molten composite layer to solidify on it. Heat flow direction is the primary determinant of the direction of cellular development. In this scenario, the greatest temperature difference was observed at the solid–liquid boundary, dictating the direction of cell growth. Beginning in a regular hexagonal array and elongated cell shape, the composite layer then solidifies outward.

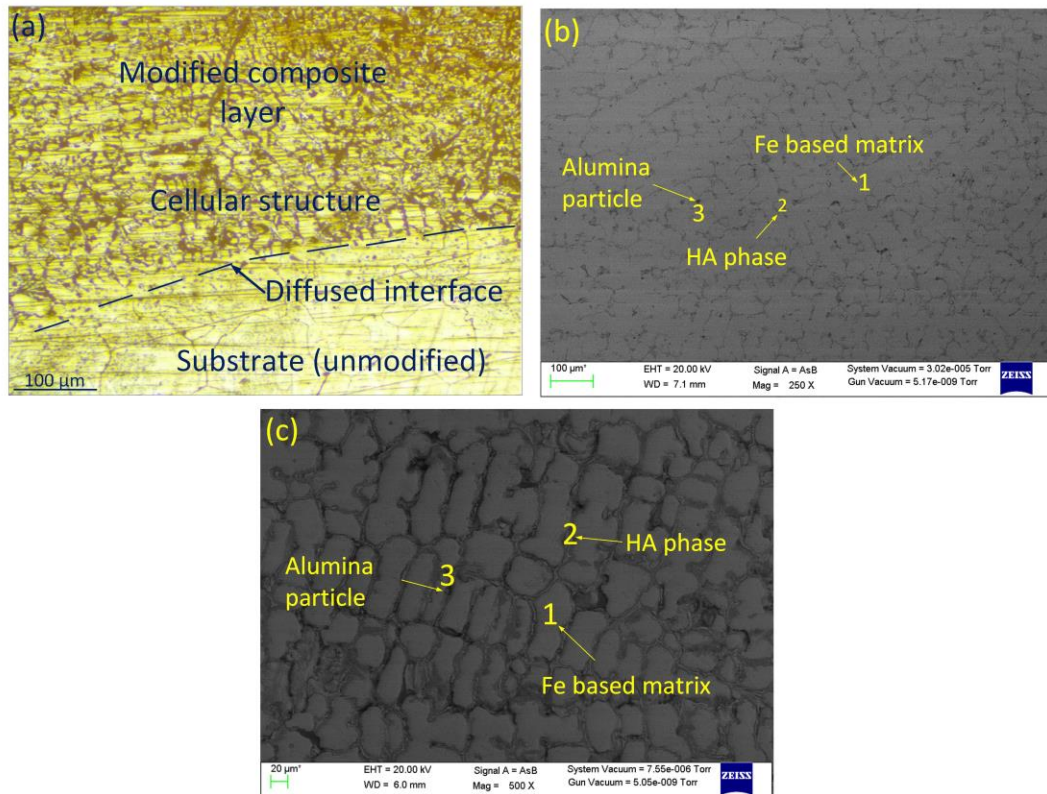


Fig. 4.14 (a) optical macrograph of the HA10AL reinforced SS-31254 in as-deposited condition. SEM micrographs of microwave surface modified specimens in (b) as-deposited condition, (c) 700 °C heat-treated conditions.

The enlarged SEM images of the changed cross-sectional microstructures are shown in Figure 4.14 (b, c). In contrast to the surface-modified samples that were in as-deposited condition (Fig. 4.14b), the sample heat-treated at 700 °C, it was observed that the HA phase has precipitated more clearly at grain boundaries after the heat-treatment performed at 700 °C and a clear mainly two-phase γ +interdendritic (HA+other reaction induced products) structure with a minimum level of porosity is seen as shown in Fig. 4.14c.

The diffusion as well as recrystallization occurred more easily at high temperature (700 °C) and HA phases were precipitated at grain boundaries through diffusion process as shown in Fig. 4.14c.

Elemental observation:

All samples (as-deposited and heat-treated) had a two-phase structure in the microwave surface modified layer, with a bright contrast of the based matrix (label as 1 in Fig. 4.14) and a dark contrast of some interdendritic phases (label as 2 in Fig. 4.14). Particles with a fully black appearance (label 3 in Fig. 4.14) were also found in the microstructure of the microwave surface modified layer. The EDS spot analysis corresponding to locations 1, 2, and 3 in Fig. 4.14 was used to calculate the elemental compositions (wt%) of these phases. Table 4.1 summarized the elemental compositions (wt%) of these phases, as quantified by the EDS spot analysis. The reported results are the average of five EDS spot analysis performed at different locations in the modified layer. From EDS analysis, it has been observed that the γ phase is a mainly solid solution phase, rich in Fe and Ni. The interdendritic phase consists primarily of HA particles, as well as certain reaction products generated during the microwave surface modification process, and the particles that seem completely black are alumina particles. The elemental results are in well agreement with XRD study also. The dispersal of key elements (Ca, P, O and Fe) existing in the interdendritic phase were also revealed by taking elemental mapping. Figure 4.15 shows a higher magnification SEM picture of the interdendritic phase for microwave processed clad. In Fig. 4.15b, the EDS maps of the key elements

(Ca, P, O, and Fe) present correlate to the SEM micrograph of Fig. 4.15a. From EDS maps, it has been observed that the Fe is the main element present in the dendrites phase along with its presence in small amount in the interdendritic regions also. Whereas, the Ca, O, and P have significantly higher concentration in the interdendritic phases. This further supports that interdendritic phase were mainly consists of HA along with some reaction induced products formed during microwave surface modification process. (Das and Shukla., 2019) had performed the HA coatings on 254SS steel by utilizing laser rapid manufacturing technique. The authors reported that the Ca is main element found in interdendritic phases. Whereas, Fe is present in both interdendritic phase and austenite dendrites. Therefore, the obtained results in this research are in agreement with earlier finding also.

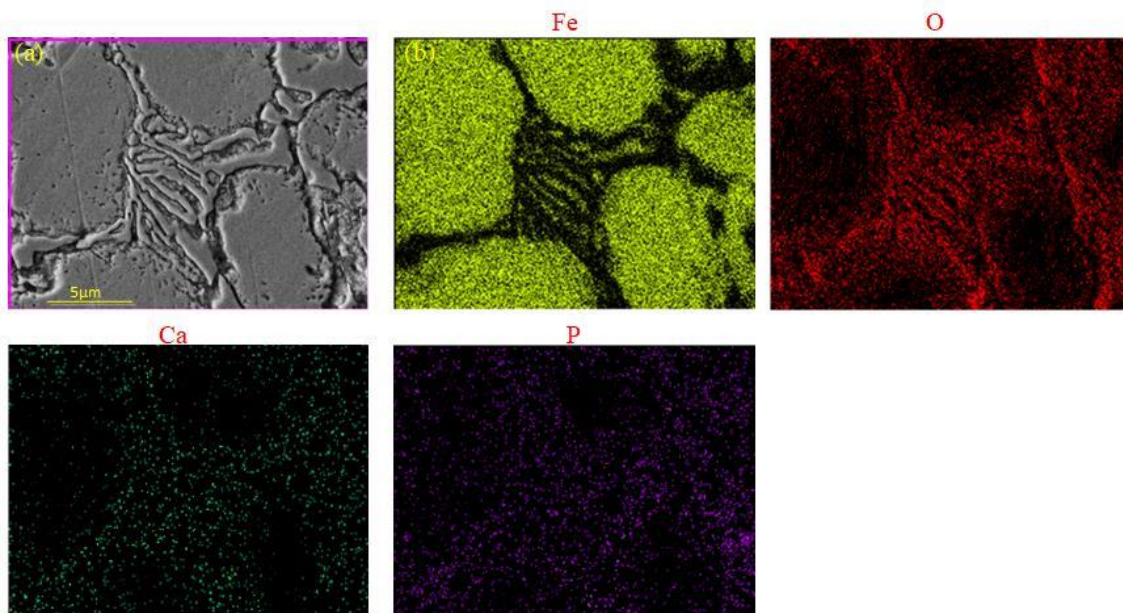


Fig. 4.15 (a) SEM microstructure of interdendritic phase in as-deposited conditions, (b) EDS maps of Fe, O, Ca, and P corresponding to Fig. 4.15a.

XRD observation:

Fig. 4.16 illustrates the typical XRD spectra of the starting HA powder along with microwave surface modified samples at different conditions. In the XRD spectra of microwave surface modified samples, several new peaks corresponding to different

reaction induced phases like α -TCP (tetracalcium phosphate), β -TCP, calcium iron oxide ($\text{Ca}_2\text{Fe}_7\text{O}_{11}$) along with main HA and Ni-Fe based face centered cubic (fcc) structure. These novel phases may have resulted from a high-temperature interaction between molten HA and 254SS.

Table 4.1 The compositions of the γ , interdendritic, and black particle phase in the microwave assisted modified layer. The values are average of five EDS spot analysis.

Element	γ (Fe-Ni based solid solution (%))	Interdendritic phase (%)	Black particles (%)
Fe	90.24	3.10	0.65
O	8.70	22.88	21.31
Al	0.12	0.07	77.53
Ca	0.55	50.09	0.45
P	0.40	23.86	0.06

The entire melting of the Fe-based substrate surface layer, as well as the melting of the HA powder, happened during microwave heating. Therefore, there is a reaction occurred between the various elements present in the melted substrate surface layer and decomposed HA, which leads to formation of new phases after rapid quenching of modified surface layer. During microwave exposures, it was discovered that the HA powder, as well as the SS-31254 surface layer was completely melted. As a result, there is a creation of two different liquids: a liquid mineral and a liquid metal. Because the bonding qualities of these two liquids are completely different (metallic vs. ionic), there is no mutual solubility between them. The solidification of the melt occurs in the form of dendrites, with the production of a Fe-Ni based austenite matrix. Because components like Ca and P (the primary elements found in the HA) have a poor solubility in the main austenite-based dendritic matrix, the residual liquid became enriched with Ca and P as additional austenite formed. As a result, HA, along with certain reaction-induced compounds, was mostly formed in the inter-dendritic zones after the solidification process was completed. It should be emphasized that (Oshkour et al., 2015) the creation of these novel phases as a result of the reaction between metallic phase alloy and ceramic

phase compounds in the composite construction of HA/SS-31254 sintered at 1200 °C. In addition, amorphous phases such α -TCP, β -TCP developed in the microwave surface modified sample due to the breakdown of de-hydroxylation of HA powder in the temperature range of 800-1350 °C in the as-deposited condition. When comparing as-deposited microwave surface modified samples to heat-treated samples at 700 °C, it is seen that the amount of these phases is greatly diminished in the microwave surface modified samples following heat treatment. The coating crystallinity was restored after being heated to 700 °C, which caused re-hydroxylation inside the composite modified layer (Deng et al., 2012a).

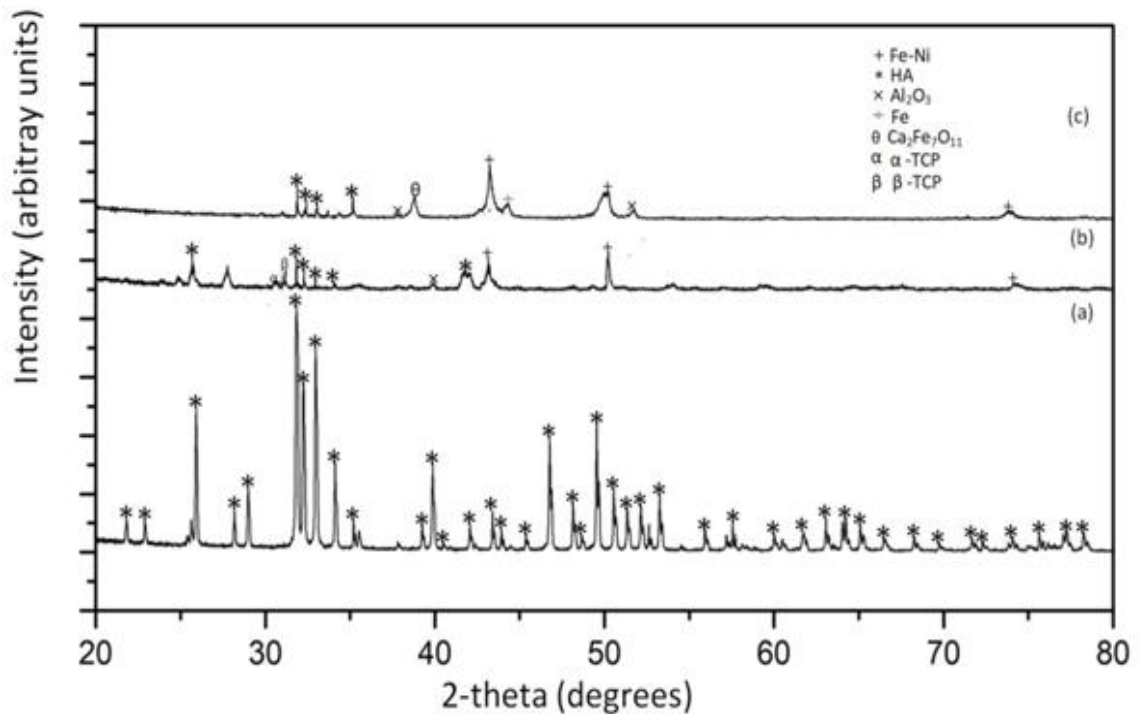


Fig. 4.16 (a) HA powder, (b) HA10AL surface modified specimens in as-deposited conditions, and (c) HA10AL surface modified layer in the post heat-treated conditions.

4.2.3 Microstructural/ elemental study and XRD analysis of as-deposited and heat-treated surface modified specimens with HA10ZR powder.

SEM images of the HA10ZR layer, both as-deposited and after heat treatment, are shown in Fig. 4.17. Beginning in a regular hexagonal array and elongated cell shape, the composite layer then solidifies outward. Figure 4.17 (b, c) shows scanning electron micrographs of the changed cross-sectional microstructures in all situations at increased magnification. In contrast to the surface-modified samples that were in as-deposited condition (Fig. 4.17a), the sample heat-treated at 700 °C (Fig. 4.17b), it was observed that the HA phase has precipitated more clearly at grain boundaries after the heat-treatment performed at 700 °C and a clear mainly two-phase γ +interdendritic (HA+other reaction induced products) structure with a minimum level of porosity is seen as shown in Fig. 4.17b. Some grain coarsening was also observed for the sample heat-treated at 700 °C as seen in Fig. 4.17b. The XRD study for the samples treated with HA10ZR condition is depicted in Fig. 4.18. From Fig. 4.18a, it has been deduced that the samples in the as-deposited condition depicts the presence of secondary phases (α , β) along with main HA based clad powder.

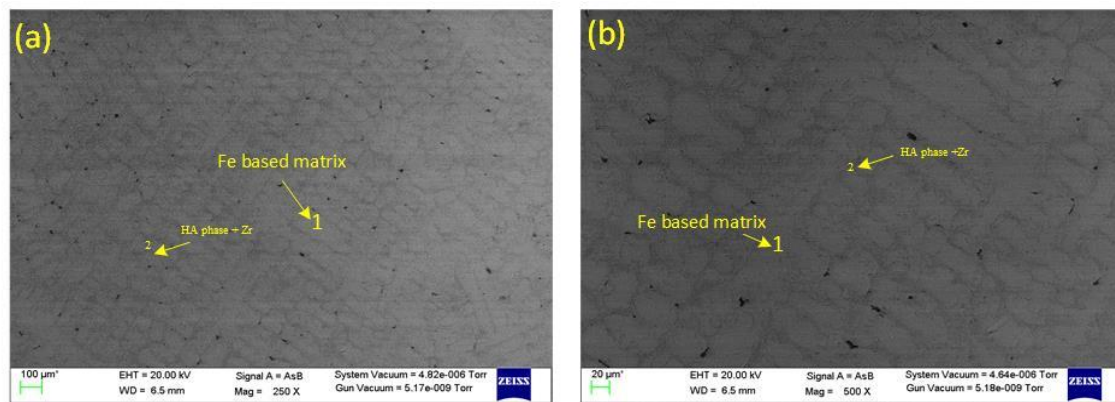


Fig. 4.17 SEM image of (a) as-deposited HA10ZR powder, and (b) heat-treated HA10ZR surface modified layer.

Whereas, the XRD spectra (Fig. 4.18b) of heat-treated surface modified specimens' reveals the absence of secondary phases (α , β) in the modified layer.

The absence of the secondary phases in the modified layer indicates that the coating crystallinity was restored after being heated to 700 °C, which caused re-hydroxylation inside the composite modified layer (Deng et al., 2012a).

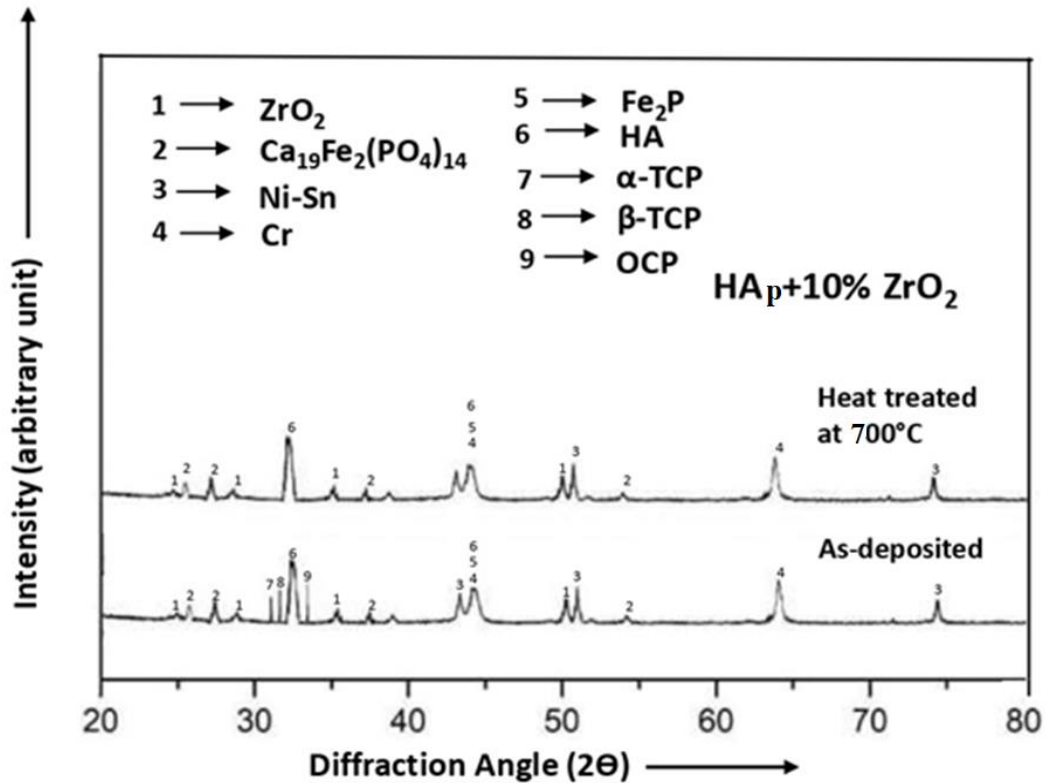


Fig. 4.18 XRD analysis of (a) as-deposited HA10ZR surface modified layer, and (b) heat-treated HA10ZR surface modified layer.

4.3 POROSITY MEASUREMENT

The porosity is another important feature that strongly influences the modified layer properties (mechanical and biological). The higher porosity leads to reduction in microhardness and allows for higher wear and corrosion rate. The inverse relationship between the hardness and porosity was also reported by Morks et al., 2008. According to their findings, when porosity improved, coating hardness deteriorated. Nevertheless, the porosity deteriorates the mechanical property of the fabricated composite modified layer. However, a certain amount of porosity is essential for the surface modified layer to allow the bone matter to grow into it, which accelerates patient healing and shortens recovery

time. The porosity (%) helps the initial bone fixation, however the high porosity content for long term mechanical stability of the HA coatings is uncertain (Deb et al., 1996). Therefore, a proper balance in porosity contents is required to optimized the performance of the fabricated composite layer in term of its mechanical property as well as its biocompatibility in human plasma environment. Percentage porosity in the as-deposited and heat-treated microwave surface modification samples was measured in this study as per procedure mentioned in section 3.5.5. Table 4.2 displays the related results. As can be seen in Table 4.2, porosity decreases dramatically during and after heat treatment. Further, there is a proportionate decrease in porosity level with corresponding increase in the heat-treatment temperature was observed. The sample heat-treated at 700 °C showed minimum porosity due to the maximum temperature involved in it. After heat-treatment, there is a reduction in pores, voids and micro cracks due to the diffusion and recrystallization process occurring at high temperature. Further, the HA10ZR heat-treated sample has minimum porosity amongst all samples. In this study, the microwave surface modified samples had lower reported porosity contents across the cross-sectional regions than the HA coatings applied using thermal spray techniques (vacuum plasma spray and low velocity oxy fuel spray). The difference between the coatings produced using thermal spray procedures (which resulted in the mainly mechanical anchorage between the impinged splats) and those deposited via diffusion bonding between the HA10AL powder and the substrate surface layer is responsible for this (Birks et al., 2006; Daram and Banjongprasert., 2020). In thermal spray processes, the few splats are present even in the un-melted state which contributes to the increase in porosity of the fabricated HA coatings.

Table 4.2 Measured porosity (%).

Sample identity	As-deposited condition	700 °C heat-treated condition
Porosity (%) only HA powder	2.5±0.5%	1.4±0.4%
Porosity (%) with HA10AL powder	2.9±0.7%	2.3±0.3%
Porosity (%) only HA10ZR powder	2.7±0.4%	1.9±0.3%

4.4 Microhardness measurement in the as-deposited and heat-treated surface modified samples at all conditions.

As mentioned in Chapter 3, the hardness of the as-deposited and heat-treated samples of the microwave surface modified materials was determined as per procedure mentioned in section 3.6.1. Table 4.3 displays the results of the measurement of microhardness for all samples at all conditions. Samples with a changed surface that underwent heat treatment showed an increase in microhardness relative to untreated substrate. The increase microhardness of the microwave surface modified specimens is beneficial from the perspective of the wear resistance of the implants. Increases in microhardness protect the orthopaedic implants from wearing down as quickly. Further, the maximum microhardness was achieved for sample heat-treated at 700°C followed by the as-deposited modified substrate, and then followed by unmodified substrate material at all conditions. The surface modified samples with HA10ZR based clad powder exhibit the maximum hardness amongst all the microwave treated samples at all conditions. The improvement in hardness may resulted due to decrease in porosity after heat-treatment process, which causes the densification of the surface modified layer of the samples. The densification of the microwave surface modified layer is due to recrystallization that occurs at high temperature in the manufactured composite modified layer. After being subjected to heat, the microwave surface modified specimens were denser, resulting in an increase in microhardness. Also, it has been shown that after heat-treatment at 700 °C, the variation in microhardness values was reduced because a more uniform microstructure was created. There is a uniform distribution of HA, reinforcement particle (Al_2O_3 and ZrO_2), and other phases were occurred mainly at the grain boundaries after heat-treatment performed at 700 °C, which resulted in decrease in variation of microhardness after heat-treatment. The SEM images (Fig. 4.19) depicts the morphology of the typical indents taken on the microwave surface modified samples layer with HA10AL based clad powders. From Fig. 4.19, it should be noted that there is a marginal decrease in dimensions of indents taken on the samples at heat-treated conditions with a corresponding increase in temperature. This further confirmed that microhardness

displayed a direct relationship with a corresponding increase in temperature of the microwave surface modified specimens.

Table 4.3 Microhardness values.

Sample identity	Clads	700 °C heat-treated condition
Porosity (%) only HA powder	260±8.8HV	271±5.2HV
Porosity (%) with HA10AL powder	272±11.1HV	315±4.2HV
Porosity (%) only HA10ZR powder	278±10.8HV	325±4.1HV

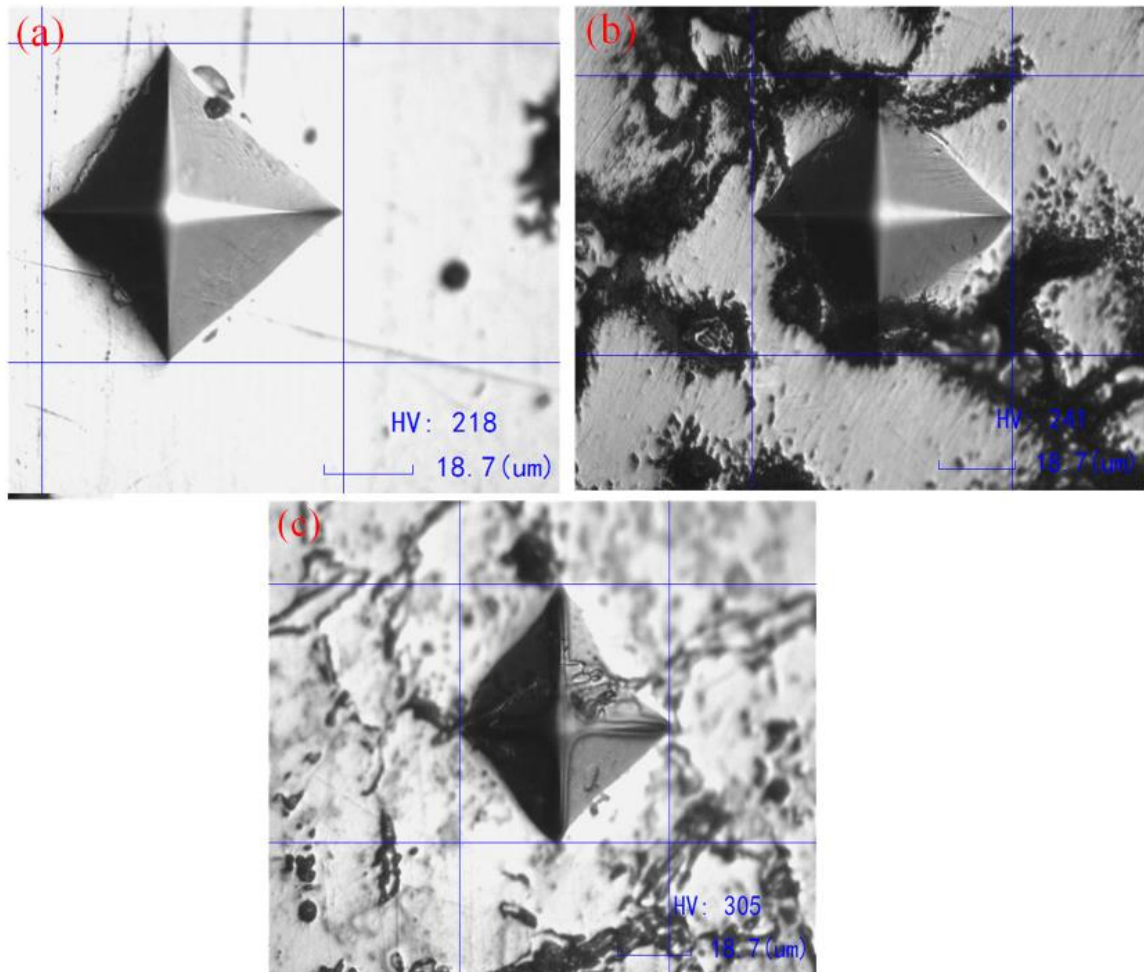


Fig. 4.19 SEM micrographs illustrates the morphology of indents taken on microwave surface modified specimens in (a) unmodified layer (b) as-deposited modified layer, (c) 700 °C heat-treated layer in case of HA10AL specimen.

4.5 SUMMARY

The metallurgical and mechanical characterization using XRD, SEM associated with EDS of specimens with all combinations (HA, HA10AL, and HA10ZR) have been presented in this chapter. The metallurgical characterization in term of microstructure, phase analysis, element composition using, FE-SEM, XRD, and EDS were used for finding the characteristics of developed clad and heat-treated (HA, HA10AL, and HA10ZR) clads at all conditions . The relevant mechanical aspects of as-deposited and heat-treated specimens, viz microhardness were evaluated. The surface modified samples have significant higher microhardness as compared with the base material (SS-31254). The microhardness of the heat-treated specimens is greater than that of the as-deposited clad specimens because the heat treatment densifies the surface changed layer.

CHAPTER 5

IN-VITRO BIOCOMPATIBILITY STUDY AND CORROSION BEHAVIOUR OF THE BASE METAL (SS-31254) AND SURFACE MODIFIED SPECIMENS AT ALL CONDITIONS

This chapter presents in-vitro corrosion behavior and biocompatibility study of the uncoated SS-31254 and microwave assisted surface modified specimens at all conditions in simulated body fluid (SBF), also termed as Ringer's solution. Polarization technique was used to assess the corrosion susceptibility of uncoated SS-31254 and microwave assisted surface modified specimens at all conditions. Growing cells in a lab is a complicated procedure known as cell culture. Prior to their use in the in-vivo setting, uncoated SS-31254 and microwave assisted surface modified specimens are initially tested in controlled circumstances using in-vitro cell culture testing. Additionally, the outcomes of FE-SEM/EDS analysis of the test materials have been integrated.

5.1 IN-VITRO STUDY FOR HA SURFACE MODIFIED SPECIMENS FOR AS-DEPOSITED AND HEAT-TREATED CONDITIONS.

The formation of the apatite layer was measured by comparing the pre- and post-submersion weights of the modified and original SS-31254 alloy in an SBF for 14 days. There is a negligible change in weight (about 0.001g) with no indication of apatite layer formation was observed in unmodified SS-31254 alloy, which indicates the non-bioactivity of SS-31254 alloy. Whereas, there is a significant change in the weight (about 0.35 g in as-deposited condition, and 0.18g in heat-treated condition) with the formation of apatite layer was observed in modified SS-31254 alloy, which indicates the bioactivity of microwave-assisted modified layer of SS-31254 alloy. Further, the precipitates of apatite, if any, can be identified as particles having brighter contrast on the surface of samples following immersion in SBF. The SEM micrographs of the unmodified and modified SS-31254 alloy is shown in Fig. 5.1. There is no formation of apatite layer was observed in the unmodified SS-31254 alloy as shown in Fig.5.1a. On the other hand, from Fig. 5.1b, it is clear that there is a formation of precipitation of the apatite layer on its surface. Further the apatite layer formation was decreases in the heat-treated specimens due to densification of pores after this heat-treatment as shown in Fig. 5.1c.

The elemental composition (wt%) of the brighter phase was further analyzed by utilizing the EDS attached to FESEM as shown in Fig. 5.1b corresponding to the selected regions. The results showed the presence of Ca and P as major constituents demonstrating the formation of apatite layer. The results are in agreement with earlier findings also in which the SS-31254 layer was modified with bioactive HA through laser technique (Chatterjee et al., 2001). Therefore, this layer containing HA provides appropriate chemistry for better osseointegration of implant.

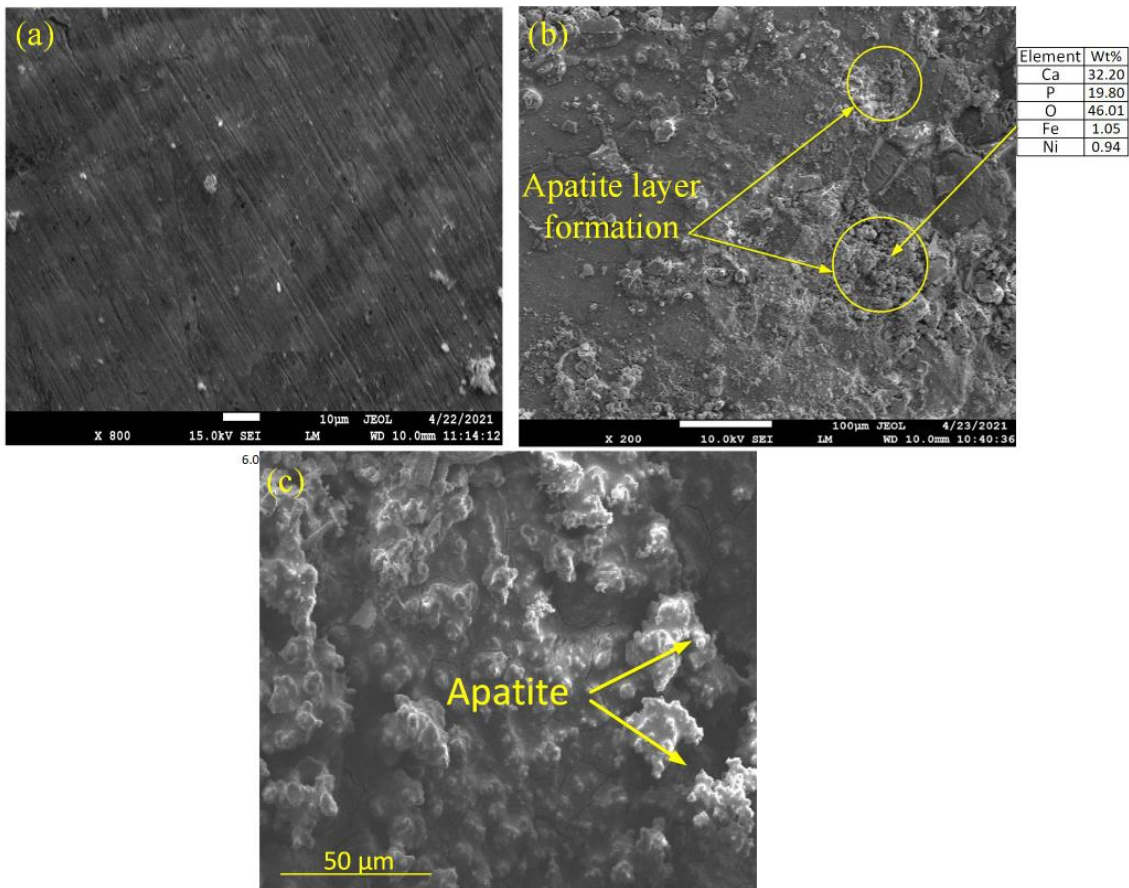


Fig. 5.1 SEM images showing the apatite precipitation after 14 days of the immersion in simulated body fluid of (a) unmodified SS-31254 alloy. (b) microwave assisted modified SS-31254 alloy along with EDS taken at brighter phase (c) microwave assisted modified SS-31254 at heat-treated conditions.

5.2 IN-VITRO STUDY FOR HA10AL AND HA10ZR SURFACE MODIFIED SPECIMENS FOR AS-DEPOSITED AND HEAT-TREATED CONDITION

The weight difference between the modified and unmodified samples following the immersion test in SBF was used to count the amount of bone-like apatite formed on the microwave-aided surface modified samples. The results are illustrated in Table 5.1 for the weight change for the tested samples in the HA10AL and HA10ZR conditions. The negligible weight gain was observed in the unmodified SS31254 steel indicating non-bioactivity of material. On the other hand, the microwave aided surface modified samples showed a significant increase in weight. The as-deposited surface modified sample in case of HA10AL gained the most weight (almost 0.33 g), and then followed by 700 °C heat-treated sample (nearly 0.16 g). Whereas, the as-deposited surface modified sample in case of HA10ZR gained the most weight (almost 0.32 g), and then followed by 700 °C heat-treated sample (nearly 0.14 g). The formation of an apatite layer on the surface modified sample is evaluated using SEM/EDS analysis. The SEM pictures (Fig. 5.2) revealed alterations in the surface morphology of microwave-modified materials with HA10AL powder, which included the production of holes, fissures, and a newly formed apatite layer in the form of agglomerates (bright contrast). This confirmed the bioactivity nature of the microwave surface modified samples. Furthermore, when the heat-treatment temperature rises, the ability to create an apatite layer decreases. The maximum apatite layer formation was observed for the as-deposited surface modified sample due to presence of maximum pores/void and amorphous phase in it (Fig. 5.2b). The heat-treatment resulted in the densification of the composite layer by covering pores and voids in it. The pore/void act as a nucleating site for apatite to grow onto it. Therefore, the as-deposited surface modified sample (Fig. 5.2b) exhibited maximum apatite layer formation followed by 700 °C heat-treated sample (Fig. 5.2c). The EDS spot analysis performed corresponding to locations 1, and 2 of Fig. 5.2 (c) showed the newly formed layer was enriched with Ca, and P, which further supports the bone-binding apatite layer on it. The SEM pictures (Fig. 5.3) revealed alterations in the surface morphology of microwave-modified materials with HA10ZR powder which also indicates the formation of apatite layer in the as-deposited and heat-treated conditions (Fig. 5.3a). The less apatite layer was formed in the heat-treated surfacd modified layer because the heat-treatment

resulted in the densification of the composite layer by covering pores and voids in it (Fig. 5.3b).

Table 5.1 Weight change of as-deposited and heat-treated surface modified specimens with HA10AL and HA10ZR powder.

Sample identity	As-deposited condition	Heat-treated condition
HA10AL powder	0.33g	0.16g
HA10ZR powder	0.32g	0.14g

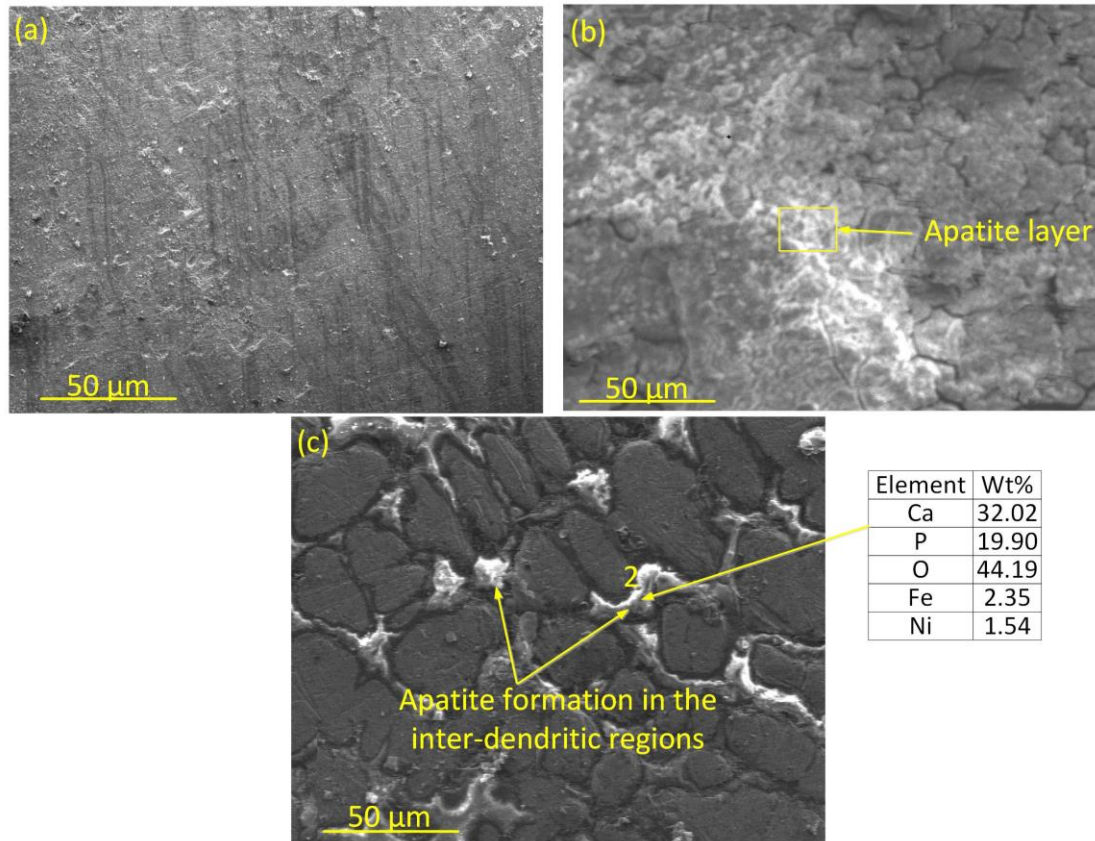


Fig. 5.2 SEM images for HA10AL (a) SS-31254 alloy. (b) clad, (c) 700 °C heat-treated layer.

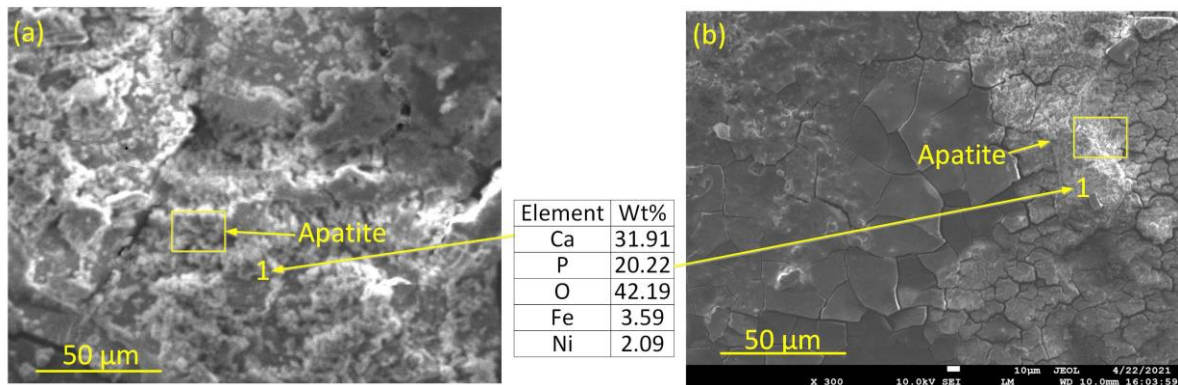


Fig. 5.3 SEM images for HA10ZR (a) as-deposited modified layer, (c) 700 °C heat-treated layer.

5.3 IN VITRO CORROSION ANALYSIS

5.3.1 Corrosion Studies

In the present work, the corrosion behaviour of materials was determined by utilizing an electrochemical technique. This technique is used because of its quickness and sensitivity to measure even a low corrosion rate. The Tafel extrapolation method based on this technique was utilized for measuring the corrosion rate (M.G. Fontana., 1987). The corrosion behavior of HA coated, HA+10wt% Al_2O_3 coated and HA+10wt% ZrO_2 coated specimens were determined by utilizing an potentiodynamic polarization test. Each experiment was run on a computer running the Gamry electrochemical programme DC105, with the help of a Potentiostat/Galvanostat (Series G-750; Gamry Instruments, Inc., USA). The Ringer's solution having similarity with the human body plasma was used as an electrolyte. Ringer's solution is a vital medium used in the corrosion testing of biomedical implants due to its physiological relevance. Ringer's solution is particularly crucial for assessing the corrosion characteristics of biomedical implants due to its ability to accurately replicate the ionic composition and pH levels of the human body. This creates an ideal environment for carrying out the assessment. The research examined the corrosion and tribocorrosion characteristics of TA3 alloy after the introduction of Nb ions. To replicate the circumstances of biological corrosion and tribocorrosion in the human body, Ringer's solution was used. This research emphasised the importance of Ringer's solution in assessing the efficacy of implants under physiological conditions. To ensure accurate corrosion testing of biomedical implants, it

is crucial to use a medium with a composition closely resembling that of human physiological fluids. Furthermore, the limitations associated with the use of intricate saline solutions as corrosive agents for performing corrosion experiments on magnesium, especially for biomedical purposes, further emphasise the need of Ringer's solution. This highlights the need of using testing conditions that closely resemble physiological conditions, such as Ringer's solution, to ensure the accuracy and reliability of corrosion testing results for biomedical implants. The accurate replication of the chemical environment of the human body is the main reason why Ringer's solution is very significant in the area of corrosion testing for biomedical implants. This capability allows for a comprehensive assessment of the corrosion characteristics and effectiveness of implants under physiological conditions. The chemical composition of the Ringer's solution is illustrated in Table 5.2.

Table 5.2 Chemical composition of Ringer's solution

Composition	NaCl	KCl	CaCl ₂	NaHCO ₃
Concentration (g l ⁻¹)	0.89	0.44	0.25	0.21

Prior to performing the corrosion study, each specimen was dipped in Ringer's solution for about 24 hours for stabilization (Balamurugan et al., 2002). The temperature of the electrolytic solution was maintained at 37±1 °C for performing all the experiments. This particular temperature (37±1 °C) was used because it's the normal temperature of the human body. The pH of the solution was adjusted 7.2. The specimens whose corrosion rate to be measured act as a working electrode and exposed area of the samples was about 1.54 cm². As the reference electrode, a saturated calomel electrode (SCE) was employed and all potentials measurement were taken with respect to this electrode. In the present setup, a pure graphite rod was acts as the counter electrode. The schematic illustration for performing the corrosion behaviour of the microwave treated surface modified samples at all conditions and base metal is shown in chapter 3 (Fig. 3.7). The fresh solution was utilized every time to conduct the experiment. The polarization curves were plotted between -250 mV to +250 mV with a scan rate of about 1 mV/sec. The tests

were performed after a steady open-circuit potential was achieved i.e. there is not more than ± 5 mV drift in 5 min. All the tests were conducted on three fresh samples to verify repeatability of test results. When using Tafel methods, tangents were constructed on a graph of E versus $\log I$, which extrapolated to corrosion potential (E_{corr}), intersected at a point, and gave the corrosion current (I_{corr}) value at that location on the X axis. There is an inbuilt software in the machine which gives the various corrosion parameters such as corrosion potential (E_{corr}), and corrosion current density (I_{corr}). The likelihood of a material corroding tendency increases as the corrosion current density (I_{corr}) of the material increases at a given potential. Three measurements were taken for each conditions on the fresh samples. The average value of three measurements was reported in results. All tests were carried out in a potential range of ± 20 mV with respect to the OCP of the specimen, at a scanning rate of 0.1667 mV/s. The Tafle curves corresponding to tested specimens at all conditions are shown in Fig. 5.4. After the completion of the corrosion testing, the specimens were further investigated by using various characterizations techniques like microstructure/composition analysis of the corroded specimens by utilizing SEM/EDS techniques. The various corrosion parameters obtained from the Tafle extrapolation curves are listed in Table 5.3. From Table 5.3, it has been reported that current density of uncoated steel in Ringers solution (0.56) is significantly high than the microwave surface modified specimens at all conditions (as-deposited as well as 700 °C heat-treated specimens). Therefore, the application of microwave assisted surface treatment on the 31254SS steel helps to enhance the corrosion resistance of the surface layer of microwave treated specimens. Thus, the microwave assisted surface modification with HA, HA+10wt%Al₂O₃ and HA+10wt%ZrO₂ have desired and beneficial effects on the corrosion behaviour of the SS-31254 steel, which is required for the implant material for prevention of metallic ion release in the human body. The results are in agreement with earlier findings also where the surface layer of the metallic implant was coated with HA and HA with reinforcement particles (Al₂O₃, ZrO₂ and TiO₂) in suitable quantity in the HA matrix (Fathi et al., 2003; Kannan et al., 2003; Sridhar et al., 2003; Singh et al., 2018). Further, From Table 5.3, it has been observed that the heat-treated microwave modified specimens have low corrosion current density followed by as-sprayed coated specimens and then followed by

uncoated base metal. Thus the heat-treated specimens have higher corrosion resistance (low corrosion current density) amongst all the specimens. The low corrosion rate for the heat-treated microwave assisted surface modified specimens was due to densification of coatings after the application of heat-treatment on the microwave treated specimens. The heat-treatment results in improvement in the densification of coatings through reduction of pores in it. Moreover, there is a conversion of non-apatite phases (TCP and TTCP) into crystalline phases after the application of heat-treatment, which further reduces the corrosion rate of the heat-treated specimens because these phases have higher dissolution rate in the Ringer solution. The results endorsed the earlier findings also (Singh et al., 2018).

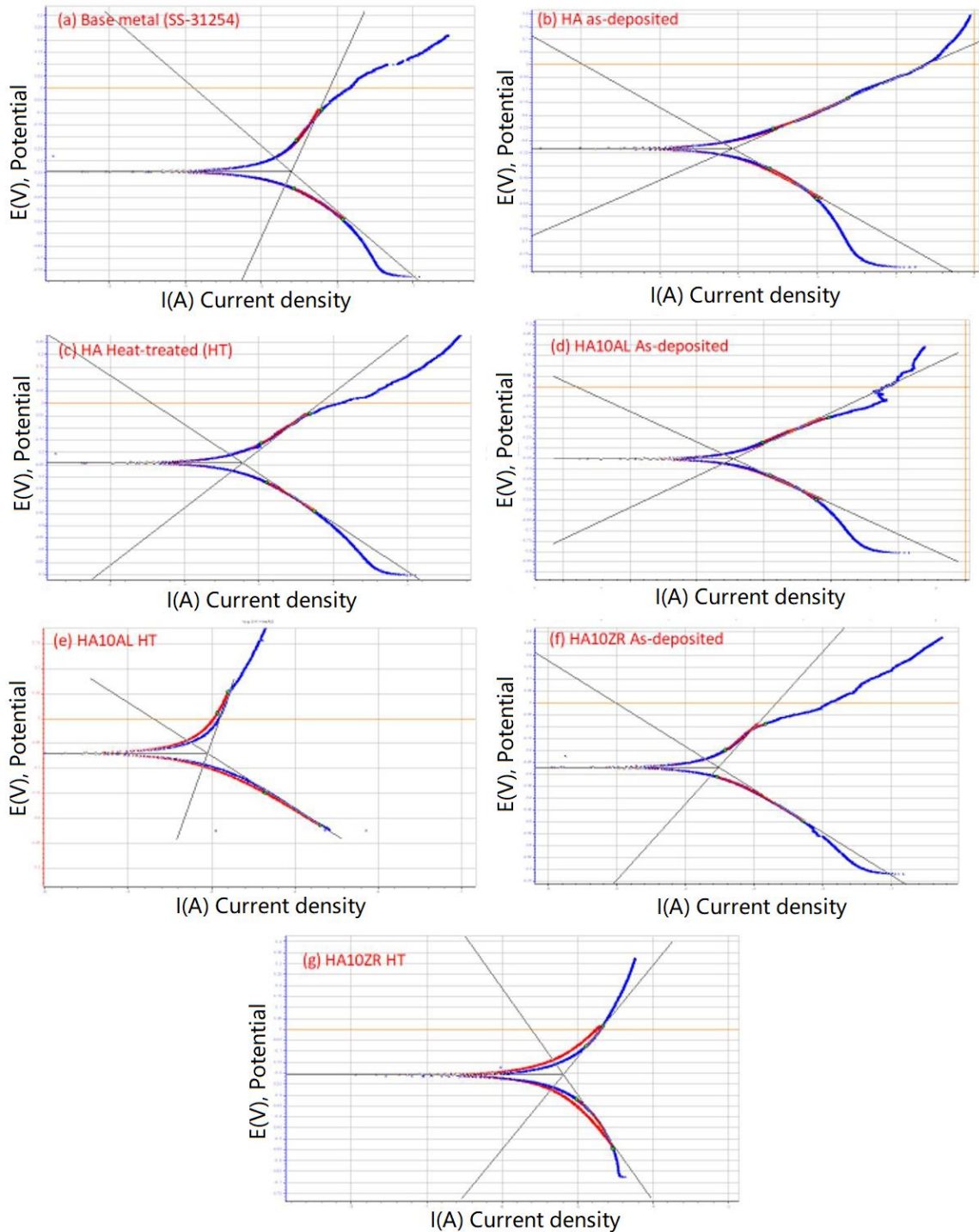


Fig. 5.4 Tafel plot curves for (a) base metal (b) HA in as-deposited condition (c) HA heat-treated (HT) condition (d) HA10AL as-deposited (e) HA10AL heat-treated (HT) (f) HA10ZR as-deposited (g) HA10ZR heat-treated (HT) condition.

Table 5.3 Various Corrosion parameters of the un-coated 254SS and the microwave surface modified samples at all conditions in Ringer’s solution at 37 ± 1 °C temperature.

Parameters	HA modified	HA modified (HT at 700 °C)	HA+10wt% Al ₂ O ₃ modified	HA+10wt% Al ₂ O ₃ modified (HT at 700 °C)	HA+10wt% ZrO ₂ modified	HA+10wt% ZrO ₂ modified. (HT at 700 °C)	Uncoated
E _{Corr} (mV)	-332.54	-241.9	-350.564	-69.496	-270.683	-208.220	-340.737
I _{Corr} (μ Acm ⁻²)	0.853	0.607	0.350	0.089	0.281	0.006	1.320

The SEM micrograph of the corroded base material is presented in **Fig.5.5**. The base material surface morphology has shown the occurrence of severe pits formed on the surface after subjected to corrosion test. This has attributed to the ions exchange between the electrolyte and metal during the test. The SEM micrographs of the HA in as-deposited condition has also shown pits (**Fig.5.6a**) and its condition has been enhanced when annealed at 700 °C (**Fig.5.6b**), which decreases the porosity level, thereby increasing the corrosion resistance. When Al₂O₃ was added to the HA, the corrosion resistance has increased and even further improved in case of annealed clad as shown in **Fig.5.6cand d**. This has attributed to the **addition of Al₂O₃** inert particles into the HA. The addition of ZrO₂ showed the highest corrosion resistance as compared to HA and HA10AL clads because of its corrosion resistance capability as shown in **Fig.5.6eand f**. The ringer’s solution has not attacked much the surface of ZrO₂ reinforced claddings.

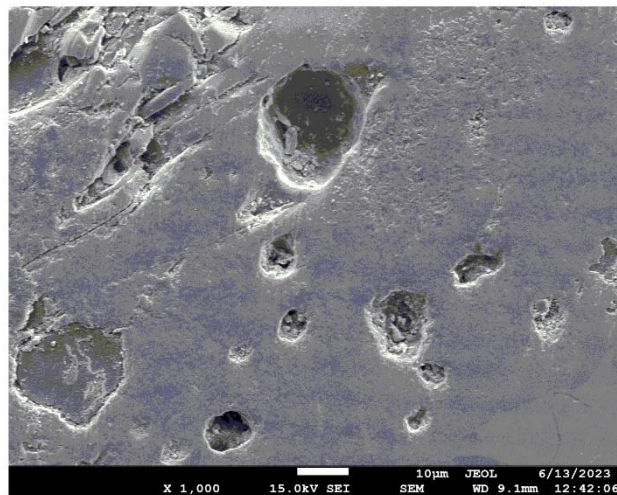


Fig. 5.5 SEM micrograph of corroded base material.

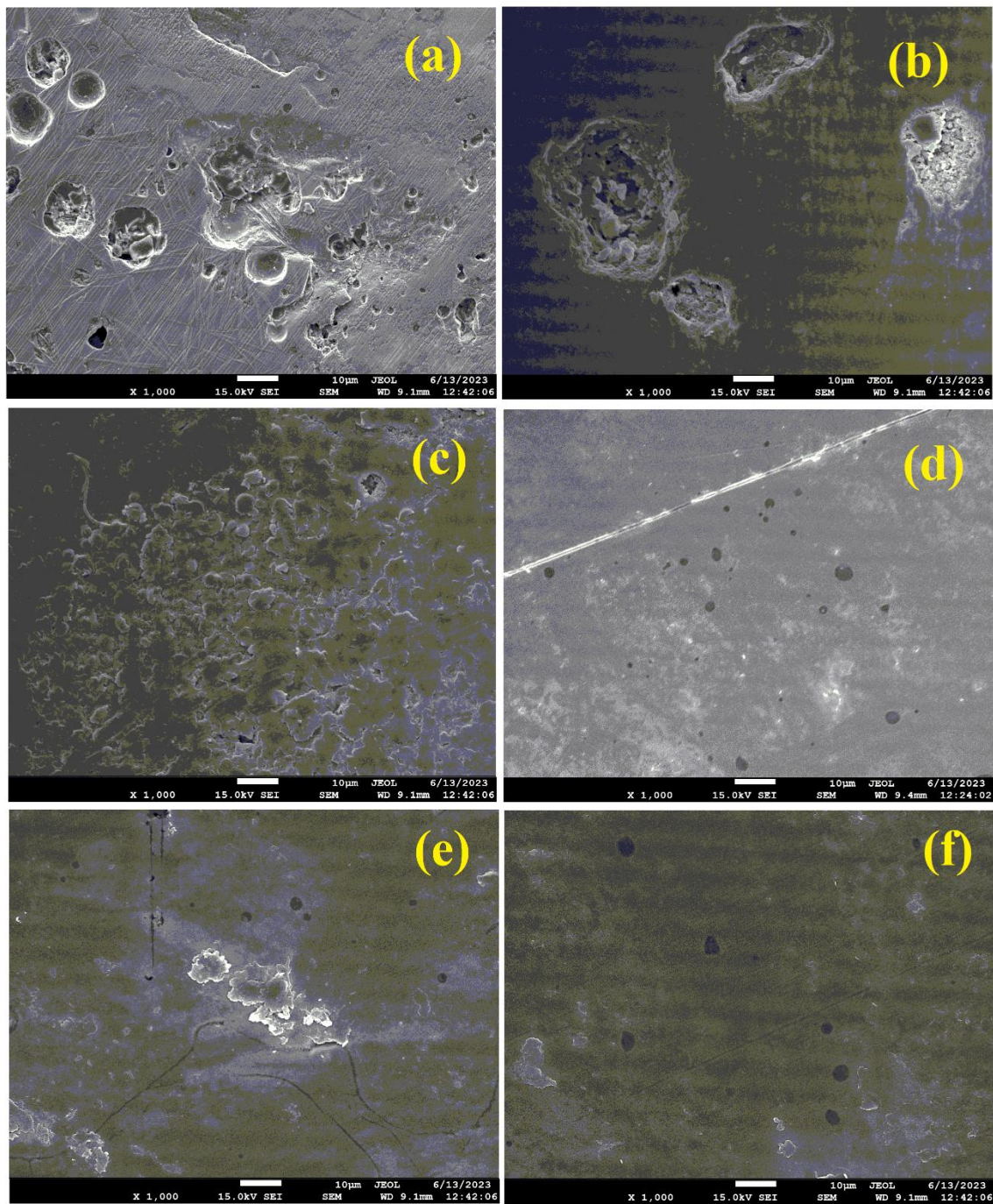


Fig. 5.6 (a) HA in as-deposited condition (b) HA heat-treated (HT) condition (c) HA10AL as-deposited (d) HA10AL heat-treated (HT) (e) HA10ZR as-deposited (f) HA10ZR heat-treated (HT) condition

5.4 SUMMARY

The in-vitro biocompatibility study of the base metal and hybrid MH assisted surface modified specimens at all conditions were investigated by immersing the samples. The SEM micrographs of the unmodified and modified SS-31254 alloy indicates that there is no apatite formation of layer was observed in the unmodified SS-31254 alloy. On the other hand, there is a formation of precipitation of the apatite layer was observed on the microwave assisted surface modified specimens at all conditions. Further the apatite layer formation was decreases in the heat-treated specimens due to densification of pores after this heat-treatment because pores will grow more rapidly on the pores or amorphous phase as compared to the crystalline structure. The electrochemical corrosion behavior of the base metal and hybrid MH assisted surface modified specimens at all conditions were investigated in a Ringer solution at room temperature by employing electrochemical technique. It has been found that the corrosion rate of the base metal was high as compared to the hybrid MH assisted surface modified specimens at all conditions. Further, the results indicate that the heat-treated specimens at all conditions exhibit improved corrosion resistance.

Chapter 6

CONCLUSIONS AND FUTURE SCOPE

The metallic materials in a pure or alloy form are widely applied as bio-implants in human body for several clinical applications due to their excellent mechanical properties and reasonable biocompatibility. Research and development on metallic biomaterials has shown that surface coating/ modifications of metallic implants by using a suitable bioactive material is a widely accepted alternative to minimize the harmful effects of corrosion.

In the present research work, a microwave assisted surface modifications has been used in metallic implants (SS-31254) by using hydroxyapatite (HA) coatings. Microwave heating is well known for uniform and volumetric heating of materials at molecular level. The uniform and volumetric heating attributes associated with this heating reduces processing time significantly and resulted in better microstructures and properties of the materials as compared to the conventional processing of materials. SS-31254 is a widely used material in clinical applications. However, it has poor biocompatibility when these materials are actually used in the human body system. Therefore, the surface layer of SS-31254 was modified with bioactive HA powder by using microwave energy. Because the HA coatings is very brittle in nature. Therefore, the effect of additions of reinforcement (Al_2O_3 and ZrO_2 by weight in 10%) in HA in suitable amount has also been discussed. The effect of heat-treatment on the microwave surface modified samples at all conditions at 700°C has also been described.

6.1 CONCLUSIONS

6.1.1 Major Conclusions of the present work

Based upon experimental results obtained and its analysis in the present work, the following conclusions have been drawn:

- It is possible to modify the surface properties of the SS-31254 by using HA, HA+10wt%Al₂O₃ and HA+10wt%ZrO₂ based bioactive powders by using the principles of hybrid MH associated with microwave energy.
- The modification of surface properties of SS-31254 by using HA, HA+10wt%Al₂O₃ and HA+10wt%ZrO₂ was carried out in a multimode home microwave applicator operating at 2.45 GHz at 900 W by using hybrid MH technique.
- The surface modification process has achieved full metallurgy bond with the substrate (SS-31254), and the modified surface layer was free from major processing defects like interface cracking.
- The as-deposited surface modified specimens at all conditions (HA, HA10AL, and HA10ZR) and heat-treated at 700 °C for 1 hr to improve its mechanical properties by conversion of amorphous phase into crystalline structure in the modified surface layer.
- Based on the X-ray diffraction (XRD) and scanning electron microscopy/energy-dispersive spectroscopy (SEM/EDS) analyses, it has been determined that the surface modification layer resulting from microwave-assisted treatment consists primarily of austenite dendrites composed of nickel-iron (Ni-Fe) alloy. Additionally, the inter-dendritic regions contain hydroxyapatite (HA) and various reaction products. The modified SS-31254 layers consists of a composite microstructure in which the inter-dendritic HA along with undesirable phases FeP, Fe₂P, and Fe₃P are embedded in the austenite dendrite matrix.
- Partial mutual diffusion of elements and the growth of grains reaching from the diluted substrate towards the clad indicate that the modified surface layer is metallurgically bonded with the medical grade stainless-steel substrate (SS-31254).

- The clads that were created and the specimens that underwent heat treatment demonstrate a notable reduction in porosity, with levels measuring below 2.5%. The significant low porosity observed in the clad specimens at all conditions (as-deposited as well as heat-treated) due to hybrid MH process.
- The modified SS-31254 layers exhibit higher microhardness than the unmodified SS-31254 layers. The modified SS-31254 alloy substrate surface showed enhanced microhardness which is beneficial for wear resistance applications of bio-implant.
- The microwave surface modified samples displayed increased microhardness and the porosity level shows the reverse trends with increasing temperature. The maximum hardness and minimum porosity level were observed in the 700 °C heat-treated samples due to maximum temperature involved in it.
- The bioactivity of the modified layer is determined by the quick development of bone-like apatite on it during an SBF immersion test. The modified SS-31254 alloy substrate surface showed the presence apatite and the bioactivity decreases as the heat-treatment temperature rises.
- The heat-treatment resulted in the densification of the composite layer by covering pores and voids in it. The pore/void act as a nucleating site for apatite to grow onto it. Therefore, the as-deposited surface modified sample exhibited maximum apatite layer formation followed by 700 °C heat-treated sample, and then uncoated samples.
- Corrosion analysis shows that the 254SS steel, necessary for the implant material to avoid metallic ion release in the human body, responds favourably to microwave-assisted surface modification with HA, HA+10wt%Al₂O₃, and HA+10wt%ZrO₂.
- Corrosion current density was found to be lowest in heat-treated microwave-modified specimens, followed by as-sprayed covered specimens, and finally by

uncoated base metal. This means that the heat-treated samples have the lowest corrosion current density and the highest corrosion protection. Densification of surfaces after heat-treatment on the microwave treated specimens was the reason for the low corrosion rate observed in these samples.

6.2 MAJOR CONTRIBUTION OF THE PRESENT WORK

1. The modification of surface properties of the SS-31254 by utilizing HA, HA+10wt%Al₂O₃ and HA+10wt%ZrO₂ has been successfully demonstrated.
2. Structure property correlation in as-deposited and heat-treated SS-31254 specimens have been explained in terms of metallurgical, mechanical, in-vitro bioactive study and corrosion aspects.
3. Contribution to the knowledge repository of microwave assisted surface modification in terms of experimental data, in-vitro bioactive study and corrosion behaviour of the surface modified SS-31254 specimens at all conditions.

6.3 SCOPE FOR FUTURE WORK

The present investigation opens up several opportunities for future work. Some of scopes can be summarised as follows:

1. Nano HA powder could be used instead of micron sized HA based powder and results can be compared.
2. The clads can be fabricated using single mode applicator and results can be compared with that of the multimode applicator.
3. The clads can be fabricated using frequency such as 30 GHz and higher power (such as 6.0 kW), and results can be compared.
4. The in-vivo test of the surface modified SS-31254 may also performed for used in actual applications.

5. A unique novel futuristic method of surface modification via electrical discharge machining (EDM) can be used for the processing of biomaterials.

BIBLIOGRAPHY

1. Awasthi, S., Pandey, S.K., Arunan, E. and Srivastava, C., 2021. A review on hydroxyapatite coatings for the biomedical applications: Experimental and theoretical perspectives. *Journal of Materials Chemistry B*, 9(2), pp.228-249.
2. Balamurugan, A., Kannan, S. and Rajeswari, S., 2002. Bioactive sol-gel hydroxyapatite surface for biomedical applications--in vitro study. *Trends in Biomaterials and Artificial Organs*, 16(1), p.18-21.
3. Balani, K., Anderson, R., Laha, T., Andara, M., Tercero, J., Crumpler, E. and Agarwal, A., 2007. Plasma-sprayed carbon nanotube reinforced hydroxyapatite coatings and their interaction with human osteoblasts in vitro. *Biomaterials*, 28(4), pp.618-624.
4. Balla, V.K., Das, M., Bose, S., Ram, G.J. and Manna, I., 2013. Laser surface modification of 316 L stainless steel with bioactive hydroxyapatite. *Materials Science and Engineering: C*, 33(8), pp.4594-4598.
5. Bansal, A. and Zafar, S., 2017. Influence of heat treatment on microstructure and mechanical properties of Inconel-625 clad deposited on mild steel.
6. Bauer, S., Schmuki, P., Von Der Mark, K. and Park, J., 2013. Engineering biocompatible implant surfaces: Part I: Materials and surfaces. *Progress in Materials Science*, 58(3), pp.261-326.
7. Beheri, H.H., Mohamed, K.R. and El-Bassyouni, G.T., 2013. Mechanical and microstructure of reinforced hydroxyapatite/calcium silicate nano-composites materials. *Materials and Design*, 44, pp.461-468.
8. Bellucci, D., Veronesi, E., Strusi, V., Petrachi, T., Murgia, A., Mastroia, I., Dominici, M. and Cannillo, V., 2019. Human mesenchymal stem cell combined with a new strontium-enriched bioactive glass: An ex-vivo model for bone regeneration. *Materials*, 12(21), p.3633.
9. Bergant, Z. and Grum, J., 2009. Quality improvement of flame sprayed, heat treated, and remelted NiCrBSi coatings. *Journal of thermal spray technology*, 18(3), pp.380-391.
10. Bergant, Z., Trdan, U. and Grum, J., 2014. Effect of high-temperature furnace treatment on the microstructure and corrosion behavior of NiCrBSi flame-sprayed coatings. *Corrosion Science*, 88, pp.372-386.

11. Bergmann, C.P. and Vicenzi, J., 2011. Protection against erosive wear using thermal sprayed cermet: a review. *Protection against Erosive Wear Using Thermal Sprayed Cermet*, pp.1-77.
12. Birks, N., Meier, G.H. and Pettit, F.S., 2006. *Introduction to the high temperature oxidation of metals*. Cambridge university press.
13. Bolelli, G., Lusvarghi, L. and Barletta, M., 2008a. Heat treatment effects on the corrosion resistance of some HVOF-sprayed metal alloy coatings. *Surface and Coatings Technology*, 202(19), pp.4839-4847.
14. Bolelli, G., Lusvarghi, L. and Giovanardi, R., 2008b. A comparison between the corrosion resistances of some HVOF-sprayed metal alloy coatings. *Surface and Coatings Technology*, 202(19), pp.4793-4809.
15. Boulos, M.I., Fauchais, P.L. and Heberlein, J.V., 2021. *Thermal spray fundamentals: from powder to part*. Springer International Publishing.
16. Calvarin, G., Molins, R. and Huntz, A.M., 2000. Oxidation mechanism of Ni—20Cr foils and its relation to the oxide-scale microstructure. *Oxidation of Metals*, 53(1), pp.25-48.
17. Campo, M., Carboneras, M., López, M.D., Torres, B., Rodrigo, P., Otero, E. and Rams, J., 2009. Corrosion resistance of thermally sprayed Al and Al/SiC coatings on Mg. *Surface and Coatings Technology*, 203(20-21), pp.3224-3230.
18. Carlisle, E.M., 1970. Silicon: a possible factor in bone calcification. *Science*, 167(3916), pp.279-280.
19. Chatha, S.S., Sidhu, H.S. and Sidhu, B.S., 2013. High-temperature behavior of a NiCr-coated T91 boiler steel in the platen superheater of coal-fired boiler. *Journal of thermal spray technology*, 22(5), pp.838-847.
20. Chatha, S.S., Sidhu, H.S. and Sidhu, B.S., 2016. Performance of 75Cr3C2-25NiCr coating produced by HVOF process in a coal-fired thermal power plant. In *Advanced Materials Research* (Vol. 1137, pp. 88-100). Trans Tech Publications Ltd.
21. Chatterjee, U.K., Bose, S.K. and Roy, S.K., 2001. *Environmental degradation of metals: corrosion technology series/14*. CRC Press.

22. Chen, H., Zhang, E. and Yang, K., 2014. Microstructure, corrosion properties and bio-compatibility of calcium zinc phosphate coating on pure iron for biomedical application. *Materials Science and Engineering: C*, 34, pp.201-206.
23. Chen, Y., Xu, Z., Smith, C. and Sankar, J., 2014. Recent advances on the development of magnesium alloys for biodegradable implants. *Acta biomaterialia*, 10(11), pp.4561-4573.
24. Chen, Y., Zhang, T.H., Gan, C.H. and Yu, G., 2007. Wear studies of hydroxyapatite composite coating reinforced by carbon nanotubes. *Carbon*, 45(5), pp.998-1004.
25. Chou, B.Y. and Chang, E., 2002. Plasma-sprayed hydroxyapatite coating on titanium alloy with ZrO₂ second phase and ZrO₂ intermediate layer. *Surface and Coatings Technology*, 153(1), pp.84-92.
26. Ctibor, P., Lechnerová, R. and Beneš, V., 2006. Quantitative analysis of pores of two types in a plasma-sprayed coating. *Materials Characterization*, 56(4-5), pp.297-304.
27. Daram, P. and Banjongprasert, C., 2020. The influence of post treatments on the microstructure and corrosion behavior of thermally sprayed NiCrMoAl alloy coating. *Surface and Coatings Technology*, 384, p.125166.
28. Das, A. and Shukla, M., 2019. Surface morphology, bioactivity, and antibacterial studies of pulsed laser deposited hydroxyapatite coatings on stainless steel 254 for orthopedic implant applications. *Proceedings of the Institution of Mechanical Engineers, Part L: Journal of Materials: Design and Applications*, 233(2), p.120-127.
29. Davis, J.R. ed., 2004. *Handbook of thermal spray technology*. ASM international.
30. Deb, D., Iyer, S.R. and Radhakrishnan, V.M., 1996. A comparative study of oxidation and hot corrosion of a cast nickel base superalloy in different corrosive environments. *Materials Letters*, 29(1-3), pp.19-23.
31. Dehnavi, F., Eslami, A. and Ashrafizadeh, F., 2017. A case study on failure of superheater tubes in an industrial power plant. *Engineering Failure Analysis*, 80, pp.368-377.
32. Delaunay, F., Berthier, C., Lenglet, M. and Lameille, J.M., 2000. SEM-EDS and XPS studies of the high temperature oxidation behaviour of Inconel 718. *Microchimica Acta*, 132(2), pp.337-343.

33. Deng, K., Shi, J., Wang, C., Wang, X., Wu, Y., Nie, K. and Wu, K., 2012a. Microstructure and strengthening mechanism of bimodal size particle reinforced magnesium matrix composite. *Composites Part A: Applied Science and Manufacturing*, 43(8), pp.1280-1284.
34. Deng, K.K., Wang, X.J., Wang, C.J., Shi, J.Y., Hu, X.S. and Wu, K., 2012b. Effects of bimodal size SiC particles on the microstructure evolution and fracture mechanism of AZ91 matrix at room temperature. *Materials Science and Engineering: A*, 553, pp.74-79.
35. Deuerling, C., Maguhn, J., Nordsieck, H., Benker, B., Zimmermann, R. and Warnecke, R., 2009. Investigation of the mechanisms of heat exchanger corrosion in a municipal waste incineration plant by analysis of the raw gas and variation of operating parameters. *Heat transfer engineering*, 30(10-11), pp.822-831.
36. Doleker, K.M., Odabas, O., Ozgurlok, Y., Askerov, H. and Karaoglanli, A.C., 2019. Effect of high temperature oxidation on Inconel 718 and Inconel 718/YSZ/Gd₂Zr₂O₇. *Materials Research Express*, 6(8), p.086456.
37. Dooley, R. and Wiertel, E., 2009, January. A survey of erosion and corrosion resistant materials being used on boiler tubes in waste to energy boilers. In *North American Waste-to-Energy Conference* (Vol. 48807, pp. 37-41).
38. Eliaz, N., Shemesh, G. and Latanision, R.M., 2002. Hot corrosion in gas turbine components. *Engineering failure analysis*, 9(1), pp.31-43.
39. Fathi, M.H., Salehi, M.A.H.D.I., Saatchi, A., Mortazavi, V. and Moosavi, S.B., 2003. In vitro corrosion behavior of bioceramic, metallic, and bioceramic–metallic coated stainless steel dental implants. *Dental materials*, 19(3), p.188-198.
40. Fontana, M.G., Corrosion Engineering, 3rd ed., McGraw-Hill Book Company, New York, (1987).
41. Frazier, W.E., 2014. Metal additive manufacturing: a review. *Journal of Materials Engineering and performance*, 23(6), pp.1917-1928.
42. Fu, L., Khor, K.A. and Lim, J.P., 2000. Yttria stabilized zirconia reinforced hydroxyapatite coatings. *Surface and Coatings Technology*, 127(1), pp.66-75.

43. Gao, T., Aro, H.T., Ylänen, H. and Vuorio, E., 2001. Silica-based bioactive glasses modulate expression of bone morphogenetic protein-2 mRNA in Saos-2 osteoblasts in vitro. *Biomaterials*, 22(12), pp.1475-1483.
44. Geetha, M., Singh, A.K., Asokamani, R. and Gogia, A.K., 2009. Ti based biomaterials, the ultimate choice for orthopaedic implants—a review. *Progress in materials science*, 54(3), p. 397-425.
45. Gross, K.A., Gross, V. and Berndt, C.C., 1998. Thermal analysis of amorphous phases in hydroxyapatite coatings. *Journal of the American Ceramic Society*, 81(1), pp.106-112.
46. Gu, Y.W., Khor, K.A., Pan, D. and Cheang, P., 2004. Activity of plasma sprayed yttria stabilized zirconia reinforced hydroxyapatite/Ti–6Al–4V composite coatings in simulated body fluid. *Biomaterials*, 25(16), pp.3177-3185.
47. Hannink, G. and Arts, J.C., 2011. Bioresorbability, porosity and mechanical strength of bone substitutes: what is optimal for bone regeneration?. *Injury*, 42, pp.S22-S25.
48. He, J.L., Chen, K.C., Chen, C.C., Leyland, A. and Matthews, A., 2001. Cyclic oxidation resistance of Ni–Al alloy coatings deposited on steel by a cathodic arc plasma process. *Surface and Coatings Technology*, 135(2-3), pp.158-165.
49. Hench, L.L. and Polak, J.M., 2002. Third-generation biomedical materials. *Science*, 295(5557), pp.1014-1017.
50. Hijón, N., Cabanas, M.V., Pena, J. and Vallet-Regí, M., 2006. Dip coated silicon-substituted hydroxyapatite films. *Acta Biomaterialia*, 2(5), pp.567-574.
51. Hofmann, D.C., Roberts, S., Otis, R., Kolodziejska, J., Dillon, R.P., Suh, J.O., Shapiro, A.A., Liu, Z.K. and Borgonia, J.P., 2014. Developing gradient metal alloys through radial deposition additive manufacturing. *Scientific reports*, 4(1), pp.1-8.
52. <https://nrc.canada.ca/en/research-development/research-collaboration/industrial-rd-groups/cold-spray-additive-manufacturing-csam-industrial-rd-group>.
53. https://www.impact-innovations.com/en/coldgas/cg_index_en.html.
54. <https://www.spee3d.com/>.
55. Huang, Y., Hao, M., Nian, X., Qiao, H., Zhang, X., Zhang, X., Song, G., Guo, J., Pang, X. and Zhang, H., 2016. Strontium and copper co-substituted hydroxyapatite-based coatings with improved antibacterial activity and cytocompatibility fabricated by electrodeposition. *Ceramics International*, 42(10), pp.11876-11888.
56. ITIRAVIVONG, P., 2001. Biomaterials: an Overview. *Journal of Metals, Materials and Minerals*, 11(1), pp. 15-21.
57. Kamachimudali, U., Sridhar, T.M. and Raj, B., 2003. Corrosion of bio implants. *Sadhana*, 28, p. 601-637.

58. Kannan, S., Balamurugan, A. and Rajeswari, S., 2003. Hydroxyapatite coatings on sulfuric acid treated type 316L SS and its electrochemical behaviour in Ringer's solution. *Materials letters*, 57(16-17), p. 2382-2389.
59. Kaushal, S., Gupta, D. and Bhowmick, H., 2018. On processing of Ni-Cr₃C₂ based functionally graded clads through microwave heating. *Materials Research Express*, 5(6), p.066405.
60. Kaya, C., 2008. Electrophoretic deposition of carbon nanotube-reinforced hydroxyapatite bioactive layers on Ti-6Al-4V alloys for biomedical applications. *Ceramics International*, 34(8), pp.1843-1847.
61. Li, H., Khor, K.A. and Cheang, P., 2002. Properties of heat-treated calcium phosphate coatings deposited by high-velocity oxy-fuel (HVOF) spray. *Biomaterials*, 23(10), pp.2105-2112.
62. Li, H., Khor, K.A. and Cheang, P., 2002. Titanium dioxide reinforced hydroxyapatite coatings deposited by high velocity oxy-fuel (HVOF) spray. *Biomaterials*, 23(1), pp.85-91.
63. Li, H., Khor, K.A., Kumar, R. and Cheang, P., 2004. Characterization of hydroxyapatite/nano-zirconia composite coatings deposited by high velocity oxy-fuel (HVOF) spray process. *Surface and Coatings Technology*, 182(2-3), pp.227-236.
64. Lin, K., Zhang, M., Zhai, W., Qu, H. and Chang, J., 2011. Fabrication and characterization of hydroxyapatite/wollastonite composite bioceramics with controllable properties for hard tissue repair. *Journal of the American Ceramic Society*, 94(1), pp.99-105.
65. Lysaght, M.J. and O'Loughlin, J.A., 2000. Demographic scope and economic magnitude of contemporary organ replacement therapies. *ASAIO journal*, 46(5), pp.515-521.
66. Mancini, C.E., Berndt, C.C., Sun, L. and Kucuk, A., 2001. Porosity determinations in thermally sprayed hydroxyapatite coatings. *Journal of materials science*, 36(16), pp.3891-3896.
67. Manivasagam, G., Dhinasekaran, D. and Rajamanickam, A., 2010. Biomedical implants: corrosion and its prevention-a review. *Recent patents on corrosion science*, 2(1). p. 40-54.
68. Marcelo, T., Mascarenhas, J.M. and Oliveira, F.A.C., 2010. Microwave sintering—a novel approach to powder technology. In *Materials Science Forum* (Vol. 636, pp. 946-951). Trans Tech Publications Ltd.

69. Martin, J.H., Yahata, B.D., Hundley, J.M., Mayer, J.A., Schaedler, T.A. and Pollock, T.M., 2017. 3D printing of high-strength aluminium alloys. *Nature*, 549(7672), pp.365-369.
70. Meng, Y.H., Tang, C.Y. and Tsui, C.P., 2008. Fabrication and characterization of needle-like nano-HA and HA/MWNT composites. *Journal of Materials Science: Materials in Medicine*, 19(1), pp.75-81.
71. Mohajernia, S., Pour-Ali, S., Hejazi, S., Saremi, M. and Kiani-Rashid, A.R., 2018. Hydroxyapatite coating containing multi-walled carbon nanotubes on AZ31 magnesium: Mechanical-electrochemical degradation in a physiological environment. *Ceramics International*, 44(7), pp.8297-8305.
72. Moridi, A., 2016. *Powder Consolidation Using Cold Spray: Process Modeling and Emerging Applications*. Springer.
73. Moridi, A., Hassani-Gangaraj, S.M., Guagliano, M. and Dao, M., 2014. Cold spray coating: review of material systems and future perspectives. *Surface Engineering*, 30(6), pp.369-395.
74. Moridi, A., Stewart, E.J., Wakai, A., Assadi, H., Gartner, F., Guagliano, M., Klassen, T. and Dao, M., 2020. Solid-state additive manufacturing of porous Ti-6Al-4V by supersonic impact. *Applied Materials Today*, 21, p.100865.
75. Nasab, M.B., Hassan, M.R. and Sahari, B.B., 2010. Metallic biomaterials of knee and hip-a review. *Trends Biomater. Artif. Organs*, 24(1), p. 69-82.
76. Ni, J., Ling, H., Zhang, S., Wang, Z., Peng, Z., Benyshek, C., Zan, R., Miri, A.K., Li, Z., Zhang, X. and Lee, J., 2019. Three-dimensional printing of metals for biomedical applications. *Materials Today Bio*, 3, p.100024.
77. Niinomi, M., 2008. Metallic biomaterials. *Journal of Artificial Organs*, 11, p.105-110.
78. Oshkour, A.A., Pramanik, S., Mehrali, M., Yau, Y.H., Tarlochan, F. and Osman, N.A.A., 2015. Mechanical and physical behavior of newly developed functionally graded materials and composites of stainless steel 316L with calcium silicate and hydroxyapatite. *Journal of the mechanical behavior of biomedical materials*, 49, p. 321-331.
79. Patterson, S.P., Daffner, R.H. and Gallo, R.A., 2005. Electrochemical corrosion of metal implants. *American Journal of Roentgenology*, 184(4), p. 1219-1222.
80. Rath, P.C., Besra, L., Singh, B.P. and Bhattacharjee, S., 2012. Titania/hydroxyapatite bi-layer coating on Ti metal by electrophoretic deposition: Characterization and corrosion studies. *Ceramics International*, 38(4), pp.3209-3216.
81. Rezaei, A., Golenji, R.B., Alipour, F., Hadavi, M.M. and Mobasherpour, I., 2020. Hydroxyapatite/hydroxyapatite-magnesium double-layer coatings as potential

- candidates for surface modification of 316 LVM stainless steel implants. *Ceramics International*, 46(16), pp.25374-25381.
82. Rocha, R.C., Galdino, A.G.D.S., Silva, S.N.D. and Machado, M.L.P., 2018. Surface, microstructural, and adhesion strength investigations of a bioactive hydroxyapatite-titanium oxide ceramic coating applied to Ti-6Al-4V alloys by plasma thermal spraying. *Materials Research*, 21(4).
 83. Roohani-Esfahani, S.I., Newman, P. and Zreiqat, H., 2016. Design and fabrication of 3D printed scaffolds with a mechanical strength comparable to cortical bone to repair large bone defects. *Scientific reports*, 6(1), pp.1-8.
 84. Roychowdhury, A., Gupta, S., Vidyasagara, P.E.C. and Pal, S., 2004. Wear studies of frequently used implant materials. *Trends in Biomaterials and Artificial Organs*, 17(2), pp.135-141.
 85. Sames, W.J., List, F.A., Pannala, S., Dehoff, R.R. and Babu, S.S., 2016. The metallurgy and processing science of metal additive manufacturing. *International materials reviews*, 61(5), pp.315-360.
 86. Singh, A., Singh, G. and Chawla, V., 2018. Influence of post coating heat treatment on microstructural, mechanical and electrochemical corrosion behaviour of vacuum plasma sprayed reinforced hydroxyapatite coatings. *Journal of the mechanical behavior of biomedical materials*, 85, pp.20-36.
 87. Singh, B., Singh, G. and Sidhu, B.S., 2018. Analysis of corrosion behavior and surface properties of plasma-sprayed HA/Ta coating on CoCr alloy. *Journal of Thermal Spray Technology*, 27(8), pp.1401-1413.
 88. Singh, B., Singh, G. and Sidhu, B.S., 2019. Investigation of the in vitro corrosion behavior and biocompatibility of niobium (Nb)-reinforced hydroxyapatite (HA) coating on CoCr alloy for medical implants. *Journal of Materials Research*, 34(10), pp.1678-1691.
 89. Singh, G., Singh, S. and Prakash, S., 2011. Post Heat Treatment of Plasma Sprayed Pure and Alumina-Titania Reinforced Hydroxyapatite Coating on SS 304 Steel. *Journal of Minerals and Materials Characterization and Engineering*, 10(2), pp.173-184.
 90. Singh, G., Singh, S. and Prakash, S., 2011. Surface characterization of plasma sprayed pure and reinforced hydroxyapatite coating on Ti6Al4V alloy. *Surface and Coatings Technology*, 205(20), pp.4814-4820.
 91. Singh, J., Chatha, S.S. and Singh, H., 2021. Characterization and corrosion behavior of plasma sprayed calcium silicate reinforced hydroxyapatite composite coatings for medical implant applications. *Ceramics International*, 47(1), pp.782-792.
 92. Singh, R. and Dahotre, N.B., 2007. Corrosion degradation and prevention by surface modification of biometallic materials. *Journal of Materials Science: Materials in Medicine*, 18(5), p. 725-751.

93. Singh, S., Pandey, K.K., Rahman, O.A., Haldar, S., Lahiri, D. and Keshri, A.K., 2020. Investigation of crystallinity, mechanical properties, fracture toughness and cell proliferation in plasma sprayed graphene nano platelets reinforced hydroxyapatite coating. *Materials Research Express*, 7(1), p.015415.
94. Sridhar, T.M., Mudali, U.K. and Subbaiyan, M., 2003. Preparation and characterisation of electrophoretically deposited hydroxyapatite coatings on type 316L stainless steel. *Corrosion Science*, 45(2), p. 237-252.
95. Tao, Y., Ke, G., Xie, Y., Chen, Y., Shi, S. and Guo, H., 2015. Adhesion strength and nucleation thermodynamics of four metals (Al, Cu, Ti, Zr) on AlN substrates. *Applied Surface Science*, 357, pp.8-13.
96. Tian, P., Hu, H., Wang, H., Liu, X. and Ding, C., 2014. TiO₂/CaF₂ composite coating on titanium for biomedical application. *Materials Letters*, 117, pp.98-100.
97. Tiwari, S. and Mishra, S.B., 2021. Post annealing effect on corrosion behavior, bacterial adhesion, and bioactivity of LVOF sprayed hydroxyapatite coating. *Surface and Coatings Technology*, 405, p.126500.
98. Tsui, Y.C., Doyle, C. and Clyne, T.W., 1998. Plasma sprayed hydroxyapatite coatings on titanium substrates Part 1: Mechanical properties and residual stress levels. *Biomaterials*, 19(22), pp.2015-2029.
99. Vasudev, H., Singh, G., Bansal, A., Vardhan, S. and Thakur, L., 2019. Microwave heating and its applications in surface engineering: a review. *Materials Research Express*, 6(10), p.102001.
100. Vayre, B., Vignat, F. and Villeneuve, F., 2012. Metallic additive manufacturing: state-of-the-art review and prospects. *Mechanics and Industry*, 13(2), pp.89-96.
101. Wang, G. and Zreiqat, H., 2010. Functional coatings or films for hard-tissue applications. *Materials*, 3(7), p. 3994-4050.
102. Wang, M., 2003. Developing novel biomaterials for new challenges. In *Materials Science and Technology in Engineering Conference Now, New and Next*, The Hong Kong Institution of Engineers, Hong Kong.
103. Wang, Y.M., Voisin, T., McKeown, J.T., Ye, J., Calta, N.P., Li, Z., Zeng, Z., Zhang, Y., Chen, W., Roehling, T.T. and Ott, R.T., 2018. Additively manufactured hierarchical stainless steels with high strength and ductility. *Nature materials*, 17(1), pp.63-71.
104. Williams, C.B., Cochran, J.K. and Rosen, D.W., 2011. Additive manufacturing of metallic cellular materials via three-dimensional printing. *The International Journal of Advanced Manufacturing Technology*, 53(1), pp.231-239.
105. Williams, D.F., 2003. Biomaterials and tissue engineering in reconstructive surgery. *Sadhana*, 28, p. 563-574.

106. Yang, C.W. and Lui, T.S., 2007. Effect of crystallization on the bonding strength and failures of plasma-sprayed hydroxyapatite. *Materials transactions*, 48(2), pp.211-218.
107. Yang, Y.C., Chen, C.C., Wang, J.B., Wang, Y.C. and Lin, F.H., 2017. Flame sprayed zinc doped hydroxyapatite coating with antibacterial and biocompatible properties. *Ceramics International*, 43, pp.S829-S835.
108. Yao, H.L., Wang, H.T., Bai, X.B., Ji, G.C. and Chen, Q.Y., 2018. Improvement in mechanical properties of nano-structured HA/TiO₂ multilayer coatings deposited by high velocity suspension flame spraying (HVSFS). *Surface and Coatings Technology*, 342, pp.94-104.
109. Yugeswaran, S., Yoganand, C.P., Kobayashi, A., Paraskevopoulos, K.M. and Subramanian, B., 2012. Mechanical properties, electrochemical corrosion and in-vitro bioactivity of yttria stabilized zirconia reinforced hydroxyapatite coatings prepared by gas tunnel type plasma spraying. *Journal of the mechanical behavior of biomedical materials*, 9, pp.22-33.
110. Zakaria, M.Y., Sulong, A.B., Muhamad, N., Raza, M.R. and Ramli, M.I., 2019. Incorporation of wollastonite bioactive ceramic with titanium for medical applications: An overview. *Materials Science and Engineering: C*, 97, pp.884-895.
111. Zhao, G.L., Wen, G.W. and Kun, W., 2009. Influence of processing parameters and heat treatment on phase composition and microstructure of plasma sprayed hydroxyapatite coatings. *Transactions of Nonferrous Metals Society of China*, 19, pp.s463-s469.
112. Zhao, Z., Du, L., Tao, Y., Li, Q. and Luo, L., 2016. Enhancing the adhesion strength of micro electroforming layer by ultrasonic agitation method and the application. *Ultrasonicsonochemistry*, 33, pp.10-17.
113. B. Beig, U. Liaqat, M. F. K. Niazi, I. Douna, M. Zahoor and M. B. K. Niazi, *Coatings* 10 (2020) 1249.
114. S. Bodhak, S. Bose and A. Bandyopadhyay, *Mater. Sci. Eng. C* 31 (2011) 755
115. Y. Chai et al., *Bioactive Mater.* 6 (2021) 4772.
116. A. Bartkowiak, A. Zarzycki, S. Kac, M. Perzanowski and M. Marszalek, *Materials* 13 (2020) 5290.
117. W. J. Basirun, B. Nasiri-Tabrizi and S. Baradaran, *Crit. Rev. Solid State Mater. Sci.* 43 (2018) 177.
118. F. E. Baştan et al., *Coll. Surf. B: Biointerf.* 169 (2018) 176.
119. J.A. Disegi, L. Eschbach, *Stainless steel in bone surgery, Injury* 31 (2001) 2–6.
120. M.L.C.A. Afonso, R.V. Jaimes, E.P.G. Arêas, M.R. Capri, E. Oliveira, S.M.L. Agostinho, The influence of albumin on the anodic dissolution of chromium present in UNS S31254 stainless steel in chloride environment, *Colloids Surf.* 317 (2008) 760–763.
121. Q. Chen, G.A. Thouas, *Metallic implant biomaterials, Mater. Sci. Eng. R. Rep.* 87 (2015) 1–57.
122. M.L.D.A. Afonso, R.F. Jaimes, P.A. Nascente, S.O. Rogero, S.M. Agostinho, Surface characterization, electrochemical behavior and cytotoxicity of UNS S31254 stainless steel for orthopedic applications, *Mater. Lett.* 148 (2015) 71–75.

123. A. Dziubińska, K. Majerski, E. Siemionek, Effect of forging temperature on the microstructure and properties of REX 734 implantable stainless steel, *Procedia Manuf* 15 (2018) 411–418.
124. E. Salahinejad, M.J. Hadianfard, D.D. Macdonald, S. Sharifi-Asl, M. Mozafari, K.J. Walker, A.T. Rad, S.V. Madihally, L. Tayebi, In vitro electrochemical corrosion and cell viability studies on nickel-free stainless steel orthopedic implants, *PLoS One* 8 (4) (2013) 61633.
125. R.F.V.V. Jaimes, M.L.C. de Andrade Afonso, S.O. Rogero, S.M.L. Agostinho, C.A. Barbosa, New material for orthopedic implants: electrochemical study of nickel free P558 stainless steel in minimum essential medium, *Mater. Lett.* 64 (13) (2010) 1476–1479.
126. L. De Micheli, A.H.P. Andrade, C.A. Barbosa, S.M.L. Agostinho, Electrochemical studies of 254SMO stainless steel in comparison with 316L stainless steel and Hastelloy C276 in phosphoric acid media in absence and presence of chloride ions, *Br. Corros. J.* 34 (1) (1999) 67–70.
127. E.A. El Meguid, A.A. El Latif, Critical pitting temperature for type 254 SMO stainless steel in chloride solutions, *Corros. Sci.* 49 (2) (2007) 263–275.
128. A. Das, M. Shukla, Hydroxyapatite coatings on high nitrogen stainless steel by laser rapid manufacturing, *JOM* 69 (11) (2017) 2292–2296.
129. A. Subash, A. Basanth and B. Kandasubramanian, *Int. J. Polym. Mater. Polym. Biomater.* (2022) 1.
130. L. Sun, C. C. Berndt and K. A. Gross, *J. Biomater. Sci. Polym. Ed.* 13 (2002) 977.
131. R. B. Thompson et al., *Proc. Natl. Acad. Sci.* 112 (2015) 1565.
132. A. Vladescu et al., *Biomed. Mater.* 13 (2018) 025011.
133. N. Vladislavić, I. Š. Rončević, M. Buzuk, M. Buljac and I. Drventić, *J. Solid State Electrochem.* 25 (2021) 841.
134. Tiwari, S. and Mishra, S.B., 2021. Post annealing effect on corrosion behavior, bacterial adhesion, and bioactivity of LVOF sprayed hydroxyapatite coating. *Surface and Coatings Technology*, 405, p.126500.

List of Publications

- Pardeep Singh et. al. “Effect of post heat-treatment on the microstructural, mechanical and bioactivity behavior of the microwave-assisted alumina reinforced hydroxyapatite cladding”, Part E: Journal of Process Mechanical Engineering-SAGE PUBLISHER; (2021) –SCI –I.F-1.6.

Special issue: Materials Engineering


Institution of
**MECHANICAL
ENGINEERS**



Effect of post-heat treatment on the microstructural, mechanical, and bioactivity behavior of the microwave-assisted alumina-reinforced hydroxyapatite cladding

Proc IMechE Part E:
J Process Mechanical Engineering
1–12
© IMechE 2022
Article reuse guidelines:
sagepub.com/journals-permissions
DOI: 10.1177/09544089221116168
journals.sagepub.com/home/pie



Pardeep Singh¹, Hitesh Vasudev¹ and Amit Bansal² 

Abstract

The current research involves using microwave energy to modify the surface layer of UNS S31254 stainless steel in order to improve its bioactivity by cladding it with alumina-reinforced hydroxyapatite. For the microwave surface modification process, an industrial microwave oven supported by an infrared pyrometer and functioned at 1.1 kW and 2.45 GHz was utilized. In addition, the surface-modified samples were thermally heat-treated in a muffle furnace for 1 h at three different temperatures 400°C, 600°C, and 800°C. Scanning electron microscopy, energy-dispersive spectroscopy, X-ray diffractometer, and simulated bodily fluid testing were used to investigate the metallographic, compositional, phase analysis, and bioactivity of microwave surface-modified samples. The presence of alumina in the microwave surface-modified samples was confirmed by X-ray diffractometer analysis. The microwave-assisted surface modification layer contains predominantly iron (Ni-Fe)-based austenite dendrites, as well as hydroxyapatite and certain reaction products, mostly in the interdendritic areas, according to the microstructural analysis. The results indicate that the heat-treated surface-modified samples exhibit lower porosity and higher hardness than the as-deposited surface-modified samples. Furthermore, the 800°C heat-treated samples exhibited the lowest porosity (about 56% less than that of the as-deposited sample) and maximum hardness (about 23.5% more than the as-deposited sample) among all the heat-treated samples. The bone binding ability of the surface-modified samples was decreased after heat treatment due to the reduction of pores and amorphous phase after the heat treatment process.

- Pardeep Singh, Hitesh Vasudev, Amit Bansal “In situ surface modification of stainless steel with hydroxyapatite using microwave heating”, *Surface Topography: Metrology and Properties*; (2021).

IOP Publishing

Surf. Topogr.: Metrol. Prop. **9** (2021) 035053

<https://doi.org/10.1088/2051-672X/ac28a9>

Surface Topography: Metrology and Properties



CrossMark

PAPER



In situ surface modification of stainless steel with hydroxyapatite using microwave heating

RECEIVED
29 June 2021

REVISED
2 September 2021

ACCEPTED FOR PUBLICATION
21 September 2021

PUBLISHED
30 September 2021

Pardeep Singh¹, Amit Bansal² , Hitesh Vasudev³  and Parmjit Singh⁴

¹ School of Mechanical Engineering; Lovely Professional University, Phagwara-144411, India

² Department of Mechanical Engineering; IK Gujral Punjab Technical University, Jalandhar-144603, India

³ School of Mechanical Engineering; Lovely Professional University, Phagwara-144411, India

⁴ Department of Mechanical Engineering; IK Gujral Punjab Technical University, Jalandhar-144603, India

E-mail: amit.bansal978@gmail.com

Keywords: SS-316L, HAP, microwave, apatite, heating

Conference Presentations

Certificate ID: NCTSEM/TECH/7

NCTSEM'22 

NATIONAL CONFERENCE
ON TRENDS IN SCIENCE, ENGINEERING & MANAGEMENT

31th May, 2022

CERTIFICATE

This is to certify that Dr./ Mr./ Ms. **Pardeep Singh** has actively Participated/
Presented paper on **Surface modification of stainless steel with hydroxyapatite using microwave heating** in the **NATIONAL CONFERENCE ON TRENDS IN SCIENCE, ENGINEERING & MANAGEMENT(NCTSEM'22)** organized by Gulzar Group of Institutions, Ludhiana (Punjab)


Dr. Deepti Sharma
Organizing Secretary


Dr. Sarbjeet Kaushal
Organizing Secretary


Dr. Sukhdev Singh
Dean Research, GGI


Dr. Honey Sharma
Convener

GULZAR GROUP OF INSTITUTES Campus: GT Road, Ludhiana (Pb.) | Email: info@ggi.ac.in
Helpline: +91 9914 666 777

Certificate ID: NCTSEM/TECH/6

NCTSEM'22 

NATIONAL CONFERENCE
ON TRENDS IN SCIENCE, ENGINEERING & MANAGEMENT

31th May, 2022

CERTIFICATE

This is to certify that Dr./ Mr./ Ms. **Pardeep Singh** has actively Participated/
Presented paper on **Study of alumina reinforced HA cladding processed using microwave route** in the **NATIONAL CONFERENCE ON TRENDS IN SCIENCE, ENGINEERING & MANAGEMENT(NCTSEM'22)** organized by Gulzar Group of Institutions, Ludhiana (Punjab)


Dr. Deepti Sharma
Organizing Secretary


Dr. Sarbjeet Kaushal
Organizing Secretary


Dr. Sukhdev Singh
Dean Research, GGI


Dr. Honey Sharma
Convener

GULZAR GROUP OF INSTITUTES Campus: GT Road, Ludhiana (Pb.) | Email: info@ggi.ac.in
Helpline: +91 9914 666 777